SEISMIC BEHAVIOR OF SEMI-PRECAST CONCRETE SHEAR WALLS

A THESIS SUBMITTED TO
THE GRADUATE SCHOOL OF NATURAL AND APPLIED SCIENCES
OF
MIDDLE EAST TECHNICAL UNIVERSITY

BY

GOLNESA KARIMI ZINDASHTI

IN PARTIAL FULFILLMENT OF THE REQUIREMENTS
FOR
THE DEGREE OF MASTER OF SCIENCE
IN
CIVIL ENGINEERING

FEBRUARY 2016

Approval of the thesis:

SEISMIC BEHAVIOR OF PRECAST CONCRETE SHEAR WALL.

submitted by **GOLNESA KARIMI ZINDASHTI** in partial fulfilment of the requirements for the degree of **Master of Science in Civil Engineering Department, Middle East Technical University** by,

Prof. Dr. Gülbin Dural Ünver
Dean, Graduate School of **Natural and Applied Sciences** _____

Prof. Dr. İsmail Özgür Yaman
Head of Department, **Civil Engineering** _____

Prof. Dr. Barış Binici
Supervisor, **Civil Engineering Dept., METU** _____

Examining Committee Members:

Prof. Dr. Güney Özcebe
Civil Engineering Dept., TED University _____

Prof. Dr. Barış Binici
Civil Engineering Dept., METU _____

Prof. Dr. Ahmet Yakut
Civil Engineering Dept., METU _____

Prof. Dr. Erdem Canbay
Civil Engineering Dept., METU _____

Assoc. Prof. Dr. Yalın Arıcı
Civil Engineering Dept., METU _____

Date: February 12, 2016

I hereby declare that all information in this document has been obtained and presented in accordance with academic rules and ethical conduct. I also declare that, as required by these rules and conduct, I have fully cited and referenced all material and results that are not original to this work.

Name, Last name : Golnesa Karimi Zindashti

Signature :

ABSTRACT

SEISMIC BEHAVIOR OF SEMI-PRECAST CONCRETE SHEAR WALLS

Karimi Zindashti, Golnesa

M.S., Department of Civil Engineering

Supervisor: Prof. Dr. Barış Binici

Febuary 2016, 146 Pages

Successful performance of well-designed and constructed precast concrete elements in earthquake resistant structures, has led to widespread use of these kind of elements all around the world. Fast construction, high quality of precast concrete units and high durability are just a few advantages of these elements to be favored over cast-in-situ structures by engineers, and thus to cause seeking the ways to minimize their disadvantages. The main disadvantage of precast concrete elements in construction is the difficult detailing of the connection between the structural elements in order to ensure the integrity of the structure. Combination of precast components with other construction materials, particularly cast-in-place concrete (hybrid system) is one of the systems overcoming mentioned problem.

In this study double wall (sandwich wall panel), as a hybrid system, which consists of two precast reinforced concrete layers encasing a cast-in-place concrete layer, and its seismic behavior as a shear wall have been studied. Four double walls, consisting two rectangular, one U-shaped, and one T-shaped section walls, were already tested as full scale specimens subjected to cyclic horizontal load in Middle East Technical University (2013). A series of spread-sheets were developed in order to construct the moment-curvature relation of the critical section of the walls. Accordingly, response of each element was calculated and compared with the results derived from the experimental program. After verifying a good agreement between the experimental observations and the analytical model, the performance of walls were evaluated according to ASCE/SEI-41, Eurocode 8, and Turkish Earthquake Code 2007. Afterwards, seismic analysis, design and detailing of a mid-rise double wall-incorporated building were performed and finally, the performance of the building was assessed according to TEC2007.

Keywords: Double Walls, Hybrid System, Section Analysis, Moment-Curvature Relationship, Performance Assessment.

ÖZ

YARI-PREKAST BETON PERDE DUVAR MODELLERİNİN DEPREM DAVRANIŞI

Karimi Zindashti, Golnesa

Yüksek Lisans, İnşaat Mühendisliği Bölümü

Tez Yöneticisi: Prof. Dr. Barış Binici

Şubat 2016, 146 Sayfa

Depreme dayanıklı yapılarda, iyi tasarlanmış ve inşa edilmiş prekast beton elemanlarının başarılı performansı, bu tür elemanların tüm dünyada yaygın kullanımına yol açmıştır. Prekast beton elemanların hızlı inşaatı, yüksek kalite ve yüksek dayanıklılıklarından ötürü mühendisler tarafından yerinde dökme beton yapılara göre tercih edilmektedir ve dolayısıyla dezavantajlarını en aza indirmek için araştırmalar yapılmaktadır. Bu elemanların esas dezavantajı, yapı bütünlüğünün sağlanması için gerekli yapı elemanları arasındaki bağlantı detayının zorluğudur. Söz konusu sorunun aşılması için, prekast betonun diğer inşaat malzemeleri, özellikle yerinde dökme beton, ile birleştirilerek kullanılması (hibrid sistem) uygulanan çözümlerden biridir.

Bu çalışmada çift duvar (sandviç duvar panel), iki prekast betonarme ve ortada bir yerinde dökme beton bölümden oluşan bir hibrid sistem olarak, ve sismik davranışı bir perde duvar olarak incelenmiştir. İki dikdörtgen, bir U-şeklinde, ve bir T-şeklinde kesitlerden oluşan tam ölçekli örnekler, daha önce Orta Doğu Teknik Üniversitesinde (2013), çevrimsel yatay yük etkileri altında test edilmiştir. Duvarların kritik kesitlerinin moment-eğrilik ilişkisini düzenlemek için bir grup hesap çizelgeleri geliştirilmiştir. Bu duruma göre, her bir elemanın tepkisi hesaplanmış ve deneysel programından elde edilen sonuçlar ile karşılaştırılmıştır. Deneysel ve analitik model sonuçlar arasında iyi bir uyum olduğu doğruladıktan sonra, duvarların performansları ASCE/SEI-41, Eurocode 8 ve Türk Deprem Yönetmeliği 2007'e göre değerlendirilmiştir. Daha sonra, bir orta yüksekliğe sahip çift duvar yapının sismik analizi, tasarımı ve detaylandırması yapılmış ve nihayeten, binanın performansı TDY2007'e göre değerlendirilmiştir.

Anahtar kelimeler: Çift Duvar, Hibrid Sistem, Kesit Analizi, Moment-Eğrilik İlişkisi, Performans Değerlendirme.

To My Beloved Mother and

the Loving Memory of My Father,

ACKOWLEDGEMENT

First and foremost I offer my sincerest gratitude to my supervisor Prof. Dr. Barış Binici. This thesis would not have been completed without his expert advice and unfailing patience. I express my heartfelt gratefulness for his guidance and invaluable support that I believed I learned from the best.

I would like to express my gratitude to Research Assistant Alper Aldemir for his invaluable advice and assistance throughout this thesis.

I am also very grateful to my friends; Nigar Madani and Saideh Nazirzadeh for their understanding, companionship and encouragement in my moments of crisis.

Deeply from my heart with love, I would like to give my appreciation to my mother, for her unconditional love and endless support which made me follow my ambitions; to my sister and brother for their constant encouragement; and to my dearest father who would be happy if he could see me following in his steps as a former civil engineer. I believe his spirit and love will always live on in me.

TABLE OF CONTENTS

LIST OF TABLES

TABLES

LIST OF FIGURES

FIGURES

CHAPTER 1

INTRODUCTION

1.1 General

The term of "Precast Concrete" is used for all the products made from concrete under factory conditions, whether in a permanent factory or in a temporary casting field built on construction site. There is a wide range of precast concrete products and construction systems used worldwide, from non-structural elements such as architectural cladding, to structural elements like wall panels, double tees, and bridge girders. With the advancement of production and machining technologies, deployment of precast factories and substitution of cast in place construction techniques with modern ones using perfectly manufactured precast elements instead of cast-in-place reinforced concrete is being more common.

The key advantages of precast concrete construction can be listed as follows:

1. Construction process is fast and the total building time can be shortened by advancing different activities simultaneously.
2. General cost of construction is usually reduced since formwork, scaffolding, and temporary supports will not be needed in large quantities in comparison to the cast-in-situ concrete work.

3. The demand for skilled worker for site production is reduced because of the considerable reduction in in-situ concrete work.
4. Since elements are produced inside of a factory, construction process is usually independent of weather conditions.
5. In comparison with in-situ concrete work, precast products can be made with better quality due to the availability of trained and specialized labor working under factory conditions.
6. Achieving desired shapes and finishes can be possible using different aggregates, cements and other materials.
7. Since precast components are cast under controlled conditions, they can usually be cast with lower water-cementitious material ratio, hence the durability of these product are improved, resulting in longer service life.
8. Adding the insulation property, precast elements can provide a more acoustical and thermal controlled environment with fast construction and installation.
9. Precast products are characterized by being sustainable due to efficiently using materials and energy recourses.
10. Prestressing, when combined with precast technology, allows improved performance and economy by allowing longer spans, better crack control and less material use.

On the other hand, there are, of course, some limitations regarding prefabrication method which are summarized below:

1. The initial cost of building a precast plant is a disadvantage of precast construction compared to cast in place construction which requires a Project basis initial investment.
2. The main structural issue regarding the precast elements is the connections. Developing connections that can transfer moments and can dissipate energy by exhibiting high ductility under seismic loadings is a major challenge. Furthermore, providing high skilled labor to employ those connections on site

has been a critical issue from the point of safety, construction speed and quality point of views.

3. A very strict design, planning and installation methodology is needed with small margin of error tolerance. In this regard, once the precast elements are cast, last minute modifications cannot be made. Therefore, a detailed and precise design and checking is required.
4. The economical aspect of precast method may not be obtained in irregular, curved or architecturally challenging buildings where precast formwork would be single used.

The idea of precasting and prefabrication for construction have been used for a long time in the form of masonry construction. This method was effectively utilized in Europe just after World War II, because of the necessity of providing mass housing for homeless (Waddell, 1974). From then on, this method has spread throughout the world for the concept of building systems.

Construction of precast concrete structures in North America started in 1950's with some remarkable structures such as the precast/prestressed Walnut Lane Memorial Bridge in 1950, Figure 1-1. Following this event, the construction industry gained interest towards precast concrete method. Afterwards, new techniques, devices and materials were gradually developed. During 1960's, one of the key achievements in the precast industry was the development of standard products. In Canada, after the first Canadian Standard for Prestressed Concrete published, the last existing doubts about this method were obviated. By 1980's, notable achievements were obtained, namely innovative applications in bridges, bringing up the topics like durability, and developing some pioneering manufacturing systems like zero-slump hollow core slabs. One of the notable precast concrete buildings, incorporating hollow-core slabs and precast concrete interior and exterior walls, is the 31-story Bromley Place built in Canada, in 1985, which is still the tallest total precast concrete building in Canada (FIB, 2003; PCI Design Handbook, 2008).

Figure 1-1: Walnut Lane Memorial Bridge (Wikipedia)

Figure 1-2: Paramount Building (Robert E. Englekirk, 2002)

Starting at the end of 20th century, significant effort was placed on finding methods to construct tall precast buildings with special energy dissipating mechanisms. One important example is the 128 m high Paramount Building constructed in 2002 in San Francisco, which had precast moment frames, precast gravity columns, prestressed beams and architectural precast panels (Figure 1-2). A special moment resisting connection composed of a post tensioning system with forged ductile rods were employed for that building (Robert E. Englekirk, 2002). During the past decades, with the increasing demand, more structural sections and various architectural surface textures treatments such as thin-set brick and stone-faced panels were emerged and new material technologies employing high-strength steel and concrete, carbon fibers and self-consolidating concrete were adopted in precast construction (PCI Design Handbook, 2008). One of the first high profile applications of SCC was the Akashi Kaikyo bridge in Japan (Koehler et al. 2007).

Figure 1-3: Akashi Kaikyo Bridge (www.bridge-info.org)

In Italy, the increase in manpower cost, needs for industrial buildings, and initiation of widespread use of prestressing method caused the precast concrete industry to grow rapidly. The employment of precast concrete elements was no longer limited to

industrial buildings as they were implemented in various buildings, such as commercial, office, and residential buildings, and parking garages. Contemporarily, load bearing wall panels were introduced and were used in residential and social buildings. Constructing precast concrete buildings became also popular in East Europe, the need being mostly in non-seismic zones perhaps due to the lack of knowledge on the seismicity of the region (FIB, 2003).

In Japan, the initial use of precast construction was with one-way slabs made of pre-tensioned precast units such as double tee and hollow-core section and two-way reinforced slabs composed of precast units with cast-in-situ topping concrete from 1950's. Starting from 1980's, widespread demand for the use of precast concrete members in structural systems of moment resisting frames and structural walls arose due to the high growth of the economy. However, precast concrete buildings was not issued until 1999 in Building Standard Law and the related designs had to be approved by the Building Center of Japan by providing the structural equivalency to cast-in-situ reinforced concrete structures. The performance-based design method was adopted by the Building Standard Law in 1990 and after that seismic performance of precast concrete structures was mostly controlled based on more modern analysis techniques (FIB, 2003).

Precast floor components was quite common even in 1960's in New Zealand. Reduction in site framework and labor, high quality control, and increased speed in construction, caused the extensive use of these elements in moment resisting frames and structural walls during 1980's. The utilization of precast concrete in walls and frames was overlooked for many years in New Zealand because of high seismicity of the region and poor performance of precast-incorporated buildings in some countries during earthquakes. The 1982 New Zealand concrete design standard contained cast-in-place concrete structures, while a revision containing seismic design provisions for precast concrete structures was published in 1995 (FIB, 2003).

During 1960's, precast construction industry was initiated in Turkey. Construction of about 90% of industrial facilities were done using precast members in 1990s (Karaesmen, 2001). During this rapid industrialization, a majority of companies operating in this sector used the system they usually adapted from Europe to carry gravity loads only (Ersoy, 1999). Due to low seismicity in many European countries, the main problem regarding using systems taken from these countries was incompatibility of such systems with seismic risk of Turkey. After some destructive earthquakes in Turkey, related seismic code and regulations of building design were once rearranged in 1998 and after that in 2007 which included important regulations related to improving the safety of prefabricated buildings.

1.2 Precast Products

Precast concrete products are manufactured in variety of customized sizes and shapes according to the required function. Totally, considering the aspect of "connection type" and "the implementation method" of these members, precast products can be divided into two total categories of "Finished Precast Elements" and "Semi-Finished Precast Elements".

The most commonly used finished precast elements are rectangular beams, double tees, I beams, box beams, bulb tees, inverted tees, ledger beams, hollow core slabs, piles, and wall panels, Figure 1-4. Once these elements are erected on site, there is no need for additional working process. Shortening the time of the construction without being influenced by climatic conditions is the main advantage of these product.

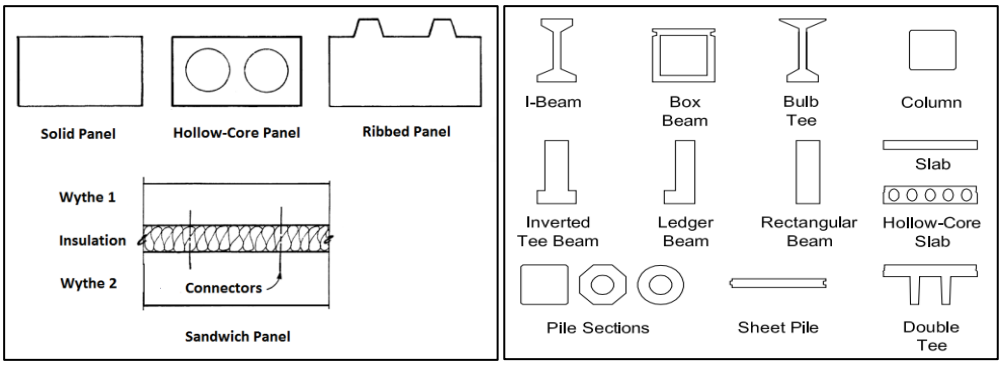

Figure 1-4: Cross Section of Commonly Used Precast Elements (PCI Design Handbook, 2004; Guide for Precast Concrete Wall Panels, 1993)

Semi-Finished Precast Elements benefit from combination of both precast and in-situ concrete construction methods. Elimination of formwork on site and reduction in costs of transportation and installation due to low-weight of these elements, in comparison with finished elements, are the main characteristics of these elements. In this category, the most known products used in the residential and industrial construction are "Double Walls" and "Filigree Slabs", Figure 1-5.

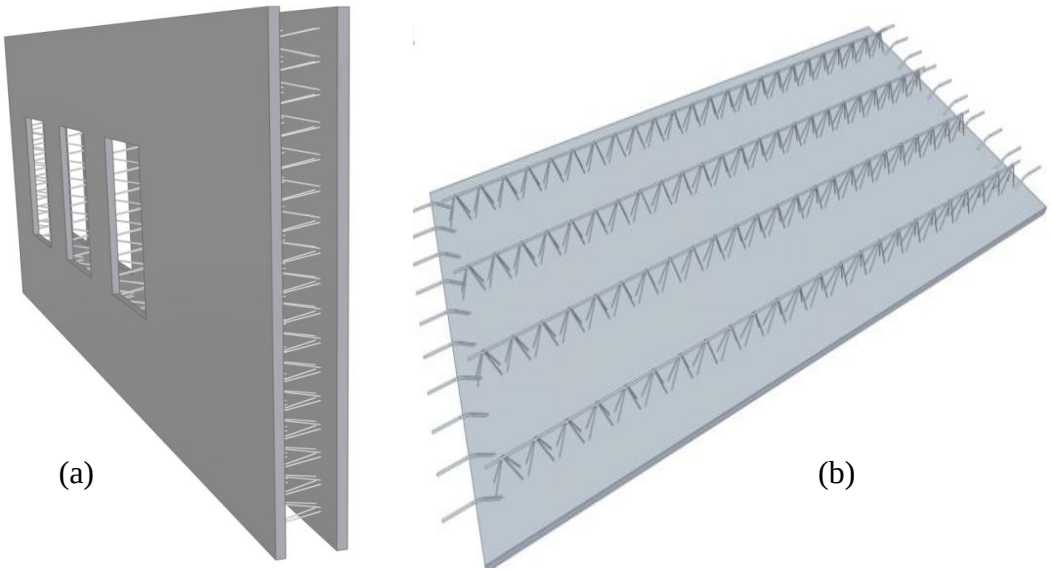

Figure 1-5: (a) Double Wall, (b) Filigree Slab

A typical double wall is composed of two reinforced concrete shells encasing a void layer, which are connected to each other through connectors, such as lattice girders or waves. Double walls are constructed with filigree slabs in general to enable monolithic behavior. Despite to its large dimensions, double walls are considered as low weight members. This enables the use of a low capacity crane to install the precast parts on the construction site. Moreover, the transport costs are relatively less compared to traditional precast concrete elements. Therefore, use of double walls in construction is a very desirable option because of lower costs, shorter construction time and high quality. An insulation layer can be added between precast concrete layers in double walls. This property enables the double walls system to be a complete structural system including exterior finish, load bearing properties and thermal/acoustic insulation. On the other hand, casting concrete in the middle layer of double walls, may lead to overcome the major disadvantage of precast products, which is the lack of monolithic connection and continuity of precast elements along the building height.

The filigree slabs, also referred as floor slabs or semi-finished slabs, are another type of precast products used in residential and industrial constructions. These slabs normally consist of a concrete shell, longitudinal and transverse reinforcement and connectors (lattice girder) in lateral direction. The bottom shell can be prestressed concrete depending in the desired span. The 5 cm thick concrete slabs (can be thicker if desired) are produced up to 3 m width. The top surface of the slab is left in an unfinished state which, in conjunction with the connectors, allows perfect bonding between the precast parts and in-situ concrete. The floor slabs are preferably used in combination with double walls to create monolithic constructions and guarantee the rigid diaphragm action. After casting concrete on site, the filigree slabs must be supported during the concrete curing process. These slabs are characterized by their low weight. This enables the semi-finished precast parts to be dispatched to the site with lower cost and installed on the construction sites, using cranes with lower load capacities. Furthermore, with the use of filigree slabs, complex molding and extensive reinforcement work on the construction site can be eliminated.

Detailed information regarding double walls, which is the subject of this study, is provided in following sections.

1.3 Seismic Performance of Precast Concrete Structures

Poorly designed, detailed and constructed precast concrete structures have been severely damaged during destructive earthquakes. This outcome has made the use of precast concrete for multi-story buildings unreliable in earthquake prone countries. It should, however, be reminded that the results gained from the experimental tests conducted in laboratories, and past earthquake experiences show that well detailed and designed precast and prestressed elements provide sufficient confidence for successful performance of precast structures under earthquake loadings.

Design of precast concrete buildings is generally similar to the design of cast in place concrete structures. The key difference from cast in place concrete system design is the design and construction of the precast concrete connections such that sufficient ductility, stiffness, strength, and stability are provided. Examples of observed damage in precast buildings are summarized below:

- **Armenian Earthquake, Armenia, 1988**

A 6.8 magnitude earthquake in Nalband, Armenia occurred in 1988 causing 45000 causalities. The behavior of precast concrete structures in this earthquake showed the importance of accurate design of connections, Figure 1-6. A number of one to five story precast frame buildings with hollow-core slabs collapsed due to poor connection between floors and walls. Beam-column connections were assembled by welding beam bars to the steel angles extended beyond precast columns in these buildings. In addition, floor diaphragms were improperly jointed to the frame elements providing insufficient diaphragm action. Bar splices in columns were made by welding longitudinal bars, which caused insufficient ductility.

Furthermore, columns were detailed poorly with inadequate confining reinforcement. Despite these inadequate reinforcement details, structures with significant amounts of precast panels attached to the framing system survived the earthquake without collapse, showing the importance of wall elements for seismic resistance. (Wyllie, 1989; Fintel, 1995)

Figure 1-6: Collapse of Precast Buildings in Armenian Earthquake (Wyllie, 1989)

- **Kocaeli Earthquake, Turkey, 1999**

A devastating earthquake occurred in Kocaeli in 1999, causing death of about 25000 people and a monetary loss of over 25 billion dollars. In this earthquake, although several improperly detailed and designed buildings collapsed, the behavior of a few buildings composed of large-span frames and precast walls with proper detailing and sufficient diaphragm reinforcement and connections was successful. (Figure 1-7)

Figure 1-7: A Precast Concrete Building with no Damage affter Kocaeli Earthquake, 1999 (Ghosh, 2001)

Figure 1-8: Shear Failure of Precast Concrete Column (FIB, 2003)

In Figure 1-8, a precast column with shear failure due to insufficient transverse reinforcement amount is illustrated. Such failures were observed due to the lack of applying capacity design principles. An example of a ductile failure in the form of flexural yielding at the base of a precast column is shown in Figure 1-9. Figure 1-10, shows a severe distress in a precast column which occurred at the section where some of vertical bars were truncated .

Figure 1-9: Ductile Flexural Yielding at a Precast Column (FIB, 2003)

Figure 1-10: Severe Distress in Precast Concrete Column (FIB, 2003)

Furthermore, several examples regarding inadequate diaphragm action was observed confirming the importance of diaphragm design in precast structures. Diaphragms were designed to be very flexible resulting in insufficient lateral load transfer from floors to the lateral force resisting system, Figure 1-11. Some of these failures occurs due to the insufficient joint connectivity between columns and beams failing due to the shear failure of the dowels or floor accelerations reducing the seating in the out of plane direction, Figure 1-12. (FIB, 2003; EERI, 1999)

Figure 1-11: Flexible Connection Between Diaphragm and Precast Concrete Beam (FIB, 2003)

Figure 1-12: Failure of Cantilever Head Connection on Top of Columns (FIB, 2003)

Figure 1-13: Failure of Columns due to Interaction with Stiff Masonry Infills (FIB, 2003)

- **Canterbury Earthquake, New Zealand, 2011**

An earthquake occurred in Christchurch on 22 February 2011 and registered 6.3 on the Richter scale. The earthquake caused widespread damage across Christchurch, killing 185 people in the nation's second deadliest natural disaster. Precast moment frames showed plastic hinging at the critical regions to a level of damage proportional to the seismic excitation, Figure 1-14. In most of the precast floor systems, the damage was observed as displacement compatibility cracks along the units, Figure 1-15. The floors cannot follow displacements of the cumulative elongation of the frame spans as a result of plastic hinge formation.

Figure 1-14: PWC Tower precast moment frame damage (Fleischman, 2014)

Figure 1-15: Damage in Floor System in Brannigans Tower (Fleischman, 2014)

Precast cladding panels generally remained intact. The collapse of precast stair elements was noted in at least three multi-story buildings, Figure 1-16, causing occupants to get stuck in the buildings for a long time. A hospital building constructed with self-centering system remained operational with little damage. In this building, unbonded post-tensioned frame was utilized in one direction, and unbonded post-tensioned rocking wall was used in the other direction. (Elwood, 2013; Fleischman, 2014)

Figure 1-16: Collapsed Precast Concrete Stair in Multi-Story Building (Elwood, 2013)

1.4 Double-Wall Technology

Structural walls are considered as widely used and costly effective lateral resistance system. Their seismic performance has been very successful in low and high rise buildings. In comparison with frame structures, they present more stability against overturning due to P-Δ effects. In addition, they effectively restrict the seismic drift demand and, hence, reduce the damage to non-structural elements. Therefore, researchers have been always seeking innovative structural wall systems.

More recently, the use of various types of precast concrete walls has been expanded. Since the early 1990s, investigation of the seismic behavior and design of precast concrete structures has been taken into consideration by researchers (Wood et al., 1987; Wyllie, 1989; Fintel, 1995; Holden et al., 2003). One of the precast products which its design is carried out to emulate the behavior of its cast-in-place equivalents, is double wall.

Double walls are considered as a "Hybrid System". A hybrid system is the result of combination of precast concrete components with other construction materials, particularly cast-in-place concrete, which utilizes the inherent characteristics of both

in order to create an optimized structural solution. Use of precast and cast-in-place concrete jointly makes construction faster, economic, with high-quality finishes. Whenever two materials are combined to create one structural system, the attributes of each material must be evaluated and addressed to ensure the proper outcome (Goodchild, 2004).

The base configuration of double walls is referred as precast concrete sandwich panel (PCSP). Sandwich wall panel is a major product in the precast concrete industry. Due to their desirable characteristics, sandwich wall panels have been widely used for decades with high demand and unprecedented success. Construction systems based on sandwich panels are commonly used worldwide for intensive building production. A typical PCSP is composed of two concrete wythes encasing a layer of insulation. Therefore, this system is able to both transfer the loading and provide insulation. Special shear connectors (i.e. truss connectors) is utilized in order to connect the wythes together. The functions of these walls vary from being used for cladding to being placed as interior and exterior walls acting as bearing or shear walls. The advantages and disadvantages of PCSPs are similar to the other precast products. Providing a layer of insulation is the unique characteristic of these products (State of the Art Precast/Prestressed Concrete Sandwich Wall Panels).

There isn't an exact time regarding the beginning of employing precast concrete sandwich walls in literature, however, they were produced in North America as early as the 1960’s. The early form of these panels is composed of a thick internal wythe, generally a double-tee or hollow core, and a layer of rigid insulation and finally an external non-structural layer (State of the Art Precast/Prestressed Concrete Sandwich Wall Panels). Currently, solid panels are used for both internal and external layers. The structural behavior of insulated wall panels is highly dependent on the connectors used to connect the wythes. Shear connectors must be able to transfer the longitudinal interface shear between the layers ensuring a fully-composite or a partially composite behavior of the PCSPs.

Several comprehensive researches have been done regarding the connectors of PCSPs. The objective of these researches is to attain a wall system which is both thermally and structurally efficient by devising a new shear connector. These connectors, generally, can provide high thermal resistance and at the same time, high shear capacity in order to optimize the composite action between wythes. One of these studies was developed in the early 1990s which combined the high structural efficiency and thermal insulation capacity through use of a special fiberglass composite truss connector (Al-Einea et al. 1994). In 2003, thorough experimental tests indicated that composite behavior is gained particularly by solid concrete regions (Pessiki & Mlynarczyk, 2003). However in 2008, after experimental and theoretical studies regarding flexural behavior of PCSPs, A. Benayoune concluded that the stiffness of the shear connectors used governs the ultimate strength and the degree of composite action Figure 1-17.

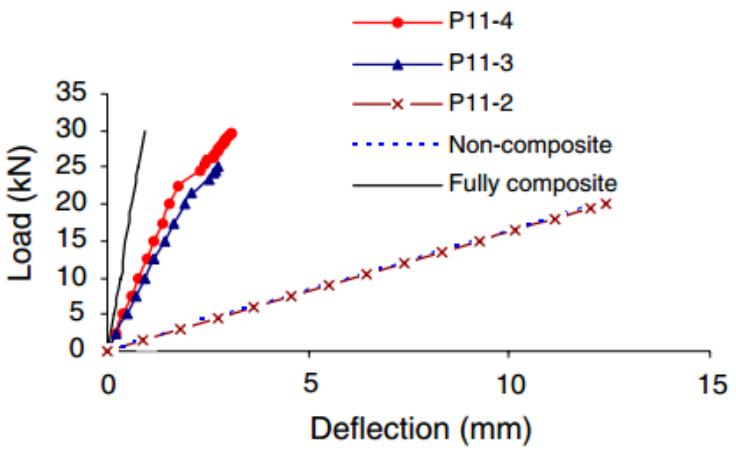

Figure 1-17: Load-Deflection Profiles for Specimens with 2, 3, and 4 Shear Connectors, Showing the Increase of Ultimate Load with the Increase of Shear Connectors' Number (Benayoune et al., 2008)

A noteworthy achievement regarding PCSPs was the publication of PCI committee in 1997 which was the summary of all the related specification including details, erection, manufacture, design, etc.

Considering the mechanism of these panels, researchers have carried out many investigations in various aspects. An experimental program was performed in Italy in order to analyze the lateral behavior of PCSPs in 1999 (De Matteis & Landolfo, 1999). In 2002, Australian researchers introduced a new fastening system which presented about 2.5 times greater shear strength and enhanced ductility (Mahendran & Subaahara, 2002). Fabrizio Gara, in Italy, studied the shear wall's buckling under vertical loading and recently, a seismic study of PCSPs was conducted in 2013 (Hamid & Fudzee, 2013).

In comparison with cast-in-place concrete walls, studies on seismic behavior of precast concrete walls are limited. So far, many studies have been carried out about various types of Precast Concrete Sandwich Panel walls, however few researches has been done concerning double walls. In 2010, Professor Xiaopu Shen in Anhui University of Architecture in China examined the seismic behavior of three full scale hybrid shear walls and the related numerical study was carried out in Illinois Institute of Technology (Xu, Shen, & Shen, 2014).

1.5 Construction of Double Walls

A double wall (twin wall) is composed of two thin precast concrete panels (usually 5cm to 6cm thick) which are connected through connectors, such as lattice girders or waves. The product is temporary fixed on the site and then, the void layer is filled with fresh concrete. Therefore, the connected precast shells act as framework and a monolithic reinforced concrete structural wall is attained. The inner surfaces of the shells are roughened in the production plant for the better integrity between layers and thus, better transferring the forces together with the connecting reinforcement. Consequently, the total cross section made of precast and cast-in-situ concrete layers has a joint structural effect in the bond and is ideally suited to carry vertical and horizontal loads. The production steps of double walls in a factory are summarized in Figure 1-18(a) to Figure 1-18(i).

Double walls are generally utilized with filigree slabs, which are composed of a concrete shell with a lattice girder. Precast concrete components are manufactured in a production facility and then are transported to the building site. On the building site, after assembly of precast structural elements, sufficient reinforcement is placed to ensure monolithic moment resisting connections. Afterwards, the void between wall shells, slab toppings, and wall-slab connections will be filled with in-situ concrete. After curing the concrete a monolithic wall-floor system will be provided which is hardly attained through standard precast construction.

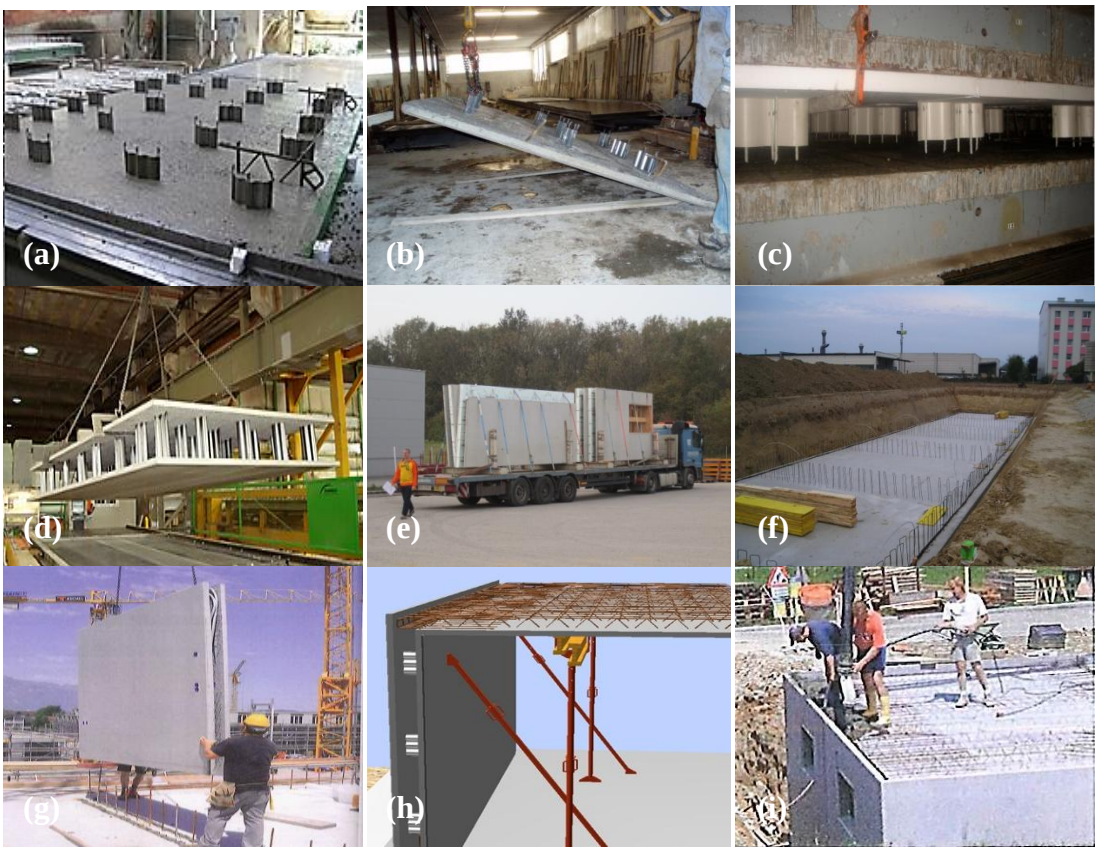

Figure 1-18: Construction Steps of Double Wall-Filigree Slab System; (a) Placement of Waves and Casting First Layer, (b) Rotating First Layer, (c) Fixing First Layer on the Second Layer with Fresh Concrete, (d) Moving to Storage, (e) Transportation, (f) Placing Starter Bars, (g) Installing Double Walls on Site, (h) Installing Filigree Slabs, (i) Casting Concrete on Site

1.5.1 Connectors

Two alternatives of connectors in connecting double walls' shells are lattice girder system and wave system (Figure 1-19). Lattice girders are classic types of connectors made from continuous steel bars bearing pressure caused from concrete casting. The main disadvantage of using this system is that it limits the development length of horizontal connection reinforcement resulting in independent behavior of adjacent walls. Furthermore, the continuous reinforcement in lattice girder restricts the placement of proper reinforcement detailing between the two shells which is necessary for seismic detailing.

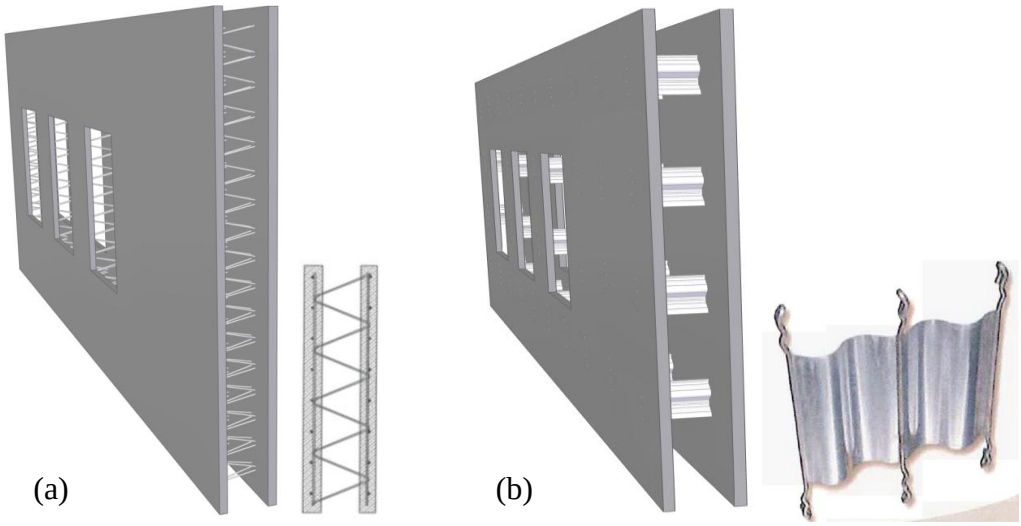

Figure 1-19: Connector Systems; (a) Girder System, (b) KAPP-Wave System

Wave systems became available from the beginning of the 21st century. This system were invented by KAPPEMA Company in cooperation with Oberndorfer Company. The special characteristic of wave system is its point connectors (steel sticks), providing the possibility of the use of horizontal steel reinforcement for connection between adjacent walls (Figure 1-20). The main advantages of these waves, with the industrial name of KAP-Waves, are (Binici and Canbay, 2014):

- Providing proper space for connecting adjacent double walls, and for placing necessary vertical and horizontal reinforcement between the two shells leading to proper design for seismic resistance,
- Thinner shell thickness,
- High pullout strength, and hence reduction in amount of reinforcement,
- Providing the possibility of installing the insulation material adjacent to one shell from inside.

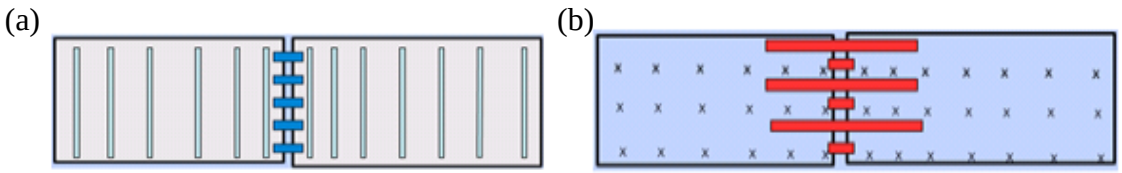

Figure 1-20: Connection of Adjacent Walls with; (a) Lattice Girder, (b) Wave System

1.6 Objective and Scope

Considering the high rigidity, strength, ductility, and integrity of cast-in-situ concrete wall structures, as well as the unique characteristics of precast concrete elements, the concept of double walls may provide an innovative shear wall system benefiting from both wall systems. In practice, double wall is not recommended as a significant seismic resisting system; it has been used as a gravity resisting components during last decades. So far, limited investigations have been done concerning its seismic behavior and hence, double walls application in seismic regions is regarded with uncertainty. The main objective of this study is the analysis and performance assessment of double walls, to be designed and detailed as a cast-in-place structural wall system and comply with the performance limit states of structural walls. In 2014, reversed cyclic test of double walls were completed in Structural Mechanics Laboratory, Civil Engineering Department of Middle East Technical University, under a research program funded by Oberndorfer International Company (Binici and

Canbay, 2014). The results obtained from this experimental program have been used in this study.

This document discussed the double wall technology in the first chapter. In chapter 2 a summary of the mentioned experimental studies is provided. Afterwards, a section analysis procedure is developed in order to determine the capacity of the specimens, estimate the response of the member, and compare with the test results. Chapter 3 contains the performance evaluation of the specimens with reference to Eurocode, ACI 318 and Turkish Earthquake Code. Chapter 4 covers the description of the analysis and design of a mid-rise double wall building, including seismic analysis, design and detailing of double walls, and performance assessment of the building according to Turkish Earthquake Code. Chapter 5 presents concluding remarks.

CHAPTER 2

SEISMIC PERFORMANCE OF DOUBLE WALLS

2.1 Review of the Experimental Study

In 2014, an experimental program was performed at Middle East Technical University, Department of Civil Engineering, Structural Mechanics Laboratory, conducted by Prof. Dr. Erdem Canbay, Prof. Dr. Barış Binici, and Erich Kastner with the funding provided by Oberndörfer GmbH in order to investigate the behavior of the double walls under reversed cyclic loading (Binici and Canbay, 2014). This research was held for the first time in literature, in order to gain a better understanding of seismic behavior of double walls. A summary of this experimental program was provided here, and more details can be found in Binici and Canbay, 2014.

Four specimens were examined during this experimental study. First two tests were conducted to compare the seismic response of two exterior double walls produced with single and two adjacent double walls, respectively, in order to simulate insulated double walls. The other two specimens were considered as interior walls of a building, hence no insulation material was used. Section shape of the specimens 3 and 4 are designed as U-shaped and T-shaped, respectively. The characteristics of all specimens and mechanical properties of the materials employed in each of them are summarized in Table 2-1 and Table 2-2.

Table 2-1: Properties of Specimens

Specimen	Section	Height (m)	Depth (m)	Thickness (m)	Insulation	Number of Precast Walls for Assembly
1	R*	2.5	3.00	0.35	+	2
2	R*	2.5	3.00	0.35	+	4
3	U	2.6	1.40	0.20	-	6
4	T	2.6	1.70	0.20	-	5

*: Rectangular Section

Table 2-2: Properties of Materials

Specimen	f'_c(s)* (MPa)	f'_c(c)** (MPa)	ϕ6 f_y, f_u (MPa)	Φ8 f_y, f_u (MPa)	Φ12 f_y, f_u (MPa)	Φ14 f_y, f_u (MPa)
1	45	28	340, 470	380, 540	490, 610	325, 455
2	43	27	340, 470	380, 540	490, 610	325, 455
3	45	25	340, 470	380, 540	490, 610	325, 455
4	45	25	340, 470	380, 540	490, 610	325, 455

*: Compressive Strength of Shell Concrete, **: Compressive Strength of Core Concrete

The details of the specimens are provided in Figure 2-1 to Figure 2-3. Specimen 1 was composed of two precast reinforced concrete shells having a length of 300 cm with 5cm and 6cm thickness. Precast layers encased a 10 cm-thick insulation layer and a 14 cm-thick void space. Specimen 2 on the other hand was produced with two adjacent double walls with lengths of 150 cm and same properties, connected with horizontal connection cages. The total thickness of these walls was 35 cm. Concrete was cast monolithically in the central void layer for both specimens. Expanded polystyrene (EPS) was installed adjacent to one of the precast concrete shells, so it was considered that the insulation layer and the concrete shell alongside it act as non-structural components.

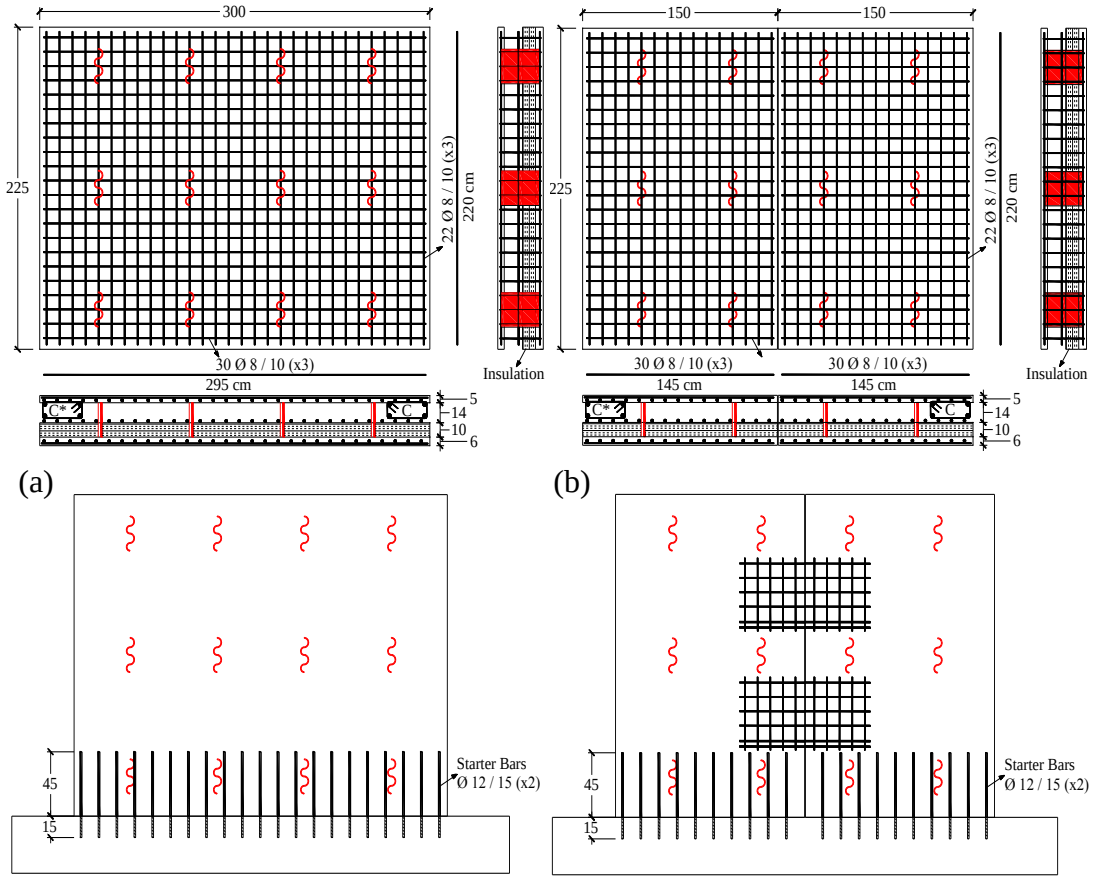

Figure 2-1: Details of; (a) Specimen 1, (b) Specimen 2 (Binici and Canbay, 2014)

Specimen 3 and 4 (U-shaped and T-shaped section walls) were composed of precast reinforced concrete layer of 5 cm, the void layer of 10 cm, and total thickness of 20 cm. These two specimens were constructed by following the regulations of Turkish Earthquake Code (TEC2007). Such walls may be utilized in buildings around stairs or elevator shafts. On the other hand, due to the lack of the experimental data regarding the seismic response of U and T-shaped section walls in literature, it was intended to evaluate the failure mechanisms and the cyclic performance for these walls. Details of the reinforcement of specimens 3 and 4 are shown in Figure 2-2 and Figure 2-3.

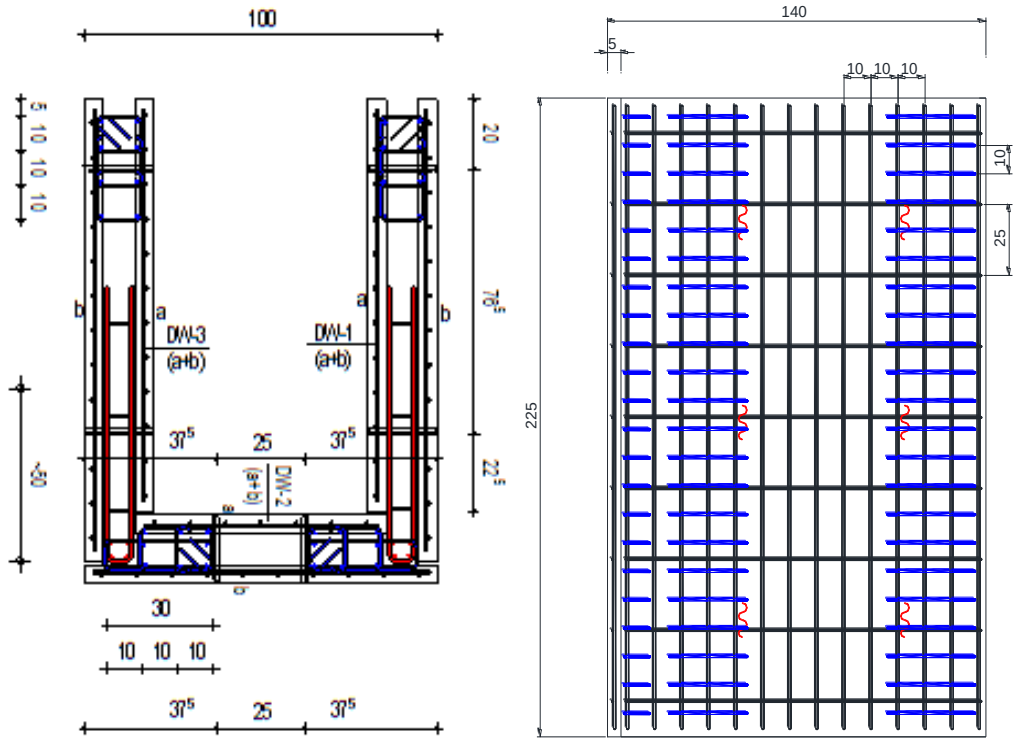

Figure 2-2: Details of Specimen 3 (Binici and Canbay, 2014)

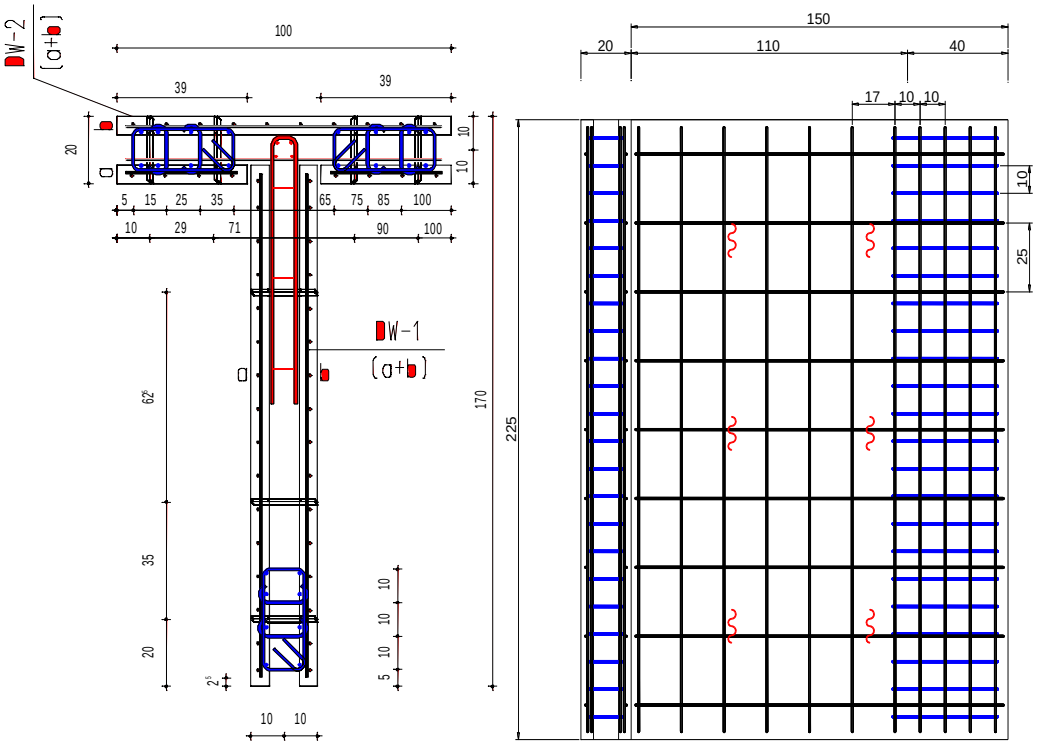

Figure 2-3: Details of Specimen 4 (Binici and Canbay, 2014)

2.1.1 Test Setup

Test setups employed for this experimental study are shown in Figure 2-4. All of the specimens were tested under lateral cyclic displacement reversals. Axial force were not applied during the tests due to insignificant axial loads for walls in actual buildings. Displacement loading history of specimens is presented in Figure 2-5.

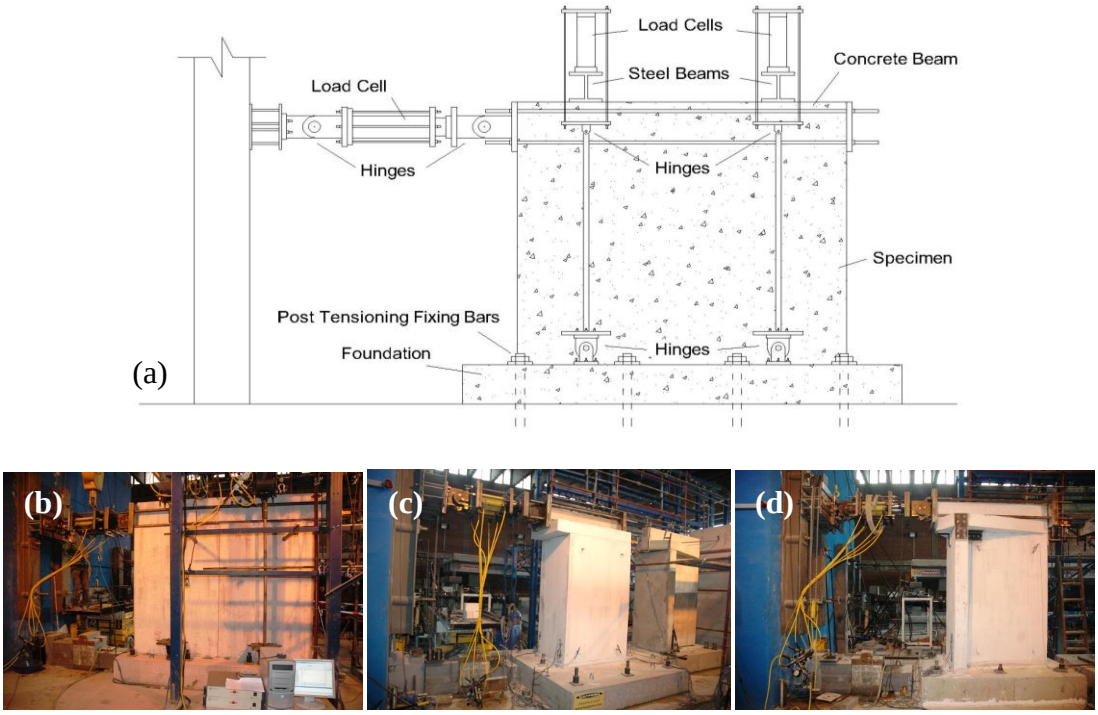

Figure 2-4: Test Setups; (a) Schematic Details of a Sample Test Setup, (b) Specimens 1&2, (c) Specimen 3, (d) Specimen 4

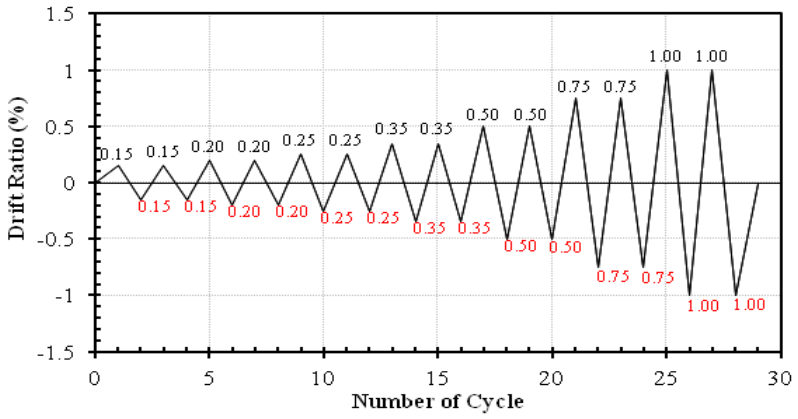

Figure 2-5: Displacement History During All Tests (Binici and Canbay, 2014)

2.1.2 Test Results

The lateral load deformation responses of all the walls are presented in Figure 2-6.

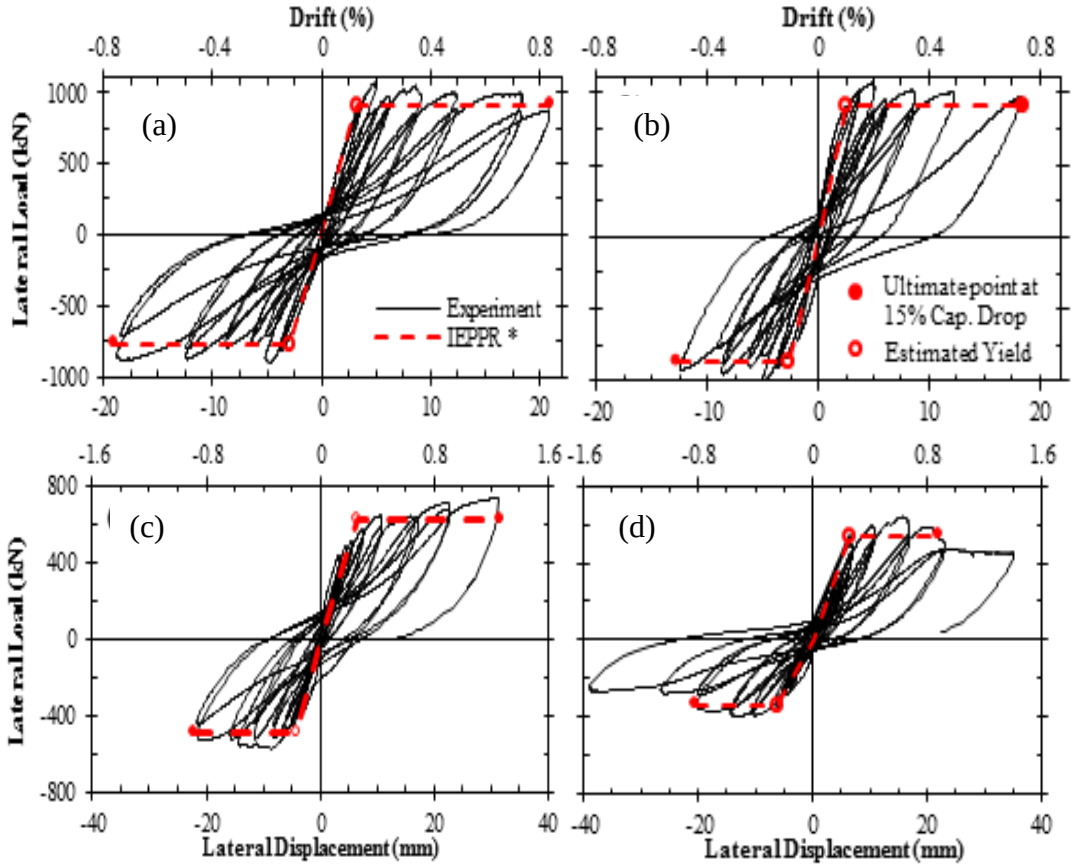

Figure 2-6: Experimental Response of (a) Specimen 1, (b) Specimen 2, (c) Specimen 3, (d) Specimen 4 (Binici and Canbay, 2014)

As shown in Figure 2-6, an idealized elastic perfectly plastic response were derived for each specimen. The yield and ultimate points may be found from these curves. First yield point was determined by drawing a line passing through the origin and 70% of the ultimate load on the initial loading curve. Extending this line to 85% of the ultimate load was considered to provide the yield point. The ultimate condition is defined at 15% capacity drop. Displacement ductility is found by dividing the ultimate displacement by the yield displacement. The damage pictures of the specimens are presented in Figure 2-7.

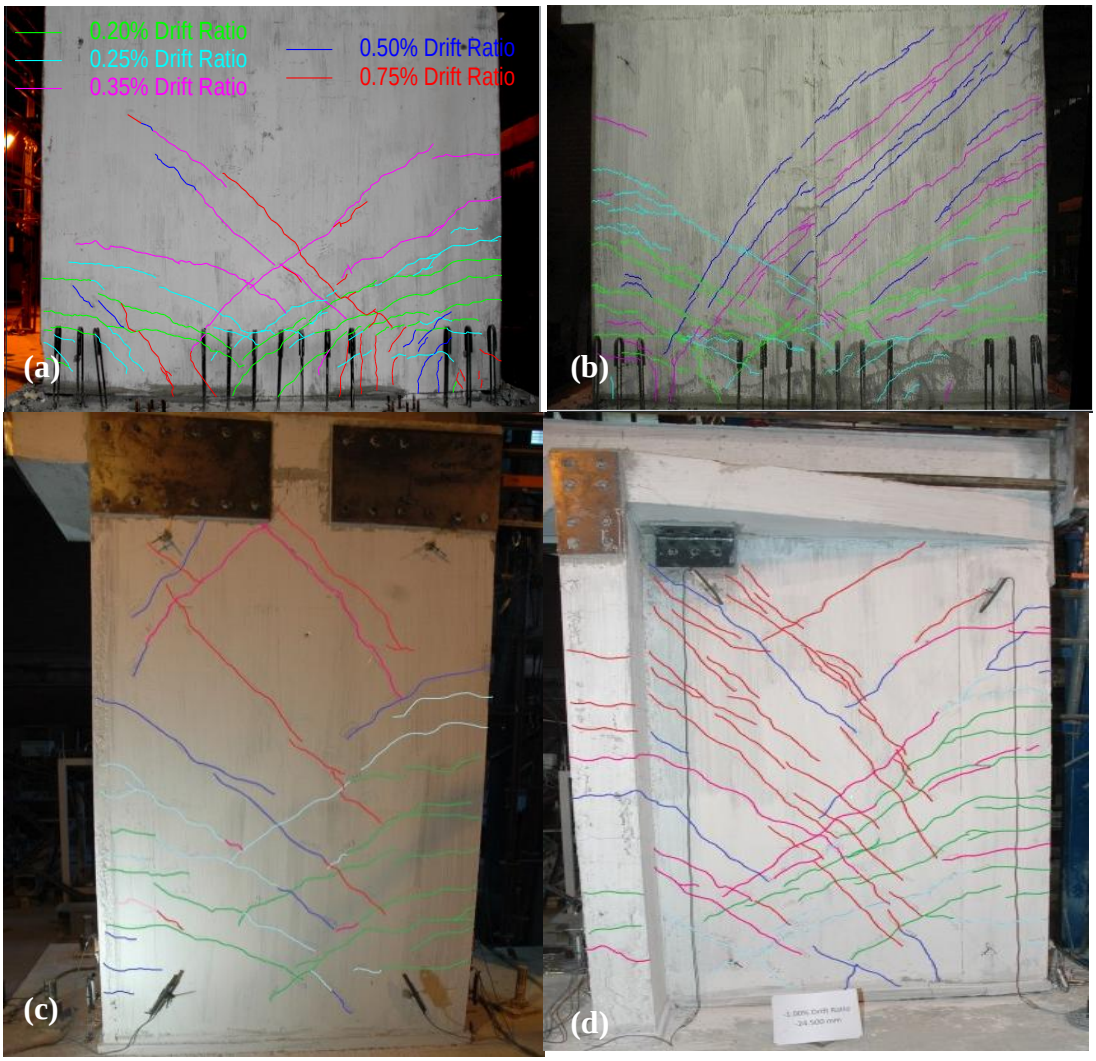

Figure 2-7: Cracks Observed for; (a) Specimen 1; (b) Specimen 2, (c) Specimen 3, (d) Specimen 4 (Binici and Canbay, 2014)

According the researchers observations (Binici and Canbay, 2014), once the specimen 1 experienced the first crack, some flexure cracks appeared starting from base towards the upper portion. The maximum base shear capacity of 1069 kN was attained in the positive and 903 kN in the negative direction. Degradation of the strength of the was observed at about 0.2% drift ratio, however lateral strength was maintained up to a drift ratio of 0.75%. Beyond 0.35% drift ratio, the width of the base cracks increased significantly (2 mm). Despite its squat dimensions (H/L≈0.85), specimen 1 behaved in a ductile manner in both directions of loading and had a displacement ductility of about 6.5 according to Figure 2-6.

Considering the important points in response of the specimen 1, specimen 2 behaved in a similar manner. The maximum base shear capacity of 1072 kN and 1017 kN was attained in positive and negative directions, respectively. The cracks were well distributed for this specimen and their widths remained limited throughout testing. Regarding the behavior of the two adjacent double wall, no cracking was observed at the interface, which is the prove of the effectiveness of the connection cage along with the central monolithic concrete.

Even though specimen 3 is much slender compared to specimen 1 ($H/L \approx 1.7$) , after the first crack, inclined cracks were seen on the two webs of the wall. These cracks extended toward the upper portion of the wall after 0.5% drift ratio. Hardening in the load deformation was observed in the positive direction, which is mainly because of the significant longitudinal reinforcement distributed on two legs of the U section. However, the same manner did not detected in the negative direction due to the reinforcement concentrated in the flange. The maximum base shear capacity of 732 kN and 575 kN was reached in positive and negative directions, respectively. Although no significant strength drop was observed in positive direction, in the opposite direction some reduction in strength monitored which is due to the concrete crushing at the toe of the wall. Based on Figure 2-6, it can be stated that Specimen 3 had a displacement ductility of about 4.8 and 5.2 in the positive and negative directions, respectively. Despite the observed shear cracks, the specimen was able to behave in a very ductile manner

After wall base cracking in specimen 4, flexural cracks on the flange and inclined cracks on the web were seen beyond a drift ratio of 0.3%. Crushing of the web corner initiated at a drift ratio of about 0.75%, after the beginning of strength degradation. The maximum base shear capacity of 639 kN and 393 kN was reached in positive and negative directions, respectively. After monitoring the crushing of wall toe and diagonal cracking, beyond a drift ratio of 1%, the wall was not able to sustain its lateral strength. Figure 2-6 indicates that the displacement ductility of the wall was about 3.4.

2.2 Moment-Curvature Analysis

In seismic analysis of reinforced concrete elements, some realistic analytical models may be needed with the aim of prognosticating characteristics of the member, namely strength, stiffness, and ductility. In order to provide this tool, a moment-curvature analysis was developed for determining the sectional response and hence, predicting the force-displacement relation of a member. In general, it has been accepted that the first loop of the hysteretic response follows the same pattern with the moment-curvature diagram under monotonic loading (Ersoy and Özcebe, 1997). For this purpose, flexural capacity of the section where the plastic hinge is expected (here, at the base of the element) was calculated and afterwards, a force-displacement relationship was obtained by integrating section curvatures over member length.

A set of spread-sheets were developed following the procedures indicated by Priestley (Priestley et al., 2007) to construct the moment-curvature relation using the properties of the critical section. Following algorithm is pursued:

1. Computing the cracking moment and cracking curvature using the equations below:

$$M_{cr} = \frac{f_{cr} \times I}{c_{bot}} \qquad (2\text{-}1)$$

$$\phi_{cr} = \frac{M_{cr}}{E_c \times I} \qquad (2\text{-}2)$$

where;

f_{cr}: is cracking force obtained from:

$$f_{cr} = 0.62\sqrt{f_c'} \qquad (2\text{-}3)$$

I: Moment of Inertia of Total Section,

c_{bot}: Distance of Neutral Axis from far most concrete tension fiber.

2. Assigning a starting strain value to the extreme concrete fiber in compression zone.

3. Finding the neutral axis depth by try and error satisfying the equilibrium between tensile and compressive forces.

4. Increasing the strain value assigned in step 1 and repeating the procedure.

Accordingly, the following assumptions were considered in constructing the moment-curvature relation:

- Plane sections remain plane before and after bending (Navier-Bernoulli hypothesis),
- Perfect bond is considered between reinforcement and concrete, so that the steel strain is equal to the strain of the surrounding concrete,
- Material models used are the unconfined and confined concrete models proposed by Mander (Mander et al., 1988a,b) and reinforcing steel model proposed by King (King et al., 1986), which are presented in details in following sections

The moment curvature graph carried out here was then compared to the results obtained from experimental results.

2.2.1 Bilinear Idealization

The recommendations provided by Priestley (Priestley et al., 2007) was followed for bilinear idealization of the moment curvature diagram. According to Priestley, 2007, the following points were considered for approximation:

1. First Yield (M_y, ϕ'_y): First yield corresponds to the yield strain of the outermost tension reinforcement or the concrete strain of 0.002 in outermost compression fiber (strain at peak stress of unconfined concrete), whichever occurs first.
2. Nominal Capacity (M_n, ϕ_y): At this point, the extreme tension reinforcement attains the strain of 0.015 (onset of 1mm crack width), or the extreme concrete compression fiber reaches the ultimate strain of unconfined concrete (onset of spalling, i.e. 0.004), whichever occurs first. The nominal curvature is calculated by linearly extrapolated from the yield point up to nominal moment capacity. ($\phi_{y=} \phi'_y M_n / M_y$)
3. Ultimate Capacity (M_u, ϕ_u): The plastic branch is defined by joining the nominal yield point to ultimate condition. This point is somehow subjective. Sometimes the ultimate condition corresponds to a critical physical event, such a confinement reinforcement fracture. On the other hand, it can be related to 20% strength drop from the maximum strength. Generally, it is defined as the extreme tension reinforcement reaches the effective ultimate strain o steel ($\varepsilon_s=0.6\varepsilon_{su}$), or the extreme concrete compression fiber is at ultimate strain of confined concrete. In this study, the ultimate point is assigned to one of the conditions above, whichever occurs first.

The schematic diagram of the described procedure is presented in the figure below.

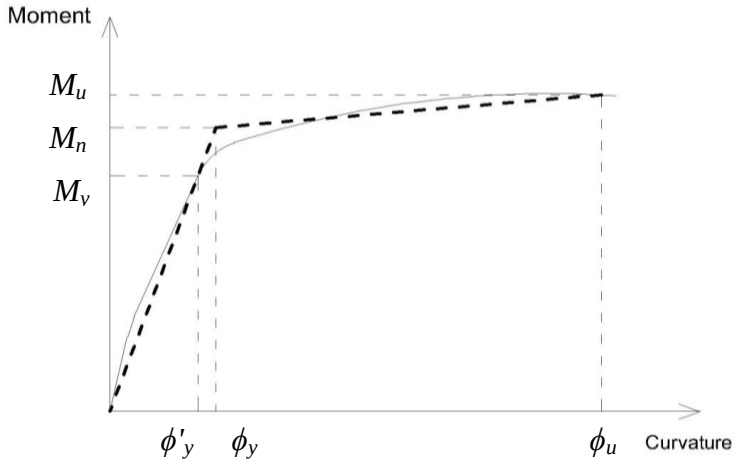

Figure 2-8: Bilinear Idealization of Moment-Curvature Curve

2.3 Material Models

2.3.1 Concrete Properties

A unified stress-strain relationship for confined concrete have been proposed by Mander et. al. (1988). The stress-strain model is presented in Figure 2-9 and is described as follows:

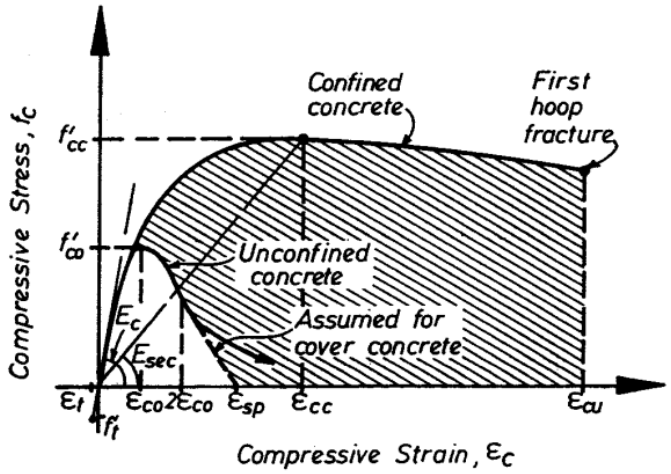

Figure 2-9: Stress-Strain Model for Monotonic Loading of Confined and Unconfined Concrete (Mander et al., 1988)

$$f_c = \frac{f'_{cc} x r}{r - 1 + x^r} \qquad (2\text{-}4)$$

where;

f'_{cc}: compressive strength of confined concrete (defined later).

$$x = \frac{\varepsilon_c}{\varepsilon_{cc}} \qquad (2\text{-}5)$$

f_c and ε_c: longitudinal compressive concrete stress and strain.

$$\varepsilon_{cc} = \varepsilon_{co}\left(1 + 5\left(\frac{f'_{cc}}{f'_{co}} - 1\right)\right) \qquad (2\text{-}6)$$

f'_{co} and ε_{co}: unconfined concrete strength and strain (generally $\varepsilon_{co} = 0.002$)

$$r = \frac{E_c}{E_c - E_{sec}} \qquad (2\text{-}7)$$

$$E_c = 5000\sqrt{f'_{co}} \qquad (2\text{-}8)$$

$$E_{sec} = \frac{f'_{cc}}{\varepsilon_{cc}} \qquad (2\text{-}9)$$

In order to determine compressive strength of confined concrete, it is necessary to study the circular and rectangular sections separately. For rectangular sections (which is the issue here) the effective lateral confining stresses in x and y directions are:

$$f'_{lx} = k_e \rho_x f_{yh} \quad , \quad f'_{ly} = k_e \rho_y f_{yh} \qquad (2\text{-}10)$$

where;

$$\rho_x = \frac{A_{sx}}{s b_c} \quad , \quad \rho_y = \frac{A_{sy}}{s d_c} \qquad (2\text{-}11)$$

A_{sx} and A_{sy}: total area of transverse reinforcement in the x and y directions,

b_c and d_c: core dimensions to centerline of perimeter hoop in the x and y directions,

s: center to center distance between hoops.

The confinement effectiveness coefficient for rectangular hoops:

$$k_e = \frac{\left(1 - \sum_{i=1}^{n} \frac{(w'_i)^2}{6 b_c d_c}\right)\left(1 - \frac{s'}{2b_c}\right)\left(1 - \frac{s'}{2d_c}\right)}{(1 - \rho_{cc})} \qquad (2\text{-}12)$$

where;

ρ_{cc}: ratio of longitudinal reinforcement area to core section area,

s': clear distance between hoops,

w'_i: i^{th} clear distance between longitudinal adjacent bars.

According to Mander, 1988, determination of confined strength (f'_{cc}) in terms of two different lateral confining stresses is presented in figure below:

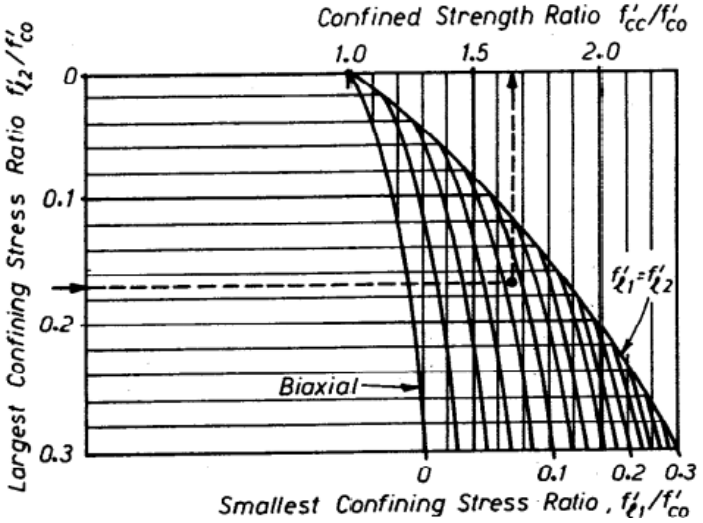

Figure 2-10: Confined Strength Determination from Lateral Confining Stresses for Rectangular Sections (Mander et al., 1988)

For unconfined concrete lateral confining pressure would be considered zero and whenever $\varepsilon_c > 2\varepsilon_{co}$, the graph was assumed to be a straight line which reaches zero at the spalling strain, $\varepsilon_{sp.}$

Tensile force of the concrete was neglected when exceeding the tensile strength (Crack point).

2.3.2 Reinforcing Steel Properties

The model proposed by King et al. (1986) was used for the stress-strain relation for the reinforcing steel.

$$f_s = E_s \varepsilon_s \qquad \varepsilon_s \leq \varepsilon_y \qquad (2\text{-}13)$$

$$f_s = f_y \qquad \varepsilon_y < \varepsilon_s < \varepsilon_{sh} \qquad (2\text{-}14)$$

$$f_s = f_y\left(\frac{m(\varepsilon_s - \varepsilon_{sh}) + 2}{60(\varepsilon_s - \varepsilon_{sh}) + 2} + \frac{(\varepsilon_s - \varepsilon_{sh})(60 - m)}{2(30r + 1)^2}\right) \qquad \varepsilon_y < \varepsilon_s < \varepsilon_{sh} \qquad (2\text{-}15)$$

where;

$$m = \frac{\left(f_{su}/f_y\right)(30r + 1)^2 - 60r - 1}{15r^2} \quad , \quad r = \varepsilon_{su} - \varepsilon_{sh} \qquad (2\text{-}16)$$

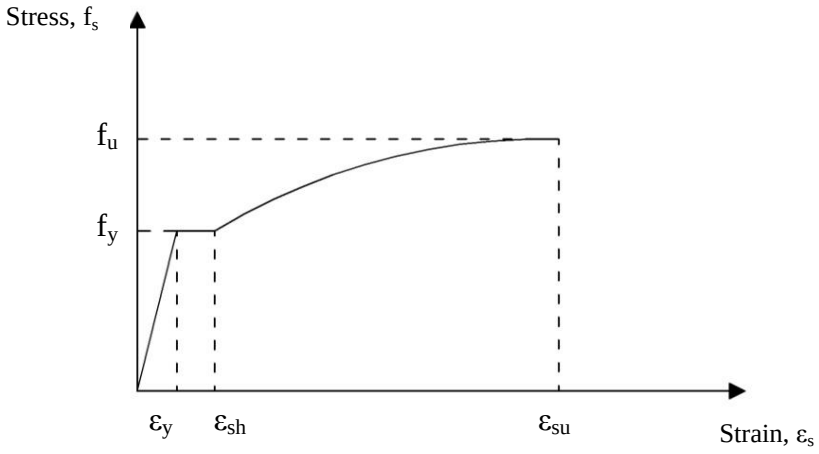

Figure 2-11: Reinforcing Steel Stress-Strain Characteristics

2.4 Member Response

2.4.1 Flexural Deformation

After performing moment-curvature analysis, it was hence possible to build the force-displacement response. Here, the procedure recommended by Priestley et al., 2007, was followed. In order to get better predictions that would be compatible with the experimental results, instead of integration from the curvature distribution along the member height, it is recommended to use a simplified solution based on the concept of the "plastic hinge". Plastic hinge length, L_p, is described as the length over which maximum strain and curvature is considered to be constant.

The plastic hinge length, proposed by Priestley, 2007, is:

$$L_p = kL_c + L_{sp} \geq 2L_{sp} \quad (2\text{-}17)$$

where;

$$k = 0.2\left(\frac{f_u}{f_y} - 1\right) \leq 0.08 \quad (2\text{-}18)$$

L_{sp}: is the strain penetration length calculated from:

$$L_{sp} = 0.022 f_{ye} d_{bl} \quad (2\text{-}19)$$

L_c: the length from the critical section from the point of contraflexure (Here, L_c=H)

Flexural deformations before cracking, after cracking and before first yield, and beyond yielding are calculated as:

Cracking: $$\Delta_{cr} = \frac{\phi_{cr} H^2}{3} \quad , \quad \mathrm{F}_{cr} = \frac{M_{cr}}{H} \quad (2\text{-}20)$$

First Yield: $$\Delta'_y = \frac{\phi'_y \left(H + L_{sp}\right)^2}{3} \quad , \quad \mathrm{F}_y = \frac{M'_y}{H} \quad (2\text{-}21)$$

After Yield: $$\Delta = \Delta'_y \frac{M}{M_y} + \left(\phi - \phi'_y \frac{M}{M_y}\right) L_p \left(L + L_{sp} - 0.5L_p\right) \quad ,$$

$$F = \frac{M}{H} \quad (2\text{-}22)$$

2.4.2 Shear Deformation

Shear deformation of the member was calculated considering 3 phase; before shear cracking, after shear cracking and before nominal moment, beyond yield.

Before the formation of shear cracks, reduction in shear stiffness is in proportion to the reduction in flexural stiffness. Hence, the shear stiffness before shear cracks start is calculated as:

$$k_{s.eff} = k_{s.gross}\frac{EI_{eff}}{EI_{gross}} \quad (2\text{-}23)$$

where;

$k_{s,gross}$: is shear stiffness of uncracked section calculated as:

$$k_{s.gross} = \frac{GA_s}{L} \quad (2\text{-}24)$$

G: is the shear modulus,

$$G = 0.43E_c \quad (2\text{-}25)$$

A_s: is the shear area for rectangular sections,

$$A_s = \frac{5}{6}A_{gross} \quad (2\text{-}26)$$

I_{eff}: is the effective moment of inertia,

$$I_{eff} = \frac{M'_y}{E_c\phi'_y} \quad (2\text{-}27)$$

Shear cracks appear after the applied shear force reaches the shear strength of concrete, V_c.

$$V_c = 0.29\sqrt{f'_c}\left(0.8A_{gross}\right) \quad (2\text{-}28)$$

The deformation in this phase is then calculated as:

$$\Delta_s = \frac{V}{k_{s.eff}} \quad , \quad V < V_c \quad (2\text{-}29)$$

After shear crack and before the nominal moment is attained, shear stiffness is calculated based on considering the shear flexibility of an equivalent strut-and-tie model. The unitary shear stiffness of this phase for rectangular sections is computed as:

$$k_{s.cr} = \frac{0.25\rho_a}{0.25 + 10\rho_a} E_s B d \qquad (2\text{-}30)$$

The deformation in this phase is then calculated as:

$$\Delta_s = \Delta_{s1} + \frac{V - V_c}{k_{s.cr}} \quad , \qquad V_c \le V \le V_N \qquad (2\text{-}31)$$

where Δ_{s1} is the displacement at onset of diagonal cracking:

$$\Delta_{s1} = \frac{V}{k_{s.eff}} \qquad (2\text{-}32)$$

After the member has attained its nominal flexural strength, it is recommended that the shear deformation be increased in proportion to the flexural deformation. That is:

$$\Delta_s = \Delta_f \frac{\Delta_{s.N}}{\Delta_{f.N}} \quad , \qquad M \ge M_N \qquad (2\text{-}33)$$

Finally total displacement of the member is:

$$\Delta = \Delta_f + \Delta_s \qquad (2\text{-}34)$$

2.5 Results

Considering the procedure described earlier, and the material and sectional properties of the specimens (which will be seen in following sections), sectional analysis was carried out and member deformation was derived employing lumped plasticity theory. In order to state the mode of failure of the specimens, the shear capacity of each wall was computed according to ACI318 (the related expressions are provided in Sec.3.2). Additionally, the capacity of specimens were determined considering the moment-shear interaction effects employing Modified Compression Field Theory (MCFT).

2.5.1 Specimen 1 and 2- Rectangular Section

Figure 2-12 shows the cross section of specimen 1.

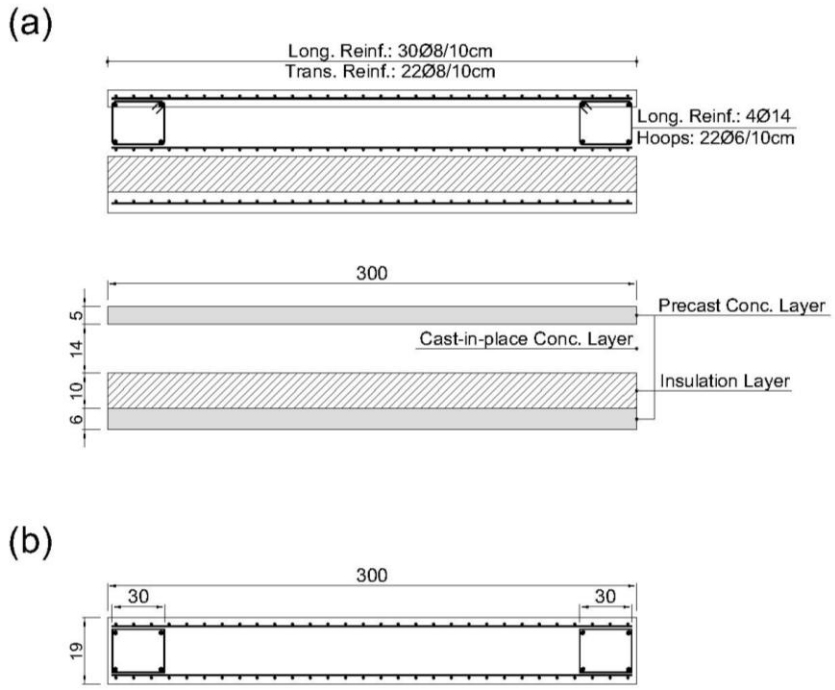

Figure 2-12: Details of the Specimen 1 & 2; (a) real cross section, (b) cross section used for analysis

Summary of the material and section properties of specimen 1 is shown in tables below.

Table 2-3: Reinforcement Steel Properties for Specimen 1 & 2

Parameters for Reinforcement			
Modulus of Elasticity	E_s	(MPa)	200000
Yield Strength-ϕ8	f_y	(MPa)	380
Ultimate Strength-ϕ8	f_u	(MPa)	540
Yield Strain-ϕ8	ε_y	-	0.0019
Yield Strength-ϕ14	f_y	(MPa)	325
Ultimate Strength-ϕ14	f_u	(MPa)	455
Yield Strain-ϕ14	ε_y	-	0.001625
Strain-Hardening Strain	ε_{sh}	-	0.008
Ultimate Strain	ε_{su}	-	0.12

Table 2-4: Concrete Properties for Specimen 1 & 2

Parameters for Concrete			
Modulus of Elasticity	E_c	(MPa)	28722
Shell Concrete Compression Strength	f'_{co}	(MPa)	45
Core Concrete Compression Strength	f'_{co}	(MPa)	28
Confined Concrete Strength	f_c	(MPa)	28.84
Spalling Strain	ε_{sp}	-	0.005
Ultimate Concrete Strain	ε_{cu}	-	0.0186

For these specimens, first yield and nominal capacity occur when the extreme tension reinforcement reaches its yield strain and the strain of 0.015, respectively. Ultimate condition is assumed to be at the onset of $\varepsilon_s=0.6\varepsilon_{su}$. Utilizing these points, the bilinear idealization is derived and the summary can be seen in Table 2-5. Comparison of the results is provided in Figure 2-14 to Figure 2-15.

Table 2-5: Bilinear Approximation Data Resulted from Hand Calculations for Specimen 1 & 2

Bilinear Idealization				
Point	**Section Response**		**Member Response**	
	Φ (1/km)	M (kN.m)	Δ (mm)	F (kN)
First Yielding (ϕ'_y, M_y)	0.7923	1484.66	3.3986	606
Nominal Yielding (ϕ_y, M_n)	1.2093	2266.08	5.1874	924.9
Ultimate Capacity (ϕ_u, M_u)	27.236	2719.69	33.7404	1110.08

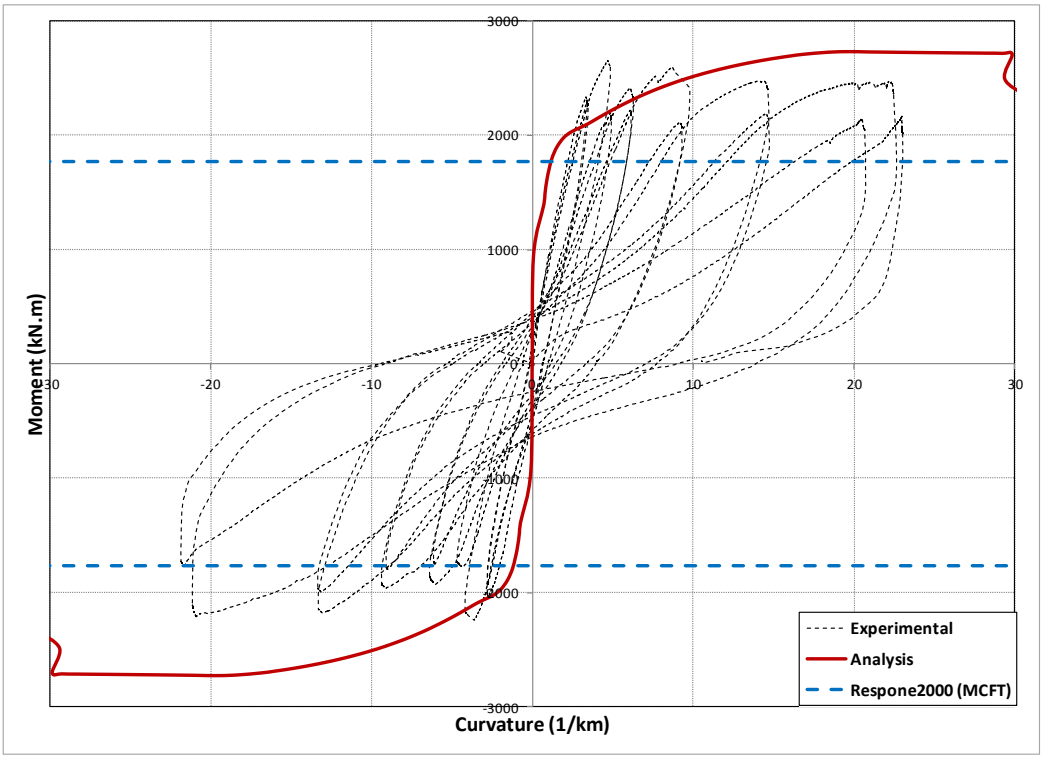

Figure 2-13: Comparison of the Moment-Curvature of Specimen 1 with Analytical Model

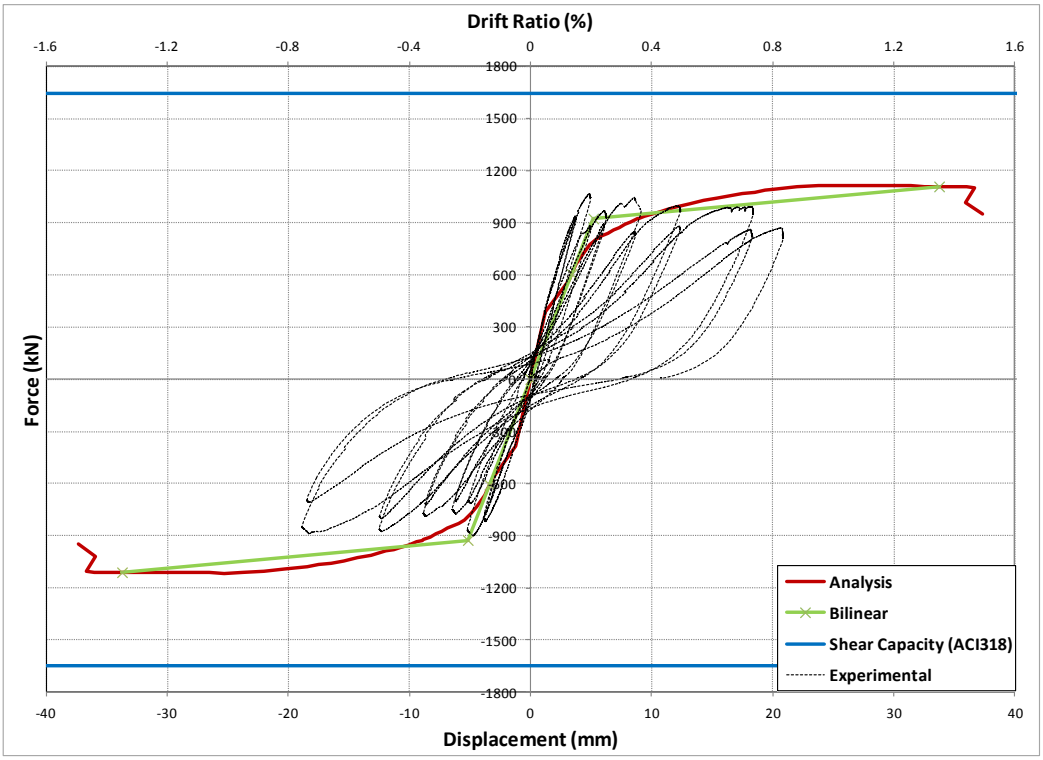

Figure 2-14: Comparison of the Response of Specimen 1 with Analytical Model

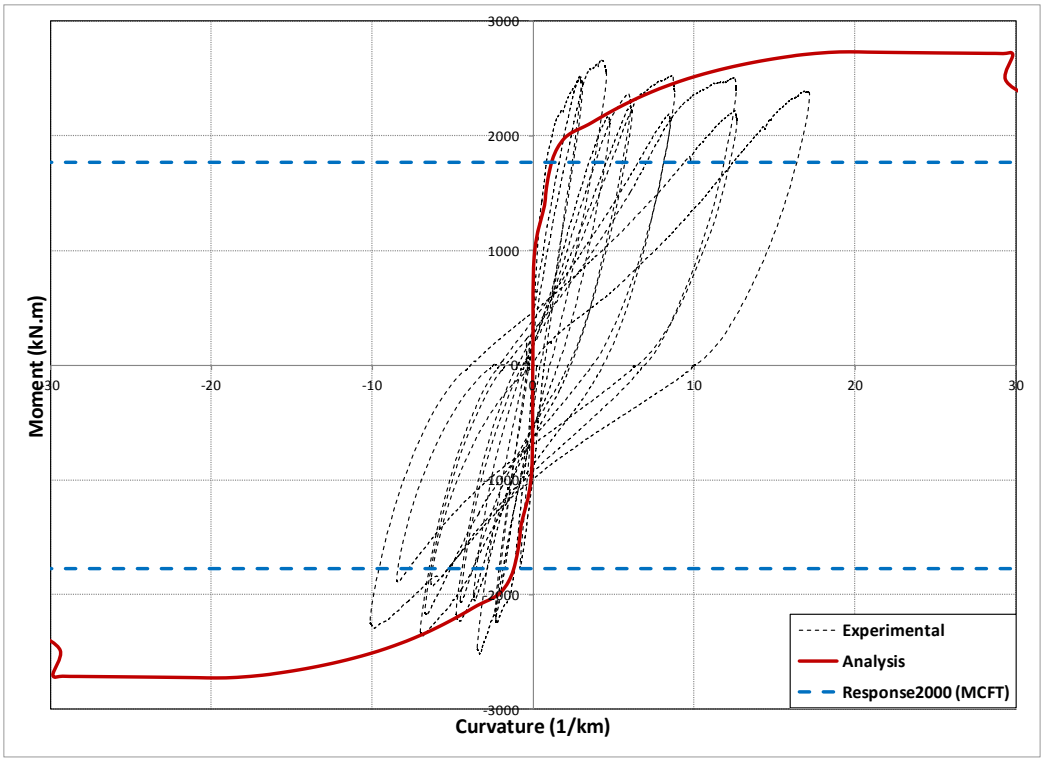

Figure 2-15: Comparison of the Moment-Curvature of Specimen 2 with Analytical Model

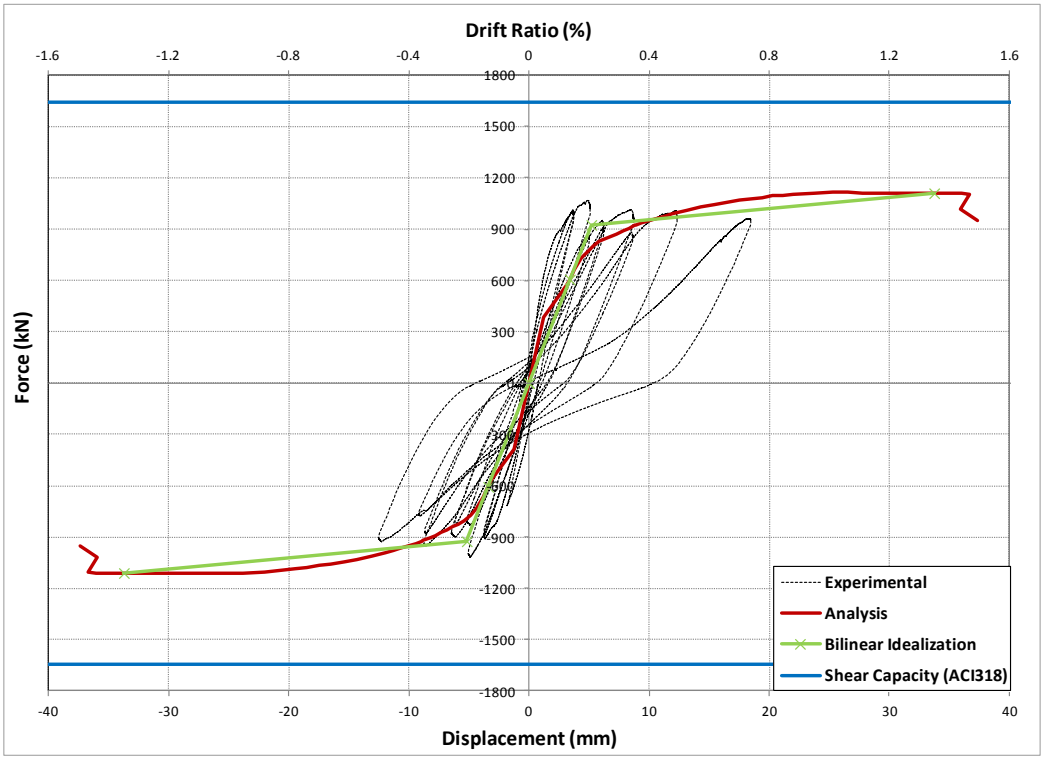

Figure 2-16: Comparison of the Response of Specimen 2 with Analytical Model

2.5.2 Specimen 3- U-Shaped Section

Figure below shows the detailed cross section of specimen 3.

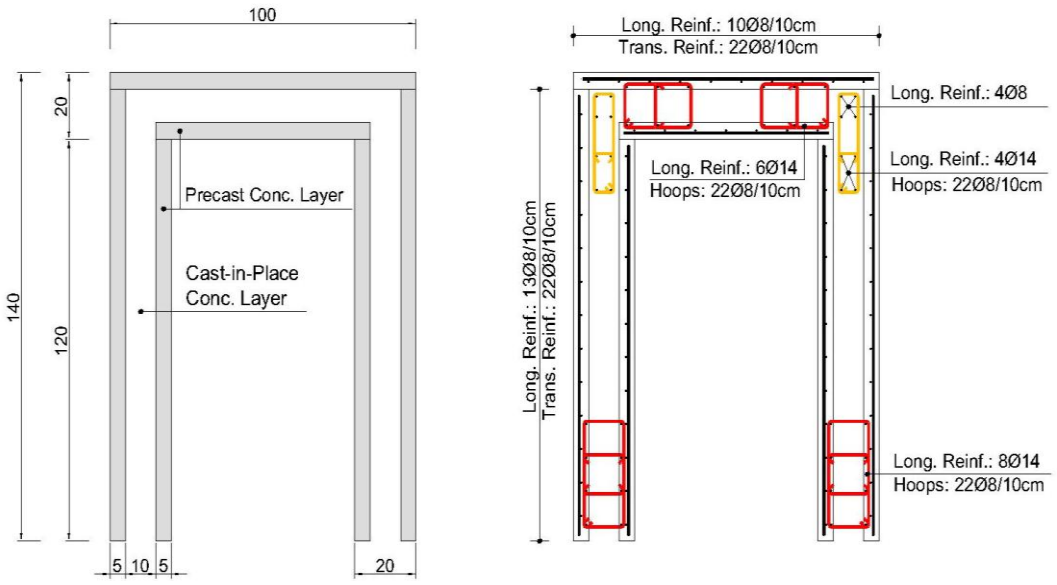

Figure 2-17: Details of the Cross Section of Specimen 3

Summary of the material and sectional properties of Specimen 3 is showed in Table 2-6.

Table 2-6: Reinforcement Steel Properties for Specimen 3

Parameters for Reinforcement			
Modulus of Elasticity	E_s	(MPa)	200000
Yield Strength-ϕ8	f_y	(MPa)	380
Ultimate Strength-ϕ8	f_u	(MPa)	540
Yield Strain-ϕ8	ε_y	-	0.0019
Yield Strength-ϕ14	f_y	(MPa)	325
Ultimate Strength-ϕ14	f_u	(MPa)	455
Yield Strain-ϕ14	ε_y	-	0.001625
Strain-Hardening Strain	ε_{sh}	-	0.008
Ultimate Strain	ε_{su}	-	0.12

Table 2-7: Concrete Properties for Specimen 3

Parameters for Concrete			
Modulus of Elasticity	E_c	(MPa)	28722
Shell Concrete Compression Strength	f'_{co}	(MPa)	45
Core Concrete Compression Strength	f'_{co}	(MPa)	25
Confined Concrete Strength	f_c	(MPa)	31.25
Spalling Strain	ε_{sp}	-	0.005
Ultimate Concrete Strain	ε_y	-	0.0328

For this specimen, because of the unsymmetrical shape, the response in two directions is different. In these calculations, the direction of positive and negative moment is according to experimental setup and is shown in Figure 2-18. In both direction, first yield and nominal capacity occur when the extreme tension reinforcement reaches its yield strain and the strain of 0.015, respectively. Ultimate condition is assumed to be at the onset of $\varepsilon_s=0.6\varepsilon_{su}$. Utilizing these points, the bilinear idealization is derived and the summary can be seen in Table 2-8.

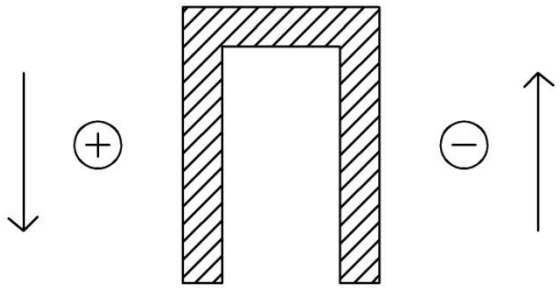

Figure 2-18: Direction of the Applied Load in Specimen 3

Table 2-8: Bilinear Approximation Data Resulted from Hand Calculations for Specimen 3

Bilinear Idealization				
	Section Response		**Member Response**	
Point	Φ (1/km)	M (kN.m)	Δ (mm)	F (kN)
First Yielding (ϕ'_y, M_y)	1.861	1493.74	5.060	609.7
	-1.684	-1275.99	-4.58	-520.81
Nominal Yielding (ϕ_y, M_n)	2.552	2048.385	6.94	836.07
	-2.311	-1751.343	-6.285	-714.83
Ultimate Capacity (ϕ_u, M_u)	65.49	2270.045	59.58	926.55
	-57.633	-2153.046	-52.241	-878.79

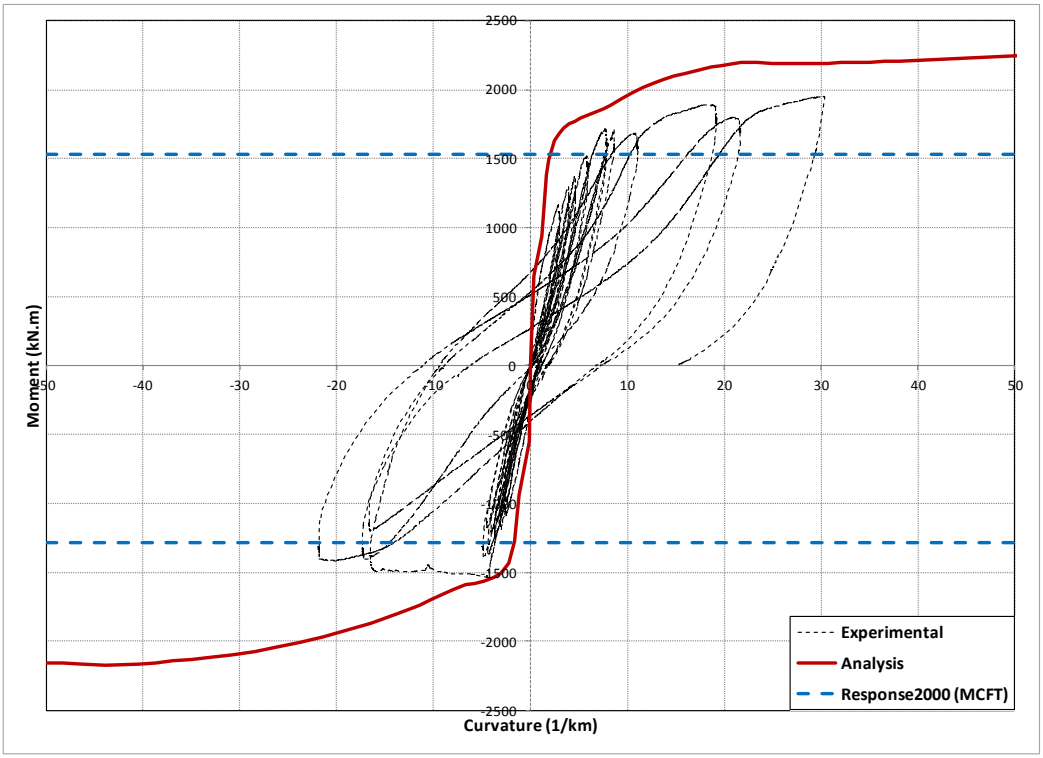

Figure 2-19: Comparison of the Moment-Curvature of Specimen 3 with Analytical Model

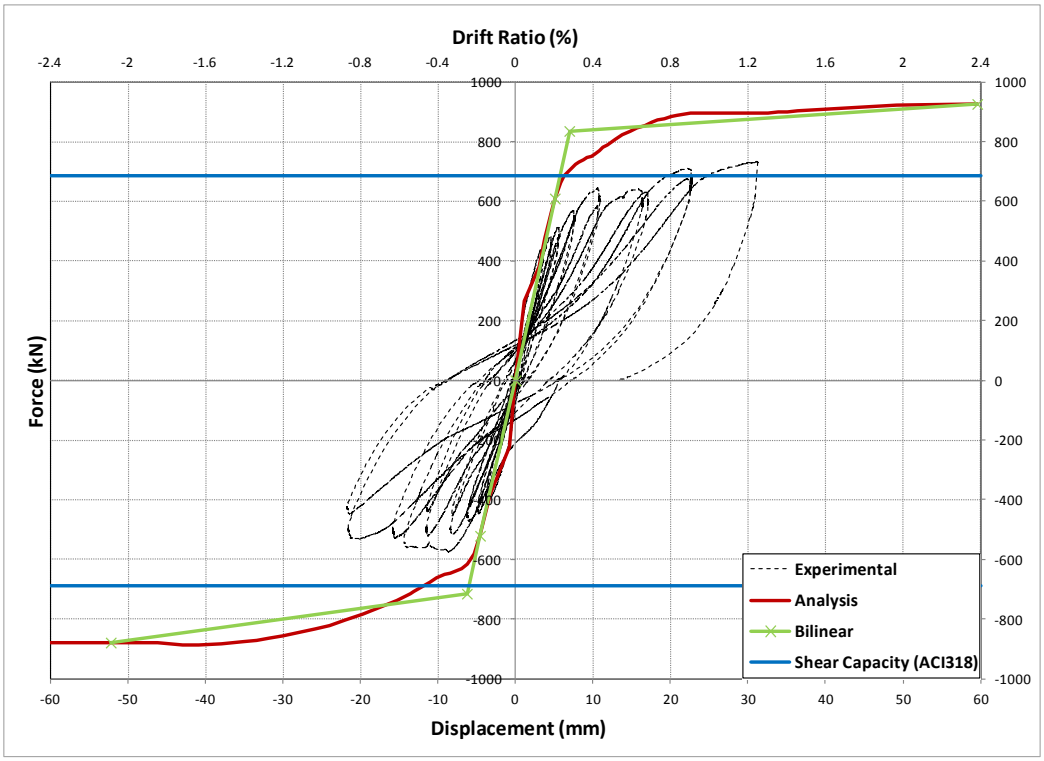

Figure 2-20: Comparison of the Response of Specimen 3 with Analytical Model

2.5.3 Specimen 4- T-Shaped Section

Figure 2-21 shows the detailed cross section of specimen 4. Summary of the material and section properties of Wall-4 are presented in Table 2-9 and Table 2-10.

For this specimen, because of the unsymmetrical shape, the response in two directions is different. In these calculations, the direction of loading is according to Figure 2-22. In both direction, first yield and nominal capacity occur when the extreme tension reinforcement reaches its yield strain and the strain of 0.015, respectively. In positive direction, ultimate condition is assumed to be at the onset of concrete spalling, while in the other direction ultimate condition is attained when the extreme tension bar reaches $0.6\varepsilon_{su}$. Utilizing these points, the bilinear idealization is derived and the summary can be seen in Table 2-11.

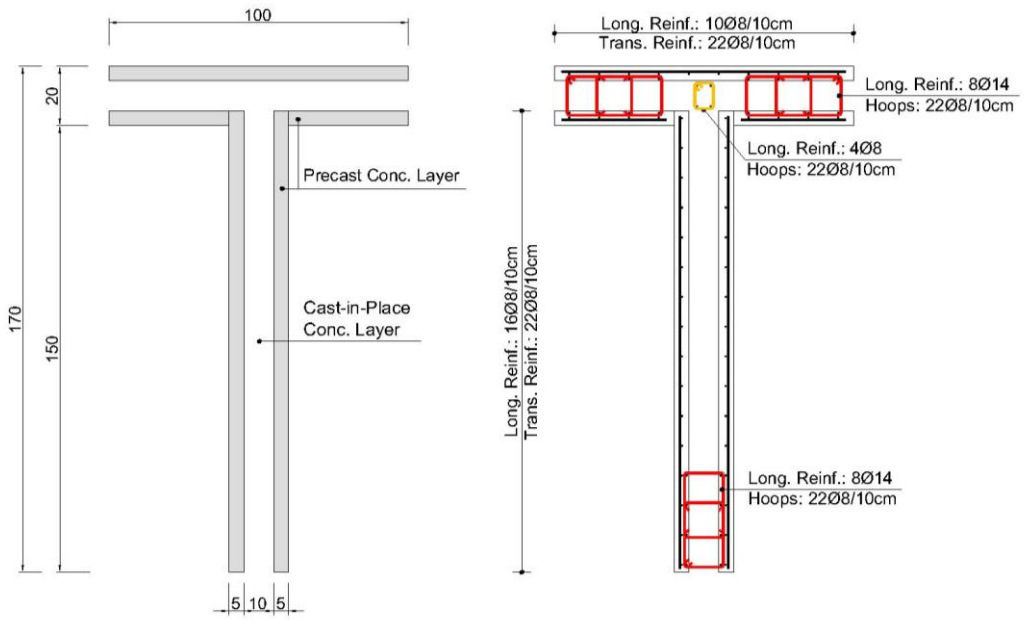

Figure 2-21: Details of the Cross Section of Specimen 4

Table 2-9: Reinforcement Steel Properties for Specimen 4

Parameters for Reinforcement			
Modulus of Elasticity	E_s	(MPa)	200000
Yield Strength-ϕ8	f_y	(MPa)	380
Ultimate Strength-ϕ8	f_u	(MPa)	540
Yield Strain-ϕ8	ε_y	-	0.0019
Yield Strength-ϕ14	f_y	(MPa)	325
Ultimate Strength-ϕ14	f_u	(MPa)	455
Yield Strain-ϕ14	ε_y	-	0.001625
Strain-Hardening Strain	ε_{sh}	-	0.008
Ultimate Strain	ε_{su}	-	0.12

Table 2-10: Concrete Properties for Specimen 4

Parameters for Concrete			
Modulus of Elasticity	E_c	(MPa)	28722
Shell Concrete Compression Strength	f'_{co}	(MPa)	45
Core Concrete Compression Strength	f'_{co}	(MPa)	25
Confined Concrete Strength	f_c	(MPa)	32.5
Spalling Strain	ε_{sp}	-	0.005
Ultimate Concrete Strain	ε_y	-	0.0317

Table 2-11: Bilinear Approximation Data Resulted from Hand Calculations for Specimen 4

Bilinear Idealization				
	Section Response		**Member Response**	
Point	Φ (1/km)	M (kN.m)	Δ (mm)	F (kN)
First Yielding (ϕ'_y, M_y)	1.6272	1837.74	7.37	750
	-1.3	-848.351	-4.01	-339.34
Nominal Yielding (ϕ_y, M_n)	2.0640	2272.7	9.12	927.6
	-1.686	-1100.446	-5.202	-440.18
Ultimate Capacity (ϕ_u, M_u)	27.67	1955.92	37.72	798.3
	-48.192	-1465.838	-46.434	-586.33

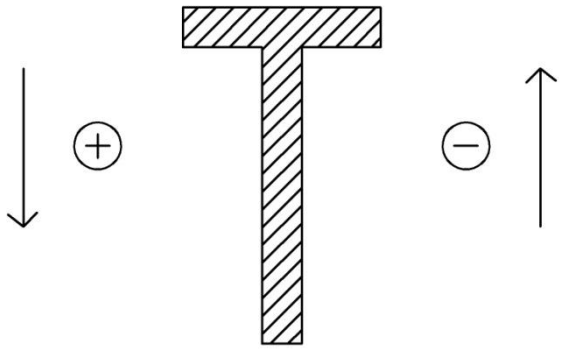

Figure 2-22: Direction of the Applied Load in Specimen 4

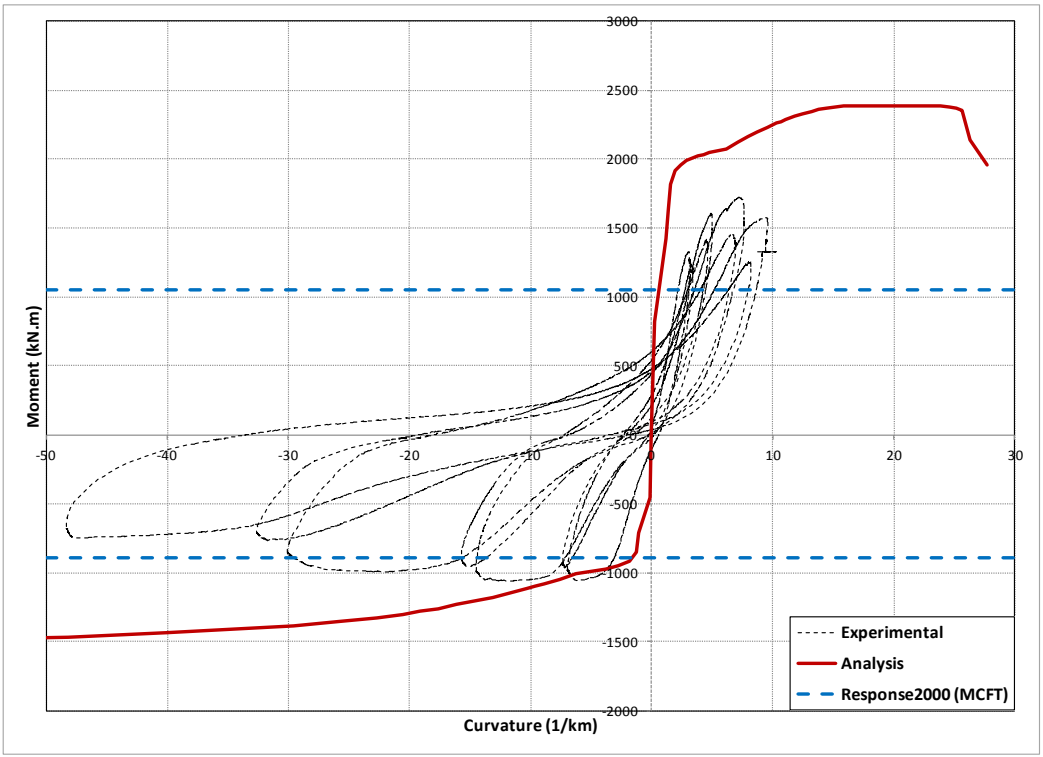

Figure 2-23: Comparison of the Moment-Curvature of Specimen 4 with Analytical Model

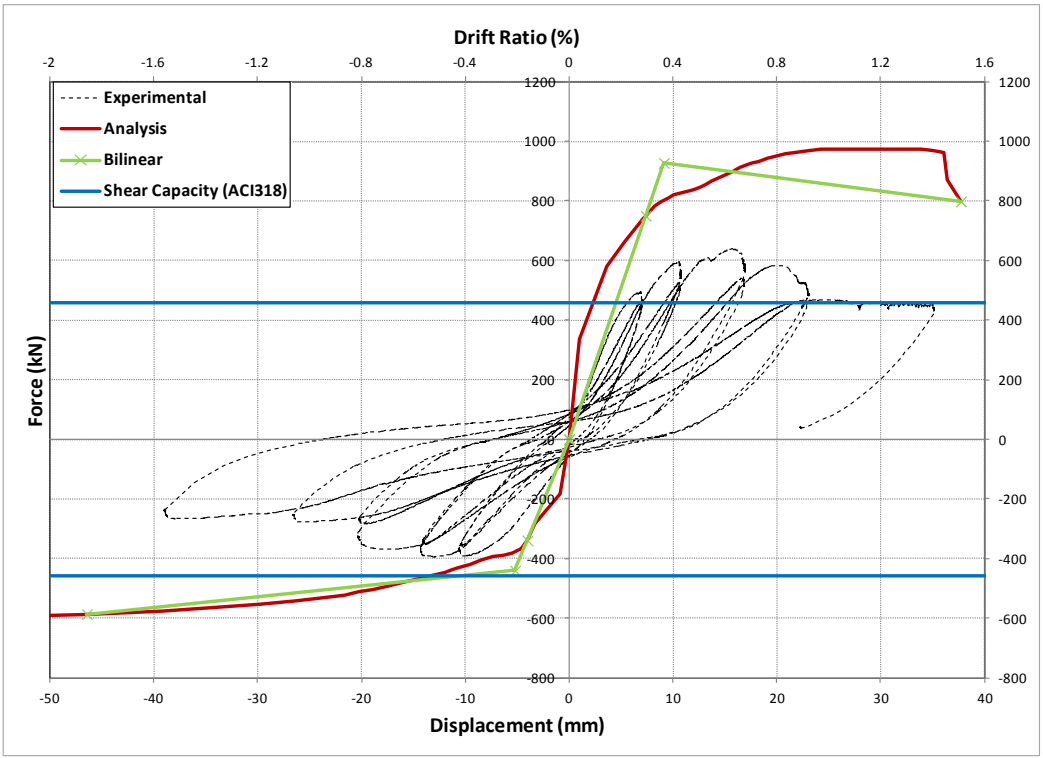

Figure 2-24: Comparison of the Response of Specimen 4 with Analytical Model

2.5.4 Discussion of the Results

According to the experimental results, limited inelastic shear deformations were monitored during the test of specimens 1 and 2, whereas significant shear strains were determined during the tests of specimens 3 and 4. These results are evaluated using the capacity calculations presented in Figure 2-13 to Figure 2-24. The results from section analysis of models provide slight overestimation of the capacity of the specimens 1 and 2. It can be observed that the estimated shear capacity for these two specimens were larger than the lateral load capacity determined based on flexural yielding. This situation indicates the estimated failure mode to be flexure dominated.

The moment capacity of concrete members is affected by the presence of shear in the member (Arlekar, 2004). Generally, the presence of shear has an effect of reducing the moment capacity of the member. While using capacity design concepts one should consider the moment-shear interaction effects for safe design and assessment. According to the observations from experimental tests, the inclined crack width was above 0.4 mm at about 0.75% drift ratio (Figure 2-25) for specimen 1. For such crack widths, shear yielding in reinforcement is expected. At this drift level, significant flexural yielding was also observed based on the strain measurements within the plastic hinge zone as shown previously. These observations support the consideration of flexure-shear interaction. Consequently, M-V interaction diagram for each specimen was computed employing the Modified Compression Field Theory (MCFT) by using Response-2000 (Figure 2-26~28). The moment capacities computed by considering shear flexure interaction were found from the interaction diagrams shown in Figure 2-13 and Figure 2-15 for specimens 1 and 2. It can be observed that, the presence of shear reduces the moment capacity of the test specimens by about 25%. Upon considering the shear effects on moment capacities, the estimations turned out to be on the safe side compared to the experimental results.

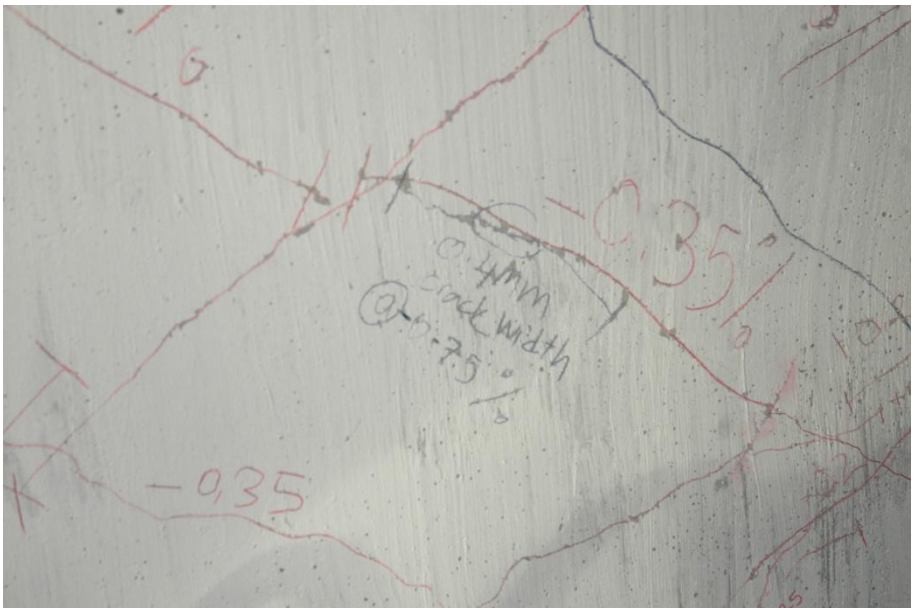

Figure 2-25: Crack Width in Specimen 1

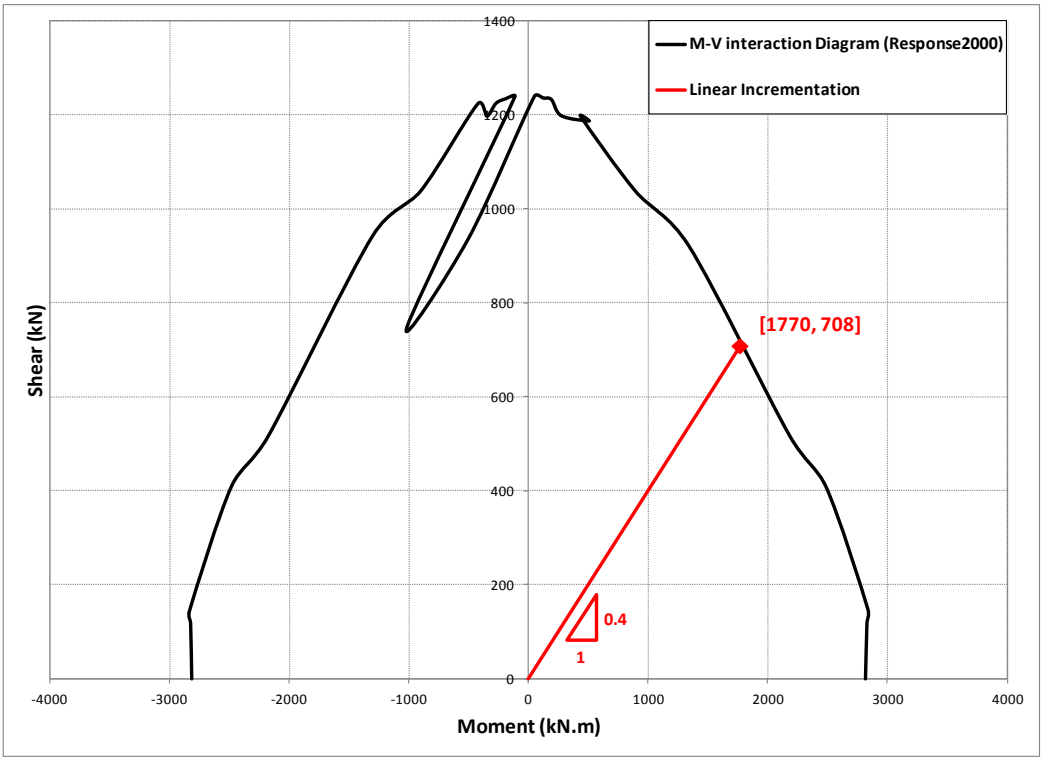

Figure 2-26: Moment-Shear Interaction Diagram by Response 2000 - Specimens 1 and 2

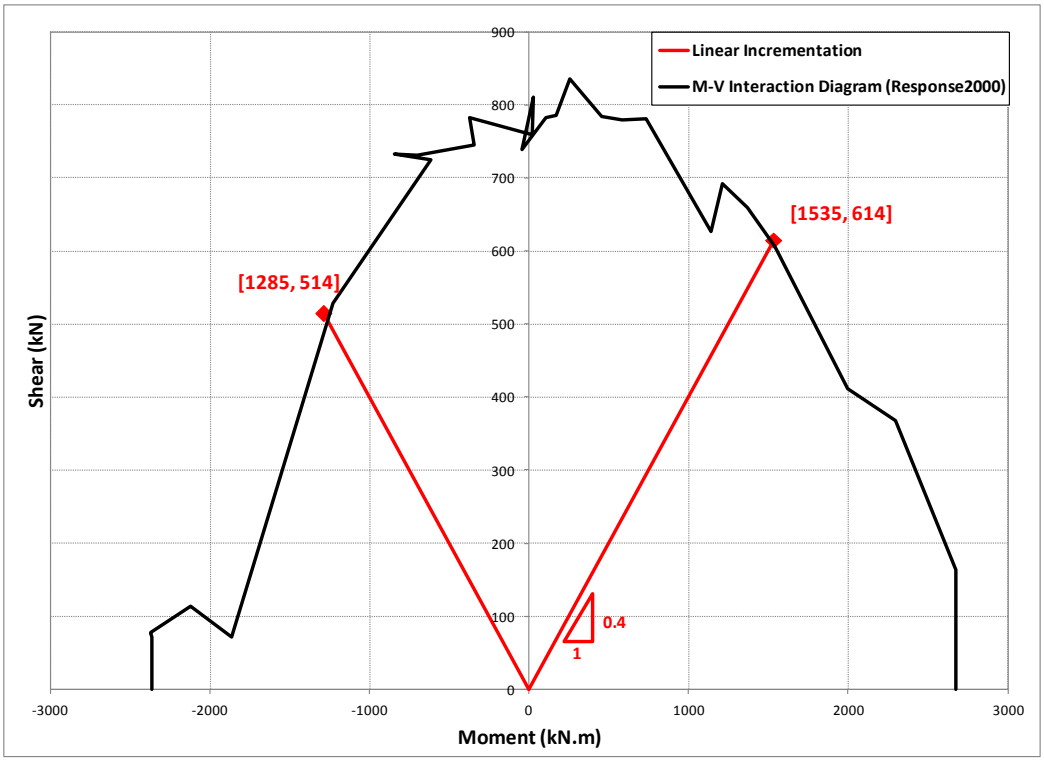

Figure 2-27: Moment-Shear Interaction Diagram by Response 2000 - Specimens 3

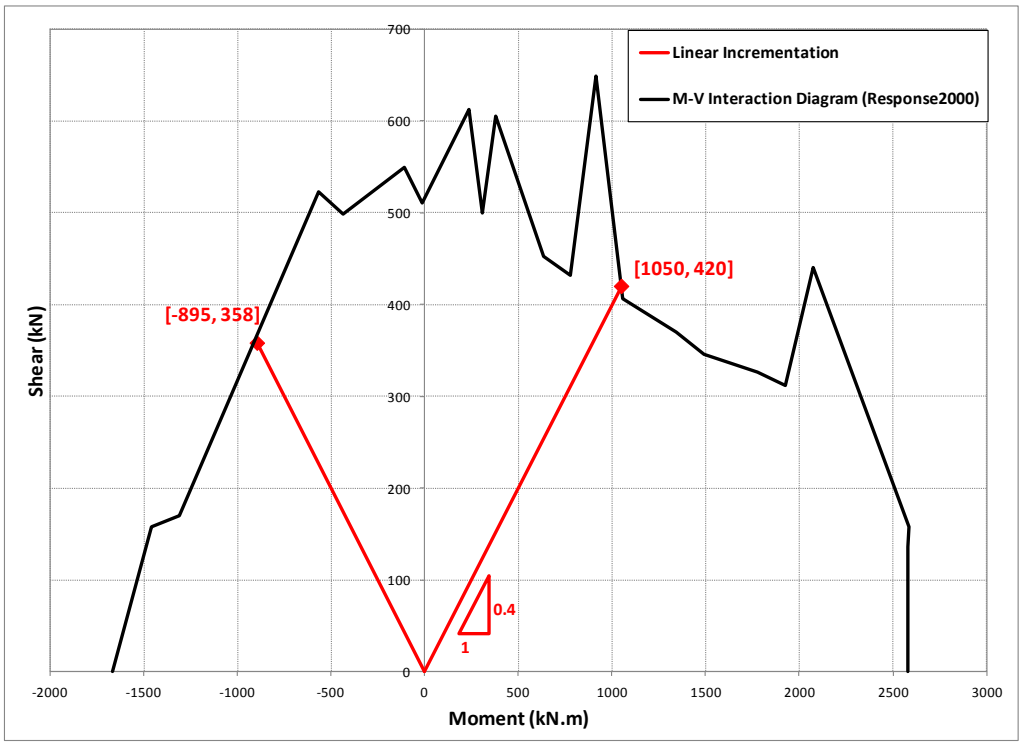

Figure 2-28: Moment-Shear Interaction Diagram by Response 2000 - Specimens 4

For specimens 3 and 4, the results demonstrate that the behavior is shear behavior dominated owing to the smaller shear capacity compared to the lateral load based on flexural yielding. The maximum bending capacity is preceded by the shear capacity of the specimens 3 and 4, indicating a brittle mode of failure. Despite the shear critical nature of specimens 3 and 4, these walls behaved in a ductile manner during the tests and the failure of these walls occurred in a flexure-shear mode. Especially, comparing the response of specimens 3 and 4, it can be seen that specimen 3 behaved in a more ductile manner in the positive direction of loading, which can be justified by presence of two webs for the U-shaped double wall resulting in high capability in sustaining compressive strains.

The moment capacities computed by considering shear flexure interaction were found from the interaction diagrams shown in Figure 2-19 and Figure 2-23 for specimens 3 and 4, respectively. It can be observed that, the presence of shear reduces the moment capacity of the test specimens by about 10% and 25% in positive and negative directions, respectively. Upon considering the shear effects on moment capacities, the estimations turned out to be closer to the experimental results still being on the safe side.

Determining the ultimate capacity of the Walls by taking it as the smaller of the moment capacity derived from section analysis and shear capacity derived using ACI recommendations, together with the capacity including the moment-shear interaction effects, the lateral strength of each specimen was estimated. Table 2-12 presents the comparison of estimated to experimental lateral strength. It should be noted that the nominal flexural capacity is taken as the point of intersection shown in the bilinear approximations (Sec. 2.2.1). Based on these limited test results, considering the average values of V/V_{test}, in all flexure-controlled and shear-controlled specimens, wall strengths can be estimated with reasonable accuracy. Comparing the capacity by considering moment-shear interaction, the estimated capacities lie on the safe side for all test specimens. However, further improvements are needed to uncover the mismatch between capacities from tests and obtained using MCFT.

Table 2-12: Comparison of the Experimental and Estimated Capacities

Specimen	V_{test}	V_S	V_M	V	$V_{(MCFT)}$	V/V_{test}	$V_{(MCFT)}/V_{test}$
1	1069	1645.2	925	925	678	0.87	0.63
	-903	-1645.2	-925		-678	-1.02	-0.75
2	1072	1645.2	925	925	678	0.86	0.63
	-1017	-1645.2	-925		-678	-0.91	-0.67
3	732	686.8	836	686.8	614	0.938	0.84
	-575	-686.8	-715		-514	-1.19	-0.89
4	639	459.2	927.6	459.2	420	0.72	0.66
	-393	-459.2	-440.2		-358	-1.17	-0.91
The values are in kN.					**AVE.**:	1.05	0.85

In the table above;

V_{test}: is the maximum capacity of the wall according to experimental results,

V_S: is the estimated shear capacity of the wall,

V_M: is the estimated flexural capacity of the wall,

V: is the minimum of V_S and V_M,

$V_{(MCFT)}$: is the capacity of the wall including moment-shear interaction effect.

CHAPTER 3

PERFORMANCE ASSESSMENT

3.1 Assessment Procedure According to Different Seismic Guidelines

In this section, the evaluation of three seismic assessment guidelines are provided. These guidelines are American Seismic Rehabilitation, ASCE/SEI 41-06 and ASCE/SEI 41-13, European seismic code, Eurocode 8 (2005), and Turkish Earthquake Code (2007), respectively.

In order to estimate the seismic performance of buildings, maximum permissible damage states (performance levels), considering certain levels of seismic hazard of the site, are specified. Hence, various performance levels have been characterized by different provisions based on the observed damage states of the building, which are thoroughly explained in this section.

ASCE/SEI-41 introduces three discrete “Structural Performance Levels” and two intermediate “Structural Performance Ranges”. These performance levels are:

- Immediate Occupancy (IO): as a post-earthquake damage state in which the structure remains safe to occupy retaining its design strength and stiffness.

Life-threatening damage is very low and some minor structural repair might be required.

- Life Safety (LS): as a post-earthquake damage state in which structural components are significantly damaged, but retain some margin against onset of either partial or total structural collapse. The total risk of life-threatening injuries is anticipated to be low. Due to economic reasons, the possibility of repairing the structure may not be practical.
- Collapse Prevention (CP): as a post-earthquake damage state in which structural components are severely damaged, including considerable degradation in the stiffness and the strength of the lateral-force-resisting system, retaining no margin against collapse, as well. However, it maintains supporting gravity loads. Significant risk of injury exist and it is not technically practical to repair the building.

Intermediate structural performance ranges are defined so that users are able to customize their building rehabilitation objectives. Structural performance ranges are described as:

- Damage Control Range: as the range between Life Safety and Immediate Occupancy Levels. In order to preserve valuable equipments and historic features, design for this range may be desirable to reduce repair time and operational interruption.
- Limited Safety Range: as the range between Life Safety and Collapse Prevention Levels

"Non-structural Performance Levels" are also determined in ASCE/SEI-41, nevertheless, the non-structural performance of the buildings are not taken into account here.

Eurocode 8 also defines three damage limit states (LS) as Damage Limitation (DL), Significant Damage (SD), and Near Collapse (NC). These LSs are characterized as:

- Damage Limitation (DL): as a damage state in which the structure is lightly damaged, retaining its stiffness and strength properties. Permanent drifts are imperceptible and the damage can be economically repaired.
- Significant Damage (SD): as a damage state in which the structure is extensiveley damaged protecting some residual lateral stiffness and strength, while the vertical elements are capable of supporting vertical loads. Limited permanent drifts exist and the repair of the structure may not be economic. The structure can undergo aftershocks with moderate intensity.
- Near Collapse (NC): as a damage state in which the structure severely damaged, remaining with low residual lateral strength and stiffness and most of non-structural elements collapsed. However, vertical loads can be still sustained by vertical elements. Large permanent drifts exist and the structure would not sustain another earthquake.

The damage range between DL and SD is designated as "damage control range", while the damage range between SD and NC indicates "limited safety range", entailing the moderate and severe damage states, respectively.

Due to the extensive life and property losses during severe earthquakes, and so the necessity of new treatments to seismic codes in Turkey, an additional chapter regarding regulation of the seismic performance evaluation of existing buildings, was added in to the Turkish earthquake code of 2007. Chapter 7 of TEC-2007 proposes three damage limits for ductile members, which are:

- Minimum Damage Limit (MN): is defined as the beginning of the behavior beyond elasticity,
- Safety Limit (SF): is defined as the limit beyond elasticity capable of safely ensuring the strength,
- Collapsing Limit (CL): is defined as the limit before collapsing..

The performance of brittle members shall not exceed the shear capacity.

Figure 3-1 presents the damage states of a member and related damage limits .

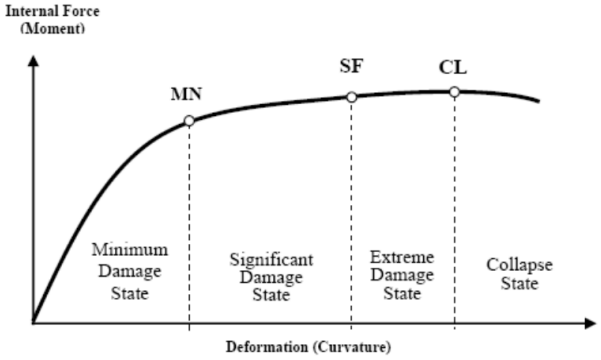

Figure 3-1: Damage States and Corresponding Damage Limits of a Ductile Member (TEC2007)

Structural component-based criteria are proposed in ASCE/SEI-41, EC8-3 and TEC-2007, by means of plastic (hinge) rotation, chord rotation and strain, respectively.

3.2 Performance Criteria of ASCE/SEI-41

In ASCE/SEI-41, component acceptance criteria for nonlinear analysis procedures are defined for columns, beams, beam-column connections and structural walls through plastic hinge rotation, for each of the structural performance levels. ASCE/SEI-41 standard does not offer any global acceptance criteria.

According to this code, concrete shear walls are planar vertical elements or combinations of interconnected planar elements that act as lateral-load-resisting components in concrete structures. Shear walls with aspect ratio (height/length) of >3, is considered to be slender which are normally controlled by flexure, while walls with aspect ratio of <1.5 is regarded as short or squat which are supposed to be shear-controlled. The behavior of walls with the aspect ratios in-between is affected by both flexure and shear.

ASCE/SEI 41 presents the modeling parameters and numerical acceptance criteria for shear walls controlled by both flexure and shear. The foresaid parameters are illustrated in Table 3-1 to Table 3-4 (considering the extent related to this study). In the tables, linear interpolation between the values is allowed.

In order to estimate the backbone response of the concrete elements for the Nonlinear Static Procedure, ASCE/SEI 41 recommends to use the "generalized load-deformation relation" shown in Figure 3-2. If the related curve is associated with flexural or tension response, the strength at $Q/Q_y = 1.0$ is defined as the yield value and the following strain-hardening is correspondent with the deformation of the member toward the expected strength. In the case that the curve is correlated with compression, the point $Q/Q_y = 1.0$ corresponds to the value at which concrete begins to spall, and the subsequent strain-hardening in well-confined sections may be related to strain-hardening of longitudinal reinforcement and confined concrete. Assuming that the force-deformation relation is indicative of shear behavior, the resistance at $Q/Q_y = 1.0$ typically represents the value at 'which the design shear strength is reached and no strain-hardening follows.

For shear walls having flexure-controlled inelastic behavior under lateral loading, the force-deformation curve with the x-axis of rotation over the plastic hinging region at the end of the member (as shown in Figure 3-3-a) shall be considered. The generalized backbone recommended by the provision is as presented in Figure 3-2-a. Following approach is permitted in ASCE/SEI 41 regarding the walls governed by flexure. At point B, corresponding to yield point, the hinge rotation is calculated with:

$$\theta_y = \left(\frac{M_y}{E_c I}\right) l_p \qquad (3\text{-}1)$$

where;

M_y: Yield moment capacity,

E_c: Concrete modulus,

I: Member moment of inertia,

l_p: Assumed plastic hinge length,

For shear walls, the value of l_p is the minimum of 0.5 times the flexural depth of the element and one story height of the shear wall.

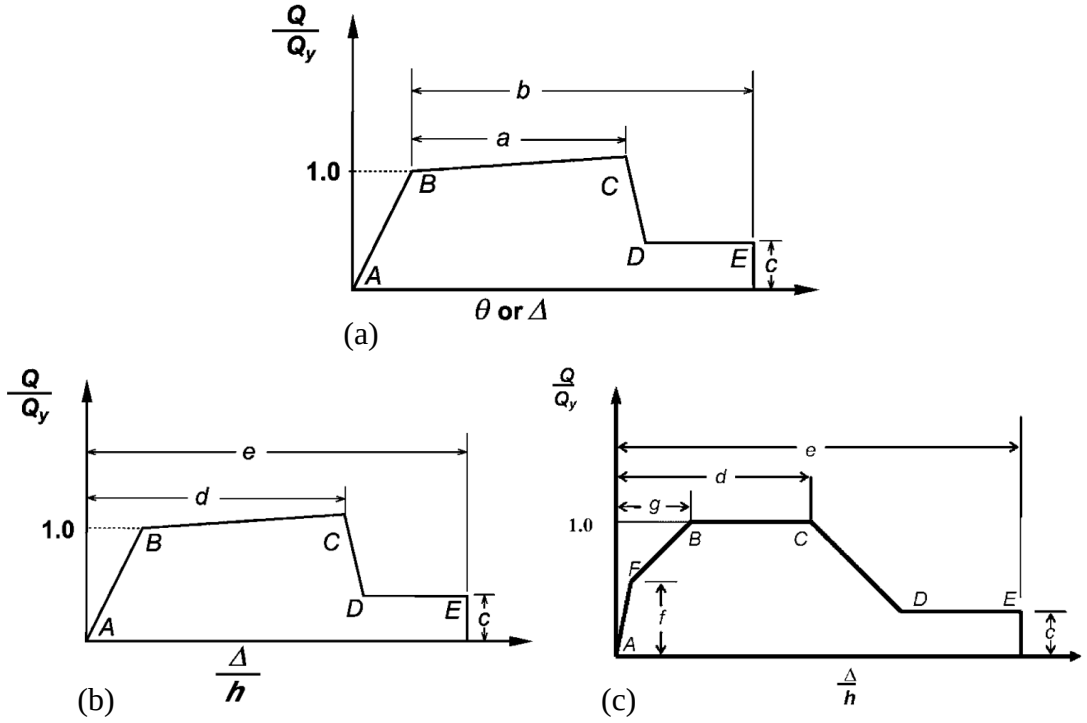

Figure 3-2: Generalized Force-Deformation Relation for Concrete Elements or Components (ASCE/SEI 41)

According to ASCE (sec. 6.7.2.3 / 41-06, sec. 10.7.2.3 / 41-13), "where determining the flexural yield strength of a shear wall, as represented by point B, only the longitudinal steel in the boundary of the wall shall be included. If the wall does not have a boundary member, then only the longitudinal steel in the outer 25% of the wall section shall be included in the calculation of the yield strength."

Point C indicates nominal flexural strength of the shear wall (M_n), which shall be calculated following the principles given in Chapter 10 of ACI 318. According to the provision, the nominal flexural strength of a member is reached when the strain in the extreme compression fiber reaches the strain limit 0.003. An equivalent rectangular compressive stress distribution (stress block) is used to replace the more exact concrete stress distribution as recommended by the code. In the this stress block, an average stress of $0.85f_c'$ is used with a rectangle of depth of $\beta_1 c$ (c as the depth of neutral axis). The values specified for β_1 are as followed:

$$\beta_1 = \begin{cases} 0.85 & f_c^{'} \leq 28\ MPa \\ \frac{0.05}{7}\left(f_c^{'} - 28\right) + 0.28 & 28 \leq f_c^{'} \leq 55 \\ 0.65 & f_c^{'} \geq 55\ MPa \end{cases} \qquad (3\text{-}2)$$

All longitudinal steel (including web reinforcement) shall be included in the calculation of nominal strength. For determining the variables a, b, and c, users are required to refer to Table 3-1 (ASCE/SEI 41-06) and Table 3-3 (ASCE/SEI 41-13).

Shear walls which inelastic response is controlled by shear, are examined considering force-deformation curve with x-axis of lateral drift ratio (as shown in Figure 3-3-b). The generalized backbone recommended by the provision is as presented Figure 3-2-b&c). Point B displays the shear capacity of the member, which shall be in accordance with ACI 318.

$$V_n = V_c + V_s \leq 0.83\sqrt{f_c^{'}}hd \qquad (3\text{-}3)$$

$$V_c = min\left\{\begin{array}{c} 0.27\lambda\sqrt{f_c^{'}}hd + \frac{N_u d}{4l_w} \\ \left[0.05\lambda\sqrt{f_c^{'}} + \frac{l_w\left(0.1\lambda\sqrt{f_c^{'}} + 0.2\frac{N_u}{l_w h}\right)}{\frac{M_u}{V_u} - \frac{l_w}{2}}\right]hd \end{array}\right. \qquad (3\text{-}4)$$

$$V_s = \frac{A_v f_y d}{s} \qquad (3\text{-}5)$$

where;

A_v: is the area of shear reinforcement within spacing ***s***

Moreover, Chapter 21 of ACI318 specifies an additional limit for shear strength of structural walls.

$$V_n = A_{cv}\left(\alpha_c \lambda \sqrt{f_c'} + \rho_t f_y\right) \qquad (3\text{-}6)$$

where;

A_{cv}: is the gross area of concrete section in the direction of shear force considered,

ρ_t: is ratio of area of transverse reinforcement to gross concrete area perpendicular to that reinforcement,

α_c: is equal to 0.25 for $h_w/l_w \leq 1.5$, 0.17 for $h_w/l_w \geq 2.0$, and varies linearly between 0.25 and 0.17 for $1.5 \leq h_w/l_w \leq 2.0$.

Values for the variables d, e, f, g and c are specified in Table 3-2 (ASCE/SEI 41-06) and Table 3-4 (ASCE/SEI 41-13) in order to find the drift ratio corresponding to points B, C, D, E, and F.

For the sharp slope between points C and D in Figure 3-2, it is recommended to assign a small slope (10 vertical to 1 horizontal) in order to avoid computational instability where used as modeling input in nonlinear analysis software.

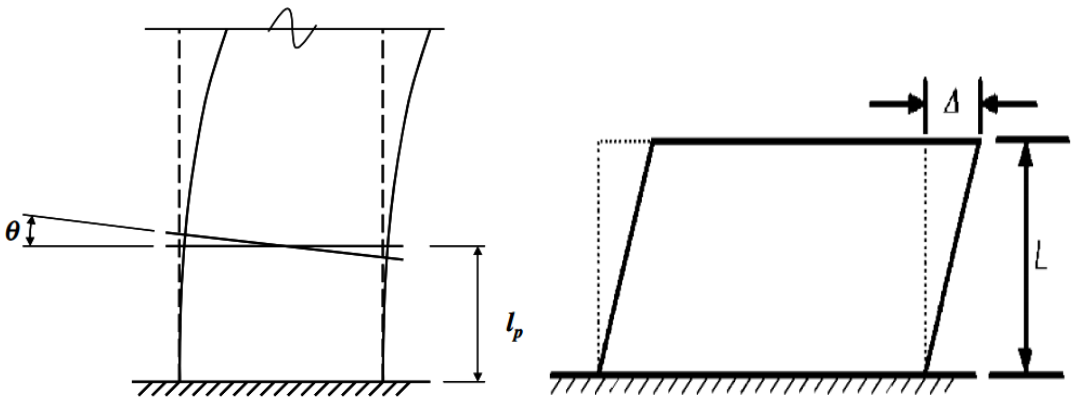

Figure 3-3: (a) Plastic Hinge Rotation in Flexure-Controlled Shear Walls, (b) Story Drift in Shear-Controlled Shear Walls (ASCE/SEI-41)

Table 3-1: Modeling Parameters and Acceptance Criteria For Shear Walls Controlled by Flexure Regarding Nonlinear Procedures (ASCE/SEI-41-06 Supplement 1, 2008)

Conditions			Plastic Hinge Rotation (radians)		Residual Strength Ratio	Acceptable Plastic Hinge Rotation[4,5] (radians)				
						Performance Level				
							Component Type			
							Primary		Secondary	
			a	b	c	IO	LS	CP	LS	CP
i. Shear walls and wall segments										
$\frac{(A_s - A'_s)f_y + P}{t_w l_w f'_c}$	$\frac{V}{t_w l_w \sqrt{f'_c}}$	Confined Boundary[1]								
≤ 0.1	≤ 4	Yes	0.015	0.020	0.75	0.005	0.010	0.015	0.015	0.020
≤ 0.1	≥ 6	Yes	0.010	0.015	0.40	0.004	0.008	0.010	0.010	0.015
≥ 0.25	≤ 4	Yes	0.009	0.012	0.60	0.003	0.006	0.009	0.009	0.012
≥ 0.25	≥ 6	Yes	0.005	0.010	0.30	0.0015	0.003	0.005	0.005	0.010
≤ 0.1	≤ 4	No	0.008	0.015	0.60	0.002	0.004	0.008	0.008	0.015
≤ 0.1	≥ 6	No	0.006	0.010	0.30	0.002	0.004	0.006	0.006	0.010
≥ 0.25	≤ 4	No	0.003	0.005	0.25	0.001	0.002	0.003	0.003	0.005
≥ 0.25	≥ 6	No	0.002	0.004	0.20	0.001	0.001	0.002	0.002	0.004

Table 3-2: Modeling Parameters and Acceptance Criteria For Shear Walls Controlled by Shear Regarding Nonlinear Procedures (ASCE/SEI-41-06 Supplement 1, 2008)

Conditions	Total Drift Ratio (%), or Chord Rotation (radians)[1]			Strength Ratio		Acceptable Total Drift (%) or Chord[5] Rotation (radians)[1]				
						Performance Level				
							Component Type			
							Primary		Secondary	
	d	e	g	c	f	IO	LS	CP	LS	CP
i. Shear walls and wall segments[2]										
$\frac{(A_s - A'_s) f_y + P}{t_w l_w f'_c} \le 0.05$	1.0	2.0	0.4	0.20	0.6	0.40	0.75	1.0	1.5	2.0
$\frac{(A_s - A'_s) f_y + P}{t_w l_w f'_c} > 0.05$	0.75	1.0	0.4	0.0	0.6	0.40	0.55	0.75	0.75	1.0

Table 3-3: Modeling Parameters and Acceptance Criteria For Shear Walls Controlled by Flexure Regarding Nonlinear Procedures (ASCE/SEI-41-13 , 2014)

Conditions			Plastic Hinge Rotation (radians)		Residual Strength Ratio	Acceptable Plastic Hinge Rotation[a] (radians)		
						Performance Level		
			a	*b*	*c*	IO	LS	CP
i. Shear walls and wall segments								
$\frac{(A_s - A'_s) f_y + P}{t_w l_w f'_c}$	$\frac{V}{t_w l_w \sqrt{f'_c}}$	Confined Boundary[b]	0.015					
≤0.1	≤4	Yes	0.010	0.020	0.75	0.005	0.015	0.020
≤0.1	≥6	Yes	0.009	0.015	0.40	0.004	0.010	0.015
≥0.25	≤4	Yes	0.005	0.012	0.60	0.003	0.009	0.012
≥0.25	≥6	Yes	0.008	0.010	0.30	0.0015	0.005	0.010
≤0.1	≤4	No	0.006	0.015	0.60	0.002	0.008	0.015
≤0.1	≥6	No	0.003	0.010	0.30	0.002	0.006	0.010
≥0.25	≤4	No	0.002	0.005	0.25	0.001	0.003	0.005
≥0.25	≥6	No	0.002	0.004	0.20	0.001	0.002	0.004

Table 3-4: Modeling Parameters and Acceptance Criteria For Shear Walls Controlled by Shear Regarding Nonlinear Procedures (ASCE/SEI-41-13 , 2014)

Conditions	Total Drift Ratio (%), or Chord Rotation (radians)[a]			Strength Ratio		Acceptable Total Drift (%) or Chord Rotation (radians)[a]		
						Performance Level		
	d	*e*	*g*	*c*	*f*	IO	LS	CP
i. Shear walls and wall segments[b]								
$\frac{(A_s - A'_s) f_y + P}{t_w l_w f'_c} \le 0.05$	1.0	2.0	0.4	0.20	0.6	0.40	1.5	2.0
$\frac{(A_s - A'_s) f_y + P}{t_w l_w f'_c} > 0.05$	0.75	1.0	0.4	0.0	0.6	0.40	0.75	1.0

3.3 Performance Criteria of Eurocode 8

Capacity models proposed in Eurocode 8 are applied to both primary and secondary elements classified as:

- Beams, columns and walls under flexure entitled as Ductile elements (with or without axial forces,
- Beams, columns, walls and joints with shear mechanism entitled as Brittle elements.

Brittle mechanisms are examined through a force/strength-based method, in order to limit brittle components to an elastic range, while the ductile failure mode is controlled following a displacement-based procedure, complying with the aim of providing the sufficient capacity for deformation and energy dissipation.

3.3.1 Ductile Mechanism

The assessment of the ductile mechanisms at component level is evaluated in terms of chord rotation (as shown in Figure 3-4) which is defined as the angle between the tangent to the axis at the yielding end and the chord connecting the mentioned end to the end of shear span (the point of contraflexure). Moreover, the chord rotation can also be considered as the component drift ratio for cantilever elements, which is the tip deflection at the shear span end with respect to the tangent to the axis at the yielding end, divided by the shear span. In this study, shear span in cantilever walls fixed at the member end is defined as the height of the wall which is equal to:

$$L_V = \frac{M}{V} \qquad (3\text{-}7)$$

with M and V accounting for bending moment and shear demands at the member end.

The chord rotation capacity may differ as both geometrical and mechanical properties, as well as the seismic action and axial load change. Eurocode 8 proposes equations for evaluation of chord rotation, based on the mentioned parameters, at Damage Limitation and Near Collapse Limit States. Conventional value defined for Significant Damage Limit State is considered as 3/4 of the value specified at Near Collapse Limit State.

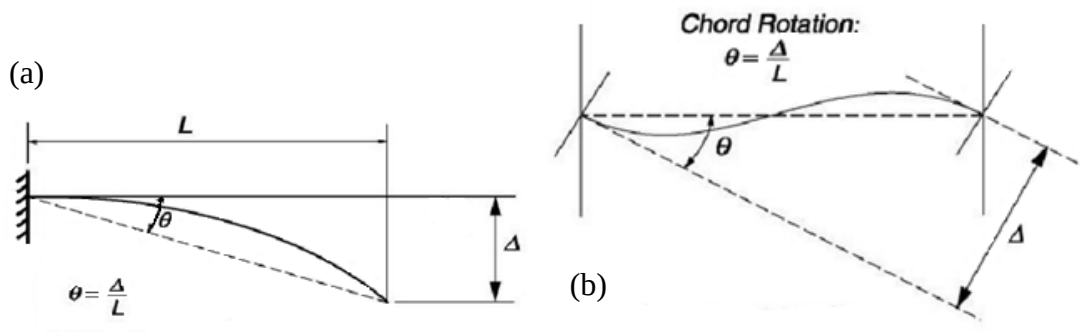

Figure 3-4: Chord Rotation in, (a) Cantilever Elements, (b) Frame Elements

At Damage Limitation Limit State, the chord rotation capacity corresponds to the yield point of member end. The following equation is suggested for walls in Eurocode 8.

$$\theta_y = \phi_y \frac{L_V + \alpha_V z}{3} + 0.002\left(1 - 0.125\frac{L_V}{h}\right) + 0.13\phi_y \frac{d_b f_y}{\sqrt{f_c}} \qquad (3\text{-}8)$$

where;

ϕ_y: is the yield curvature of the end section,

d_b: is the mean diameter of the tension reinforcement.

h: is the depth off cross-section,

$\alpha_v z$: is the tension shift of the bending moment as a result of diagonal cracking; such an increase occurs when diagonal cracking precedes flexural yielding. Therefore, if the shear resistance of the member without considering shear reinforcement (calculated according to EN 1992-1-1:2004, 6.2.2 (1)) is less than the shear force due to yielding moment, $V_y = M_y/L_v$, then $\alpha_v=1$, otherwise $\alpha_v=0$. "z" is the length of

internal lever arm, which is taken as d-d' (which are the depths to the tension and compression reinforcement, respectively) for walls with barbelled or T-section, or as 0.8h for walls with rectangular section.

The equation above consists of three terms. The first term indicates the flexural contribution which has been computed theoretically considering a triangular distribution of the curvature along the height of the member, with neglecting the influence of gravity loads. The second term implies the contribution of shear deformation, while the third term accounts for the anchorage slip of bars.

For Near Collapse Limit State, Eurocode 8 presents two different approaches, one based on theoretical assumptions and the other one based on experimental results. In this study, the empirical approach which is more convenient is used.

$$\theta_u = \frac{1}{\gamma_{el}} 0.016(0.3^{\upsilon}) \left[\frac{\max(0.01,\omega')}{\max(0.01,\omega)} f_c\right]^{0.225} \left(\frac{L_V}{h}\right)^{0.35} 25^{\left(\alpha\rho_{sx}\frac{f_{yw}}{f_c}\right)} (1.25^{100\rho_d}) \qquad (3\text{-}9)$$

(In walls the value obtained from the above equation must be divided by 1.6.)

where;

γ_{el}: is equal to 1.5 for primary seismic structural members,

ω and ω': are the mechanical reinforcement ratios of the tension (including the web reinforcement) and compression longitudinal reinforcement, respectively,

υ: is equal to N / bhf_c , N positive for compression,

ρ_{sx}: is equal to A_{sx} / $b_w s_h$, which is the ratio of transverse steel area parallel to the X-direction of loading (s_h is stirrup spacing),

ρ_d: is the steel ratio of diagonal reinforcement (if any),

α: is the confinement effectiveness factor,

$$\alpha = \left(1 - \frac{s_h}{2b_0}\right)\left(1 - \frac{s_h}{2h_0}\right)\left(1 - \frac{\sum b_i^2}{6h_0 b_0}\right) \qquad (3\text{-}10)$$

where;

h_o and b_o: are the dimensions of confined concrete core, and b_i is the i-th space between adjacent longitudinal bars laterally restrained by hoops.

Regarding the assessment of R.C. members without seismic detailing, Eurocode 8 requires the value obtained from Eq. (3-9) to be multiplied by 0.825. In this study, this factor was applied to the specimen 1, which lacks the detailing for earthquake resistance.

3.3.2 Brittle Mechanism

The assessment of brittle mechanism is performed at section level, comparing the shear demand and related shear capacity at the end of the shear wall. In Eurocode, this procedure is only assessed at the most severe Limit State, Near Collapse.

The effects of cyclic nature of seismic loading, as well as probable development of nonlinear behavior in member ends have been taken into consideration. Shear resistance, V_R, decreases with growth of the inelastic deformation, hence V_R is supposed to be function of the plastic part of ductility demand, μ^{pl}_{Δ}. This parameter may be determined as the ratio of the plastic portion of the chord rotation, θ, normalized to the chord rotation at yielding, θ_y. (Eq. (3-11))

$$\mu_{\Delta}^{pl} = \mu_{\Delta} - 1 = \frac{\theta - \theta_y}{\theta_y} \qquad (3\text{-}11)$$

where θ_y can be calculated through Eq. (3-8).

The following expression is proposed for V_R:

$$V_R = \frac{1}{\gamma_{el}}\left[\frac{h-x}{2L_V} min(N; 0.55A_c f_c) + \left(1 - 0.05min\left(5; \mu_{\Delta}^{pl}\right)\right)\right. \qquad (3\text{-}12)$$
$$\left. \times \left[0.16max(0.5; 100\rho_{tot})\left(1 - 0.16min\left(5; \frac{L_V}{h}\right)\right)\sqrt{f_c}A_c + V_w\right]\right]$$

where;

γ_{el}: is equal to 1.15 for seismic elements,

h: is the depth of cross section,

x: is the compression zone depth,

N: is the compressive axial force (taken positive for compression and zero for tension),

A_c: is the cross-section area,

ρ_{tot}: is the total longitudinal reinforcement ratio (A_{sl}/bd),

V_w: is the contribution of transverse reinforcement, which for rectangular cross-sections is equal to:

$$V_w = \rho_w b_w z f_{yw} \qquad (3\text{-}13)$$

which ρ_w is the transverse reinforcement ratio and z is as defined for Eq. (3-8).

Eq. (3-13) implies two distinct behavior regarding shear failure (Mpampatsikos, 2008):

- Brittle Shear in which ultimate shear failure happens before flexural yielding. This state is characterized with considerable drop in strength of the member and takes place in rather low deformation. In other words, when the shear force corresponding to the flexural yielding, $V_y = M_y$[1]$/L_v$, is preceded with the elastic shear resistance, V_R (Eq. (3-12)) with $\mu^{pl}_{\Delta} = 0$, brittle shear occurs ($V_{R,0}<V_y$).
- Ductile Shear in which concrete elements may first go through flexural yielding, but finally fail in shear. In this state, V_y is smaller than $V_{R,0}$ but larger then V_R at ultimate conditions ($V_{R,U}< V_y < V_{R,0}$). As shown in Figure 3-5, due to the linear degradation of V_R with respect to μ^{pl}_{Δ}, there is an plastic deformation interval correlating with this ductile shear failure.

[1] Determined as M_n in Sec.2.2.1.

Accordingly, with considering "x" constant for ductilities higher than 5 in Eq. (3-12), V_R remains constant at its ultimate condition. Hence, it can be summarized that if:

- $V_{R,0} < V_y$, the element goes through a “brittle shear” failure;
- $V_{R,U} < V_y < V_{R,0}$, the element undergoes a “ductile shear” failure;
- $V_y < V_{R,U}$, the element does not fail in shear.

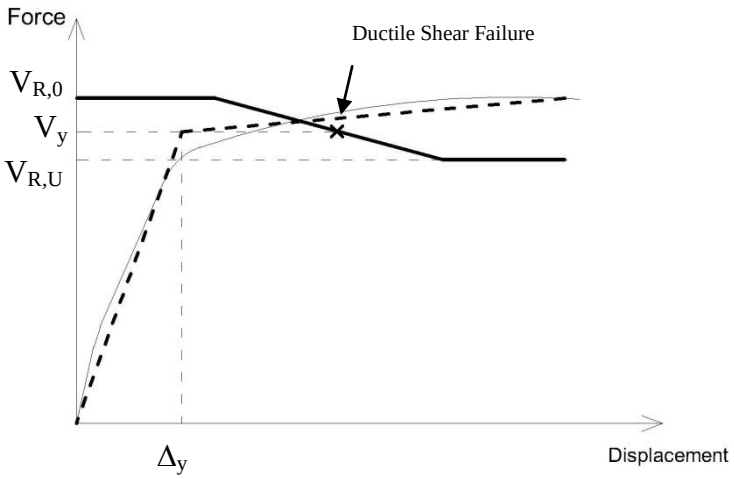

Figure 3-5: Effect of Development of Plastic Hinge in Shear Capacity

Eq. (3-12) accounts only for the shear failure by diagonal tension of structural members. However, according to Eurocode 8, It is not permitted that the shear strength of a concrete wall, V_R, to be taken greater than the value corresponding to failure by web crushing, $V_{R,max}$ which shall be determined through the following expression:

$$V_{R,max} = \frac{0.85\left(1 - 0.06\min\left(5; \mu_\Delta^{pl}\right)\right)}{\gamma_{el}}\left(1 + 1.8\min\left(0.15; \frac{N}{A_c f_c}\right)\right) \times \left(1 + 0.25\max(1.75; 100\rho_{tot})\right)\left(1 - 0.2\min\left(2; \frac{L_V}{h}\right)\right)\sqrt{f_c} b_w z \qquad (3\text{-}14)$$

where;

γ_{el}: is equal to 1.15 for seismic elements.

Similar to Eq. (3-12), the shear failure due to diagonal compression, Eq. (3-14), decreases by the development of inelastic deformation at member ends, but unlike the diagonal tension failure, the shear failure as a result of web crushing must be regarded as brittle, even if the member undergoes flexural yielding before diagonal compressive failure.

3.4 Performance Criteria of Turkish Earthquake Code 2007

Similar to the other two codes, the acceptance criteria for elements have been specified in TED 2007. However for nonlinear analysis procedures, the material strain parameter (compressive strains for concrete and tensile strain for reinforcement) has been employed for performance assessment of ductile components rather than chord rotation or plastic hinge rotation.

Concrete and steel strain limits at the outmost fibers of a cross section for damage states are provided as follows:

- Minimum Damage Limit (MN):

$$(\varepsilon_{cu})_{MN} = 0.0035 \quad ; \quad (\varepsilon_s)_{MN} = 0.010 \qquad (3\text{-}15)$$

- Safety Limit (SF):

$$(\varepsilon_{cg})_{SF} = 0.0035 + 0.01\left(\frac{\rho_s}{\rho_{sm}}\right) \leq 0.0135 \quad ; \quad (\varepsilon_s)_{SF} = 0.040 \qquad (3\text{-}16)$$

- Collapse Limit (CL):

$$(\varepsilon_{cg})_{CL} = 0.004 + 0.014\left(\frac{\rho_s}{\rho_{sm}}\right) \leq 0.018 \quad ; \quad (\varepsilon_s)_{CL} = 0.060 \qquad (3\text{-}17)$$

where;

ε_{cu}: is the concrete strain at the outer fiber,

ε_{cg}: is the concrete strain at the outer fiber of the confined core,

ε_s: is the reinforcement strain,

ρ_s: Existing volumetric ratio of transverse reinforcement which are detailed as "special seismic hoops and crossties" according to section 3.2.8 of TEC2007,

ρ_{sm}: Volumetric ratio of the required transverse reinforcement according to TEC2007.

Transverse reinforcement of the structural members of buildings under assessment must be detailed according to the rules given by the Code. Transverse reinforcement which do not conform the necessary requirements shall be neglected.

To control the brittle behavior of the components, shear capacity of the walls are calculated as provided in TEC2007 and TS500.

$$V_r = A_{ch}\left(0.65 f_{ctd} + \rho_{sh} f_{ywd}\right) < 0.22 A_{ch} f_{cd}$$

where;

A_{ch}: Gross section area of the wall,

ρ_{sh}: Volumetric ratio of transverse web reinforcement of the wall,

f_{ctd}: Design tensile strength of concrete which is:

$$f_{ctd} = 0.35\sqrt{\frac{f_{ck}}{\gamma_{mc}}}$$

f_{cd}: Design compressive strength of concrete which is:

$$f_{cd} = \frac{f_{ck}}{\gamma_{mc}}$$

f_{ck} is the characteristic compressive strength of concrete and γ_{mc} shall be considered as 1.5 for cast-in-place concrete and as 1.4 for precast concrete,

f_{ywd}: Characteristic yield strength of transverse reinforcement.

Table 3-5: Summary of Regulations of Different Codes Regarding Performance Assessment

	Flexure Mechanism	Shear Mechanism
ASCE	Referring to parameters and acceptance criteria (IO-LS-CP) in related tables in terms of plastic hinge rotation	Referring to parameters and acceptance criteria(IO-LS-CP) in related tables in terms of story drift
EC8	Evaluating in terms of chord rotation at DL, SD, NC DL: $\theta_y = \phi_y \frac{L_V + \alpha_V z}{3} + 0.002\left(1 - 0.125\frac{L_V}{h}\right) + 0.13\phi_y \frac{d_b f_y}{\sqrt{f_c}}$ SD: $\theta = \frac{3}{4}\theta_u$ NC: $\theta_u = \frac{1}{\gamma_{el}} 0.016(0.3^{\upsilon}) \left[\frac{\max(0.01, \omega')}{\max(0.01, \omega)} f_c\right]^{0.225} \left(\frac{L_V}{h}\right)^{0.35} 25^{\left(\alpha\rho_{sx}\frac{f_{yw}}{f_c}\right)} (1.25^{100\rho_d})$	comparing the shear demand and related shear capacity at the critical section (assessed at NC) $V_R = \frac{1}{\gamma_{el}}\left[\frac{h-x}{2L_V} min(N; 0.55A_c f_c) + \left(1 - 0.05 min(5; \mu_\Delta^{pl})\right) \times \left[0.16 max(0.5; 100\rho_{tot})\left(1 - 0.16 min\left(5; \frac{L_V}{h}\right)\right)\sqrt{f_c} A_c + V_w\right]\right]$ $V_{R,max} = \frac{0.85\left(1 - 0.06\min(5; \mu_\Delta^{pl})\right)}{\gamma_{el}}\left(1 + 1.8\min\left(0.15; \frac{N}{A_c f_c}\right)\right) \times \left(1 + 0.25\max(1.75; 100\rho_{tot})\right)\left(1 - 0.2\min\left(2; \frac{L_V}{h}\right)\right)\sqrt{f_c} b_w z$
TEC2007	Evaluating in terms of material strains at MN, SF, CL MN: $(\varepsilon_{cu})_{MN} = 0.0035 \quad ; \quad (\varepsilon_s)_{MN} = 0.010$ SF: $(\varepsilon_{cg})_{SF} = 0.0035 + 0.01\left(\frac{\rho_s}{\rho_{sm}}\right) \le 0.0135 \quad ; \quad (\varepsilon_s)_{SF} = 0.040$ CL: $(\varepsilon_{cg})_{CL} = 0.004 + 0.014\left(\frac{\rho_s}{\rho_{sm}}\right) \le 0.018 \quad ; \quad (\varepsilon_s)_{CL} = 0.060$	comparing the shear demand and related shear capacity at the critical section $V_r = A_{ch}\left(0.65 f_{ctd} + \rho_{sh} f_{ywd}\right) < 0.22 A_{ch} f_{cd}$

3.5 Performance Assessment of the Components

Performance assessment of all the specimens are provided in this section. In order to evaluate the performance limits specified by the codes, performance of each specimen is additionally estimated from experimental results considering the idealized elastic perfectly plastic response described in Sec. 2.1.2. In this study, estimated Collapse Prevention state is considered as the ultimate point where the maximum strength is dropped by 15 percent. Immediate Occupancy is defined as the state where the elastic behavior gives place to plastic behavior (Yakut and Solmaz, 2012). This situation is attained when the outermost tension reinforcement is reached the strain value of 0.015 or the outer compression fiber of concrete is reached the strain value of 0.004 (defined as yield point). Here, the yield point is determined by connecting the origin with a line passing through 70% of the ultimate load on the initial loading curve (defined as first yield point) and extending this line to 85% of the ultimate load. Accordingly, Life Safety state may be estimated as the 75 percent of the ultimate point (Binici and Canbay, 2014).

3.5.1 Comparison of the Results According to ASCE/SEI-41

Plastic hinge rotations, determined for each limit states described in Sec.3.2 for each specimen, were converted to displacements in order to compare the experimental results with the acceptance criteria of ASCE/SEI-41.

3.5.1.1 Analysis According to ASCE/SEI-41

Response of the specimens are compared with the backbone shapes derived from ASCE/SEI-41-06 and ASCE/SEI-41-13. The backbones obtained from both versions, considering the ultimate conditions, are totally in compliance with the experimental results. It is also possible to determine the expected failure modes of the walls. For Specimens 1 and 2 (Figure 3-6~Figure 3-9), the capacity associated with the shear-type failure is higher than the flexural capacity of these walls, which means that the

specimens 1 and 2 are governed by flexure, while the specimens 3 and 4 (Figure 3-10~Figure 3-13) fail in shear and are categorized as a brittle component.

On the other hand, two approaches where used for defining the yield point (point B) in backbone shapes of flexure-controlled specimens; one following the procedure proposed in ASCE considering the reinforcement in boundary zones, and the other by including all the reinforcement in calculation. The difference is also presented in Figure 3-6 to Figure 3-13 as method 1 and method 2, respectively. Comparing with the experimental results, it can be seen that the backbone shapes obtained including all reinforcement provide a better agreement with the walls response.

3.5.1.2 Performance Assessment According to ASCE/SEI-41

The load-deformation relation of walls and the related backbone curves are compared with the acceptance criteria (Figure 3-14~21). According to ASCE/SEI-41-06, in specimens 1 and 2, the state of Collapse Prevention is quite close to the ultimate step of the tests, which means in case of proceeding the loading, this state would be passed before complete failure. For specimens 3 and 4, the damage limits were found to be on the safe side. Generally, the Immediate Occupancy state is overestimated in all walls. On the other side, Collapse Prevention limit state is overestimated by ASCE/SEI-41-13. Considering this result, one can derive that ASCE 41-13 does not set the collapse state assuming the strength degradation; it rather recommends performing complete analysis and afterwards, determining collapse state.

The shear capacity estimated by ACI318 for specimen 3, is in good agreement with the test results, while this value is smaller in the case of specimen 4. However, the shear strengths predicted by ACI318 remain on the safe side in this study.

Totally, capacity of the specimens are well-estimated by both ASCE/SEI-41-06&13, however, ASCE/SEI-41-06 determines a good approximation for ultimate conditions, while overestimating the Immediate Occupancy.

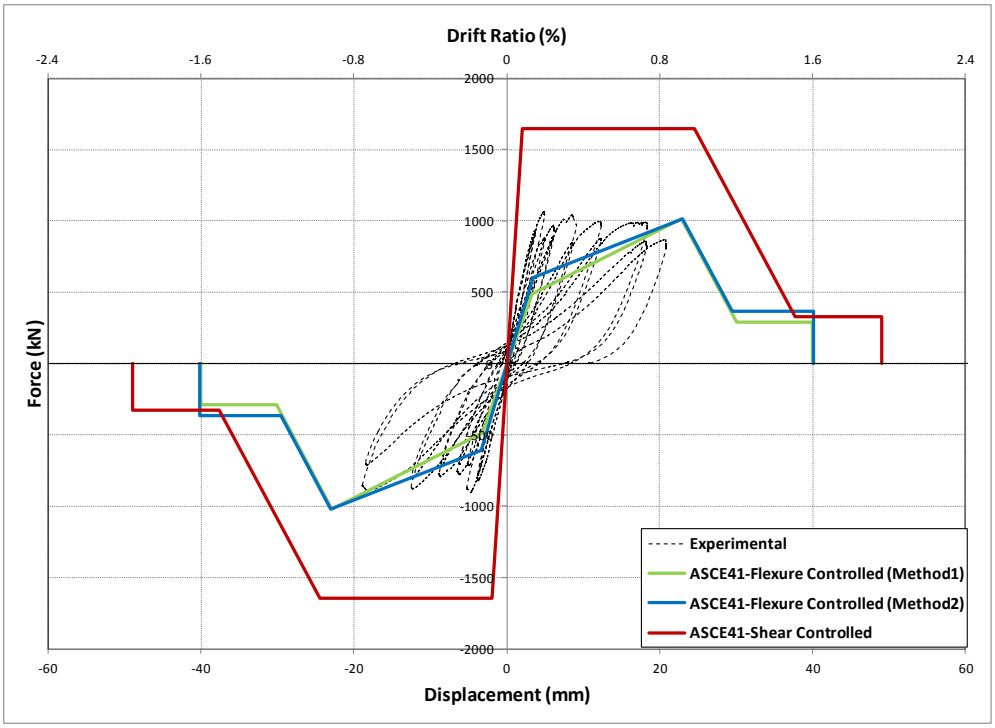

Figure 3-6: Comparison of Experimental Results of Specimen 1 with Backbone Shapes Obtained from ASCE/SEI-41-06 Supplement 1

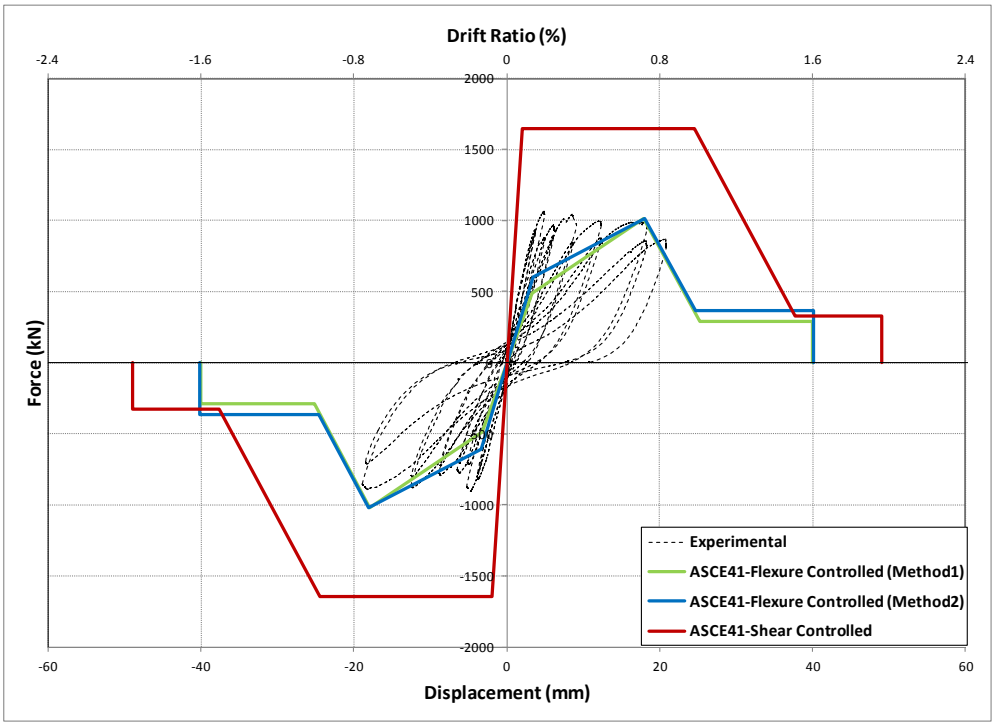

Figure 3-7: Comparison of Experimental Results of Specimen 1 with Backbone Shapes Obtained from ASCE/SEI-41-13

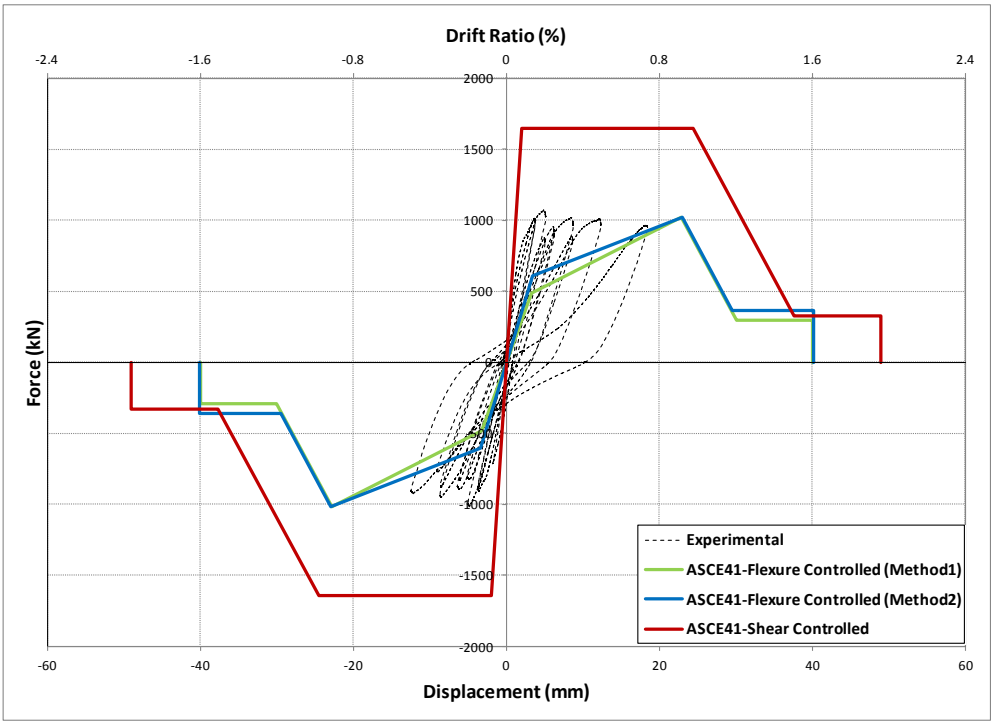

Figure 3-8: Comparison of Experimental Results of Specimen 2 with Backbone Shapes Obtained from ASCE/SEI-41-06 Supplement 1

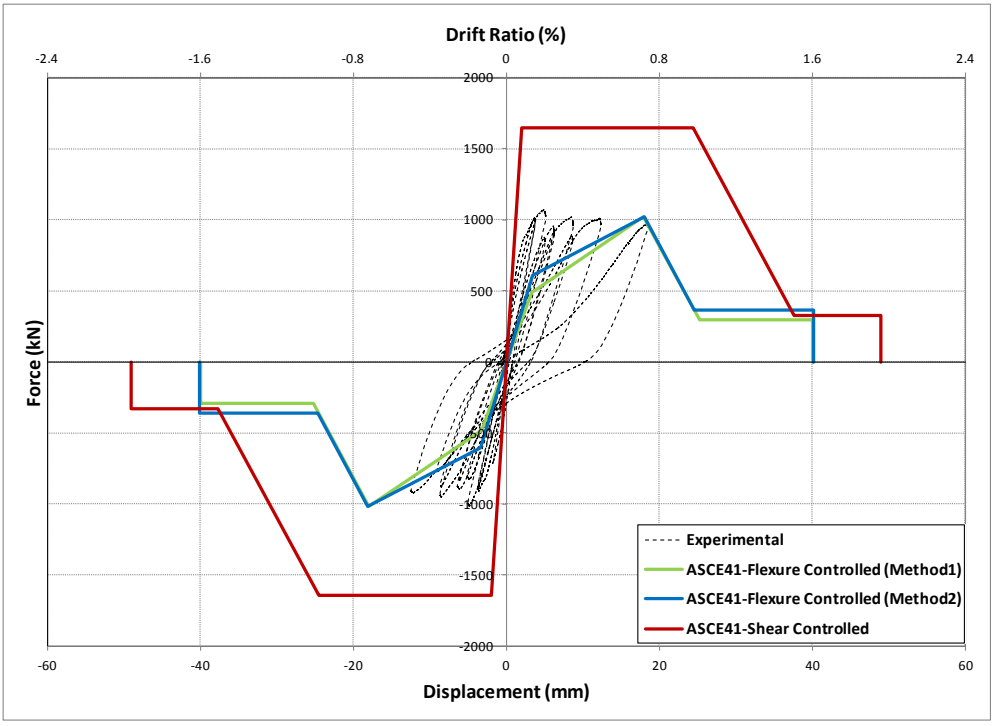

Figure 3-9: Comparison of Experimental Results of Specimen 2 with Backbone Shapes Obtained from ASCE/SEI-41-13

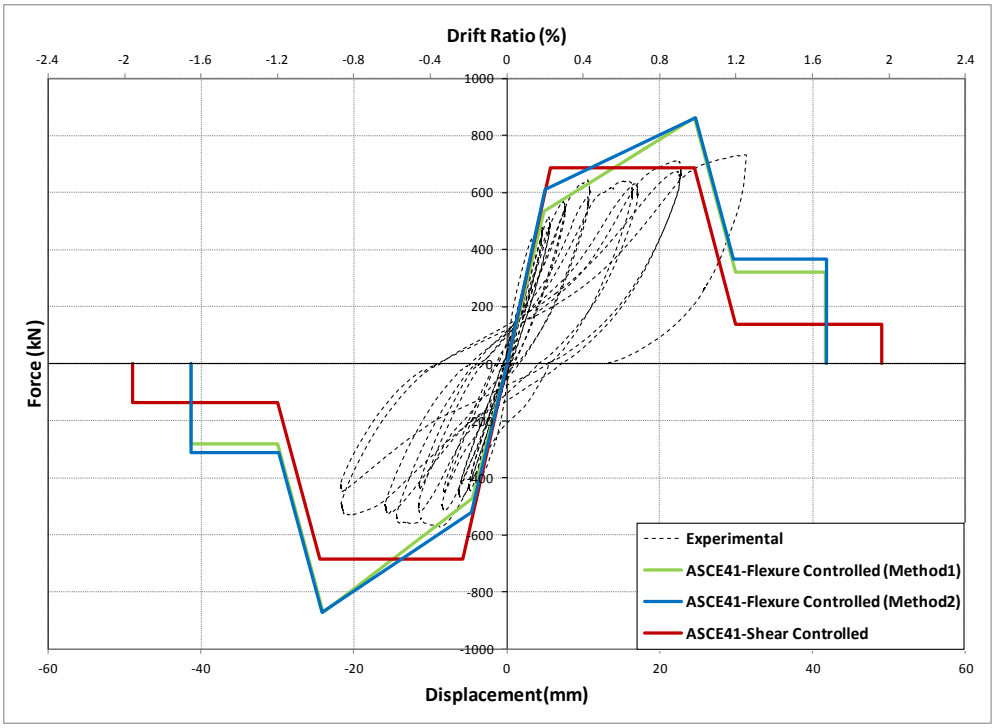

Figure 3-10: Comparison of Experimental Results of Specimen 3 with Backbone Shapes Obtained from ASCE/SEI-41-06 Supplement 1

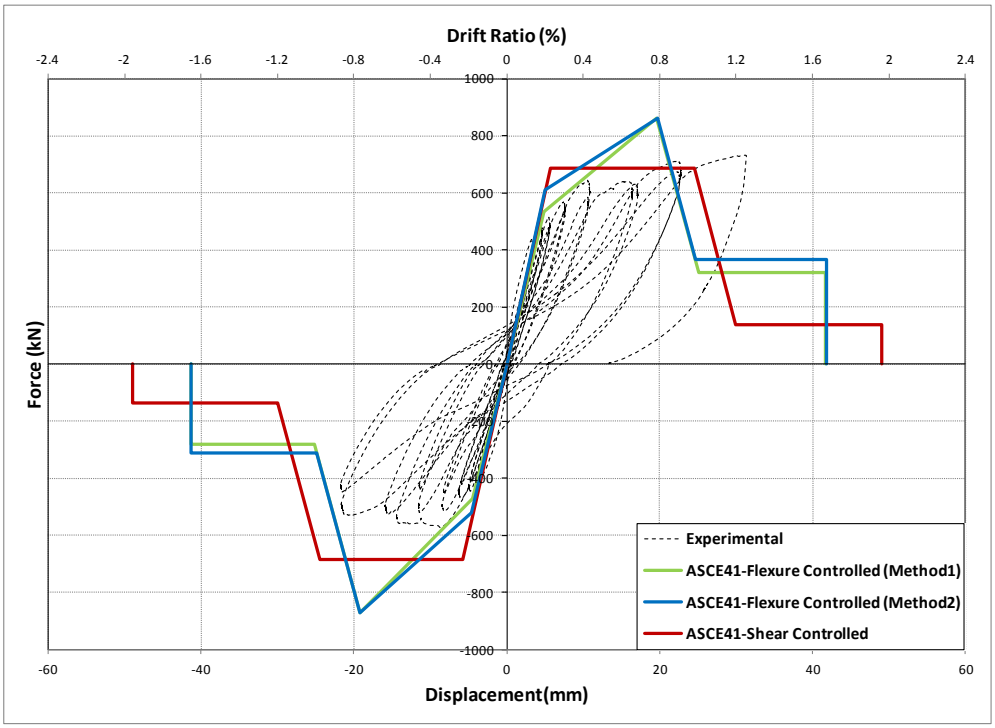

Figure 3-11: Comparison of Experimental Results of Specimen 3 with Backbone Shapes Obtained from ASCE/SEI-41-13

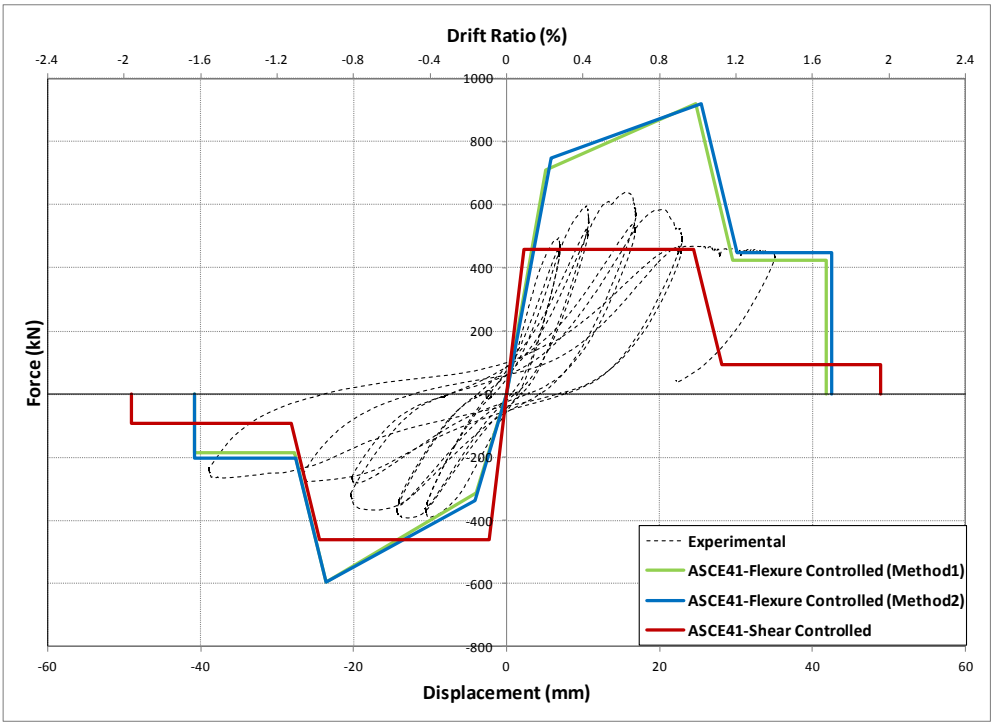

Figure 3-12: Comparison of Experimental Results of Specimen 4 with Backbone Shapes Obtained from ASCE/SEI-41-06 Supplement 1

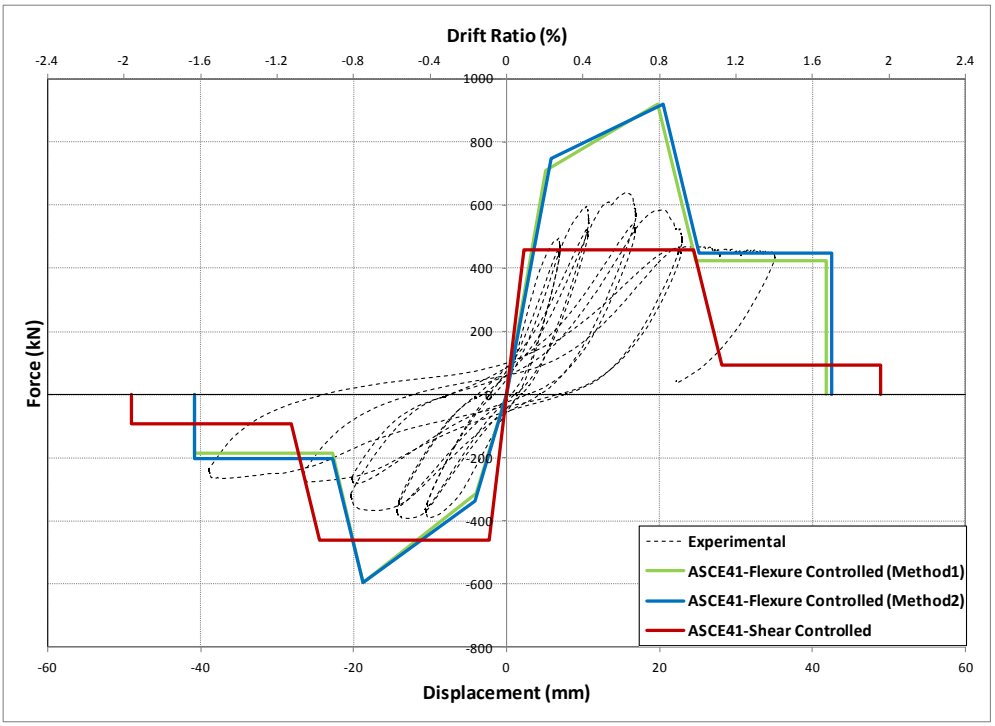

Figure 3-13: Comparison of Experimental Results of Specimen 4 with Backbone Shapes Obtained from ASCE/SEI-41-13

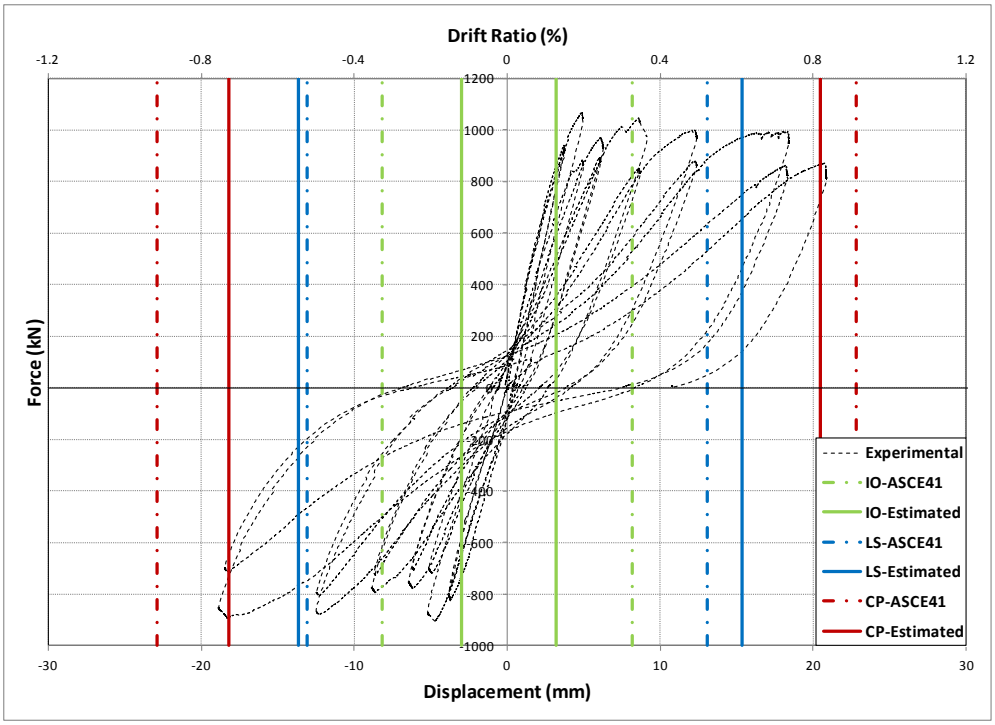

Figure 3-14: Comparison of Experimental Results of Specimen 1 with Damage States According to ASCE/SEI-41-06 Supplement 1

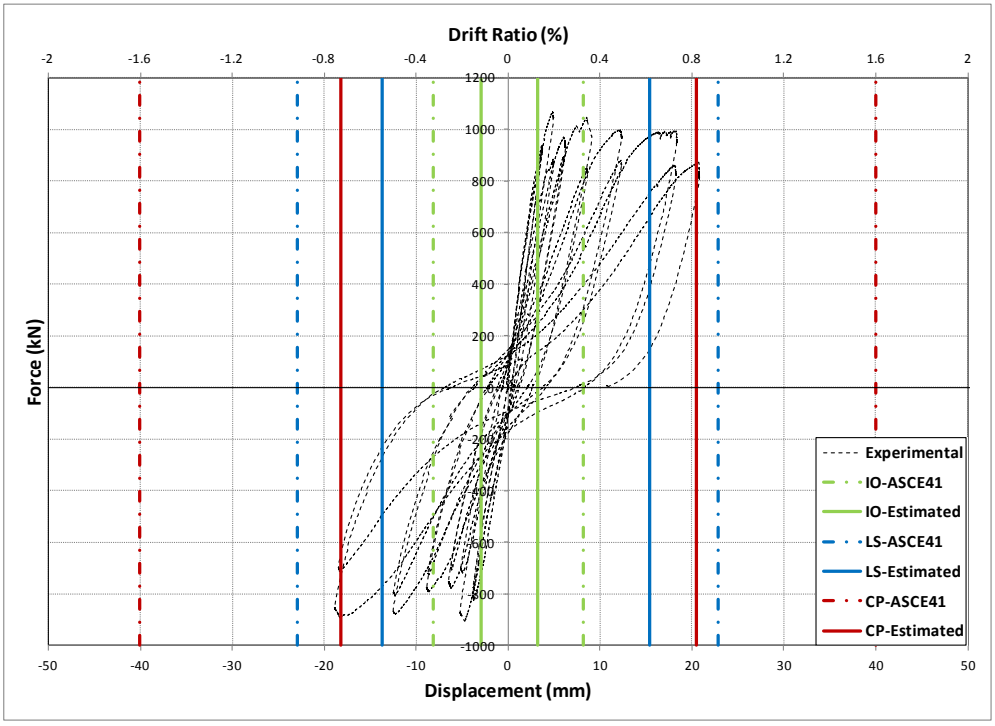

Figure 3-15: Comparison of Experimental Results of Specimen 1 with Damage States According to ASCE/SEI-41-13

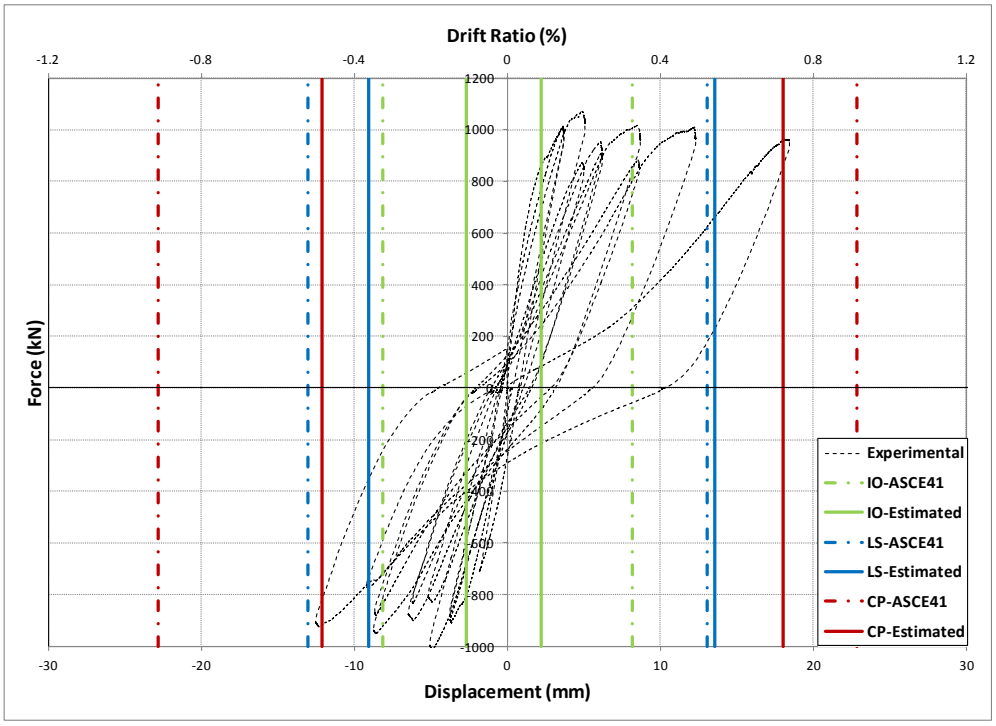

Figure 3-16: Comparison of Experimental Results of Specimen 2 with Damage States According to ASCE/SEI-41-06 Supplement 1

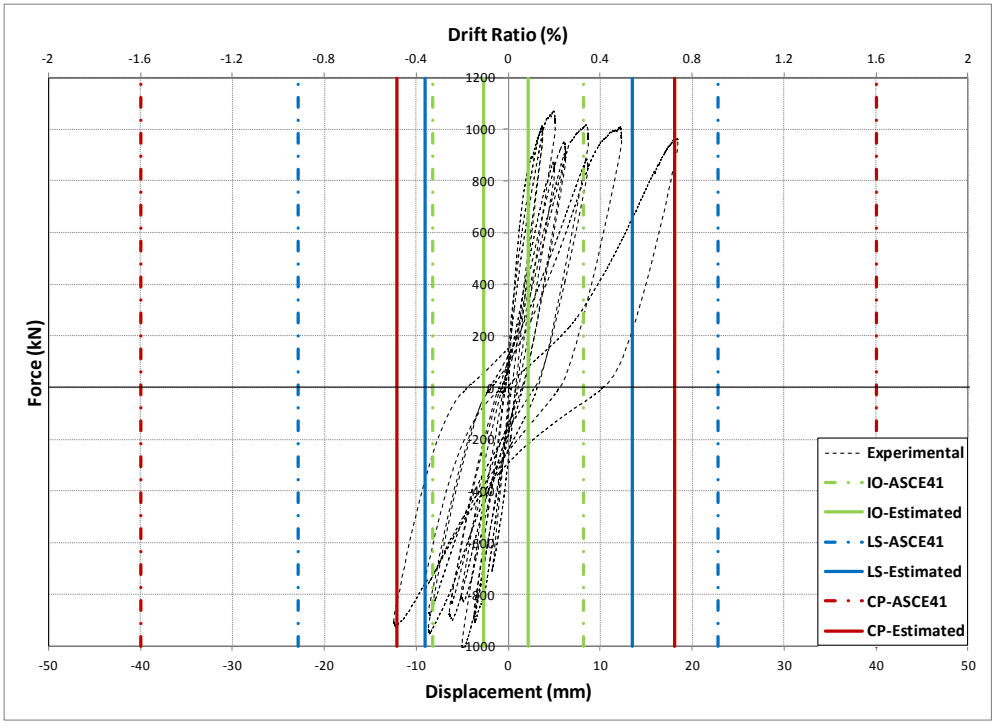

Figure 3-17: Comparison of Experimental Results of Specimen 2 with Damage States According to ASCE/SEI-41-13

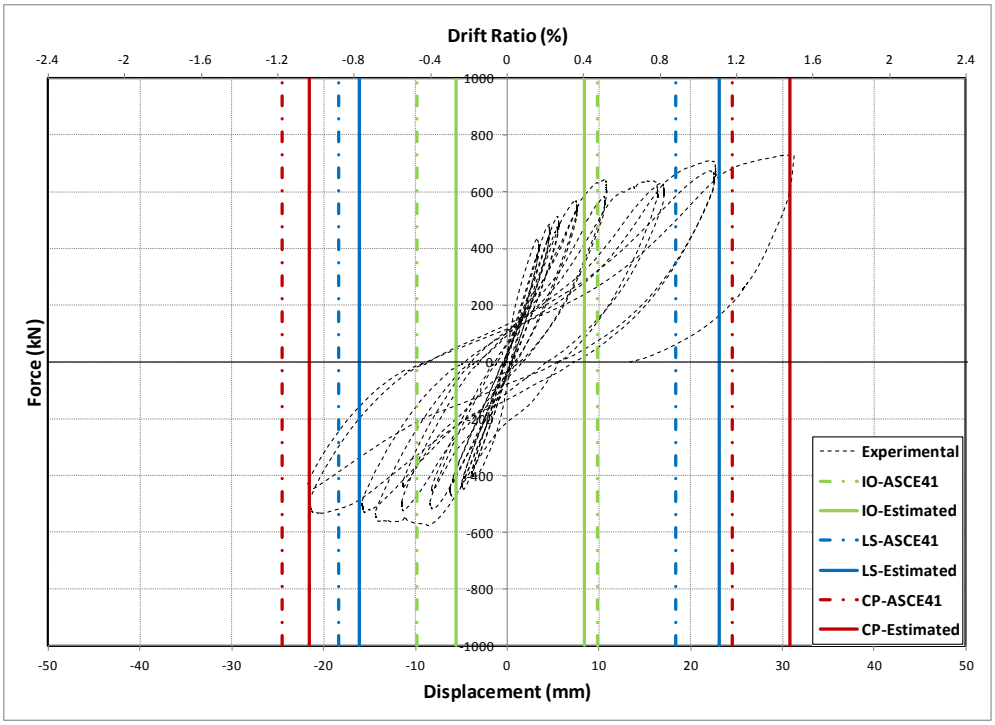

Figure 3-18: Comparison of Experimental Results of Specimen 3 with Damage States According to ASCE/SEI-41-06 Supplement 1

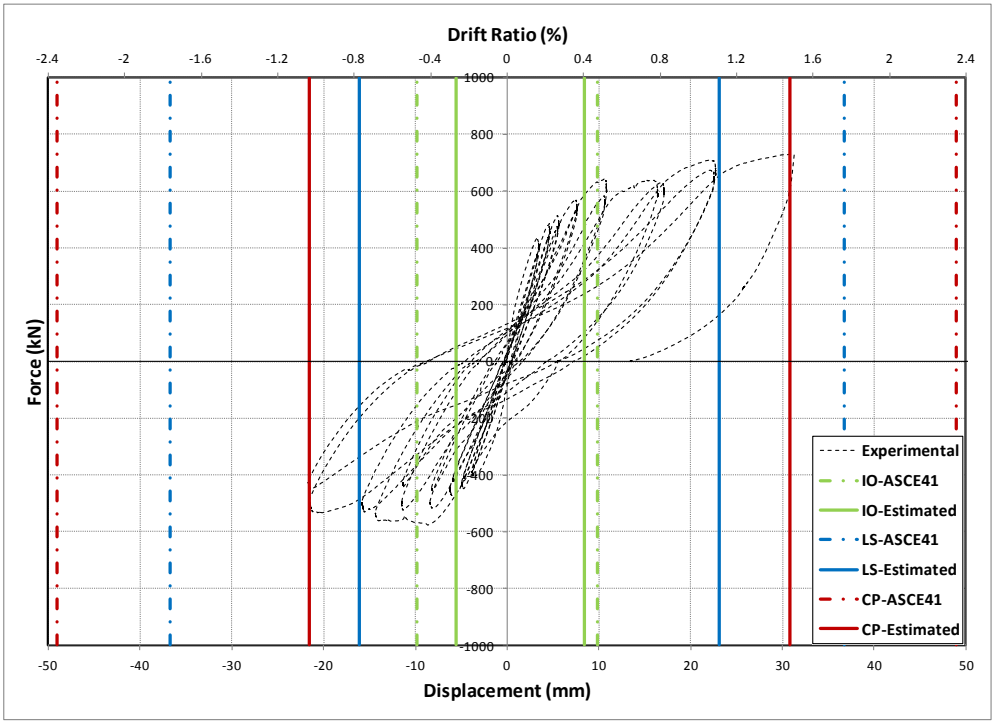

Figure 3-19: Comparison of Experimental Results of Specimen 3 with Damage States According to ASCE/SEI-41-13

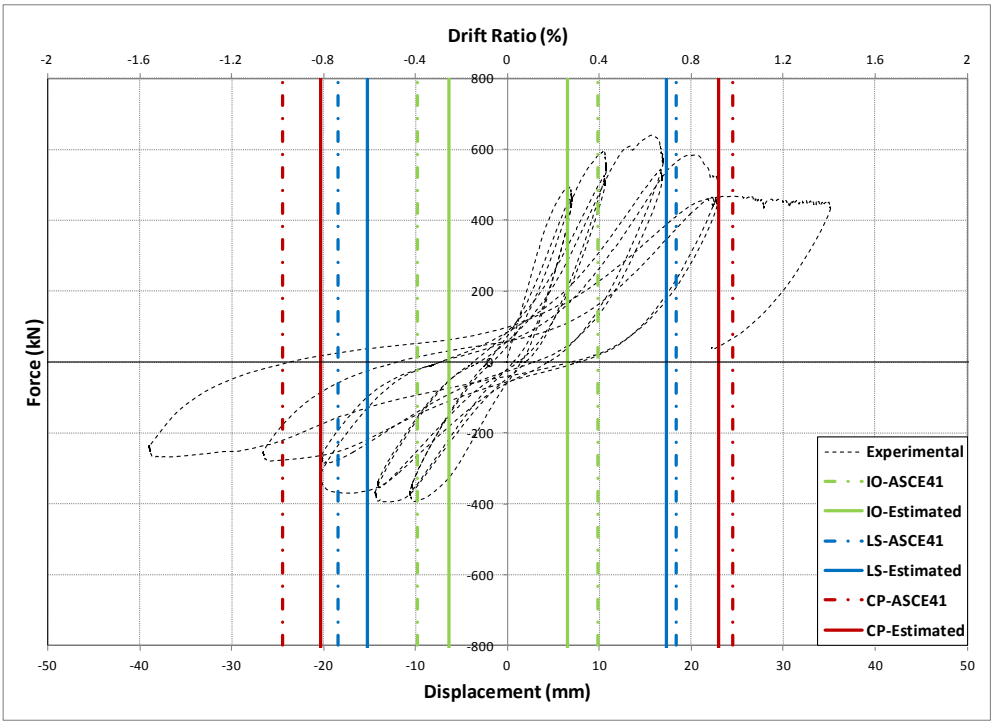

Figure 3-20: Comparison of Experimental Results of Specimen 4 with Damage States According to ASCE/SEI-41-06 Supplement 1

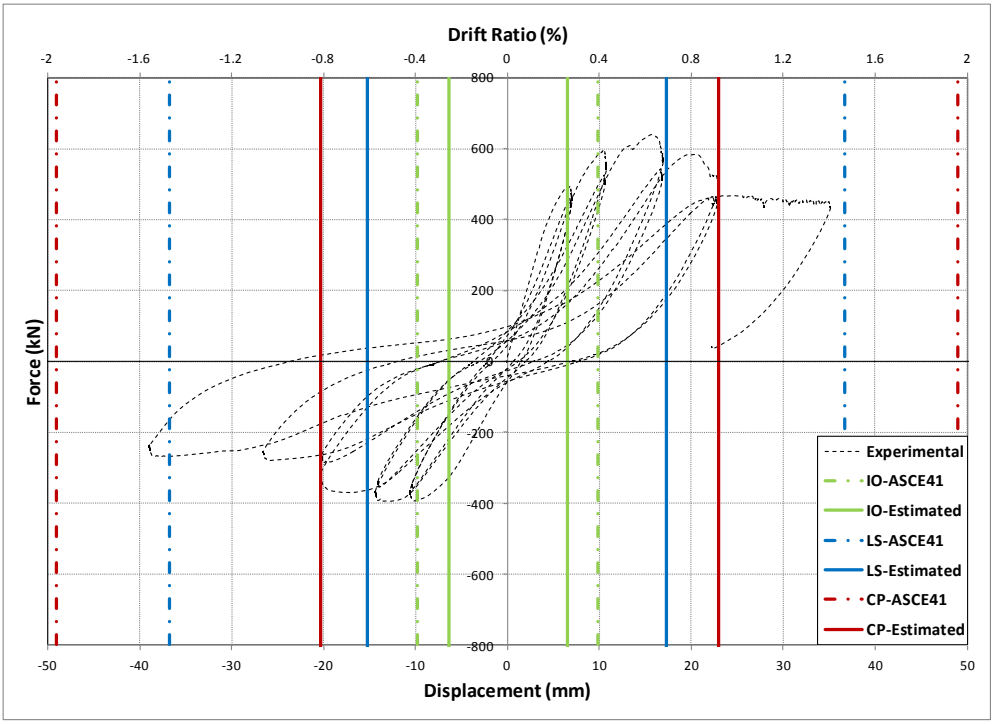

Figure 3-21: Comparison of Experimental Results of Specimen 4 with Damage States According to ASCE/SEI-41-13

3.5.2 Comparison of the Results According to EC8

Using the expressions explained in Sec.3.3 , chord rotation limits are calculated for each wall and are later converted to displacements for each limit state.

It can be seen that Eurocode 8 is presented almost the same results as ASCE/SEI-41. Figure 3-22 and Figure 3-23 prove the flexure failure mode for specimens 1 and 2, while brittle behavior may be observed in specimens 3 and 4 due to lower shear capacity compared to flexure capacity (Figure 3-24 and Figure 3-25). Eurocode 8, provides performance assessment for ductile elements; in this study this evaluation is presented for specimens 1 and 2, in Figure 3-26 and Figure 3-27. It can be observed that the proposed NC limit states exhibit a good agreement with the test results, while the other two limit stated are on unsafe side in both specimens.

The behavior of specimen 3 is well predicted according to EC8. During the experimental tests, despite the observed shear cracks, the specimen was able to behave in a very ductile manner, which according to Figure 3-24, it can be seen that the wall is expected to go through a flexure-shear failure, especially in negative direction. The same behavior may be expected for the specimen 4 on the negative direction, while on the positive direction a brittle failure is determined which is not in compliance with the real response of the specimen. Shear capacity is in good agreement with the experimental results for both specimens.

Totally, in performance assessment of flexure-controlled elements, EC8 provides the same results with ASCE; Ultimate conditions are well-predicted, while Damage Limit states are generally overestimated. Capacity of the walls are well-estimated by EC8.

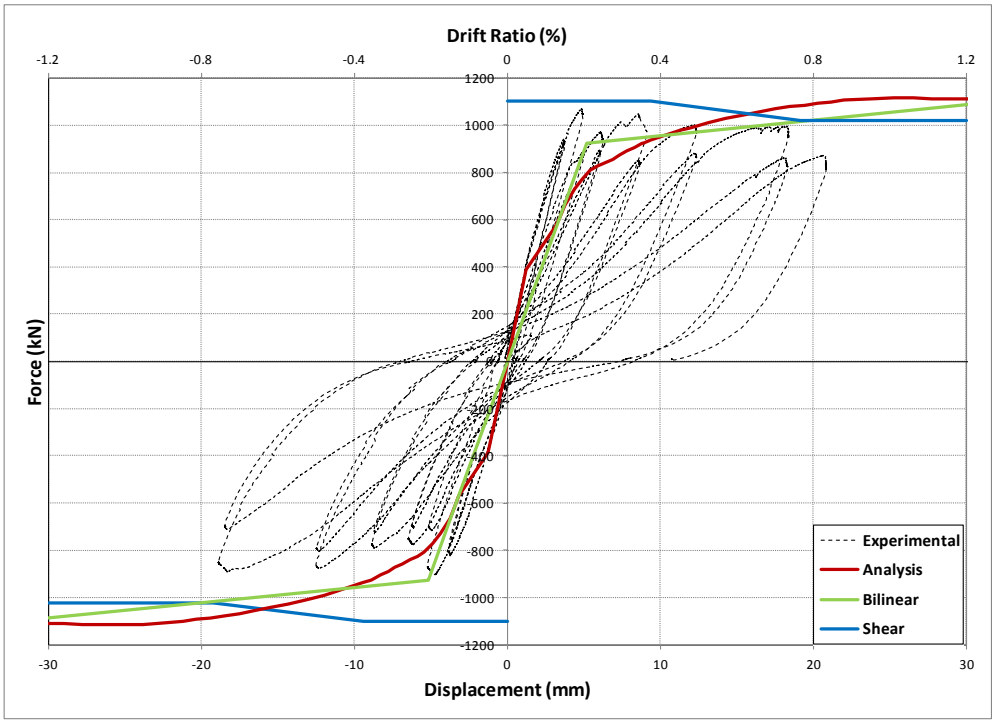

Figure 3-22: Comparison of Flexural and Shear Capacity of Specimen 1 According to Eurocode 8

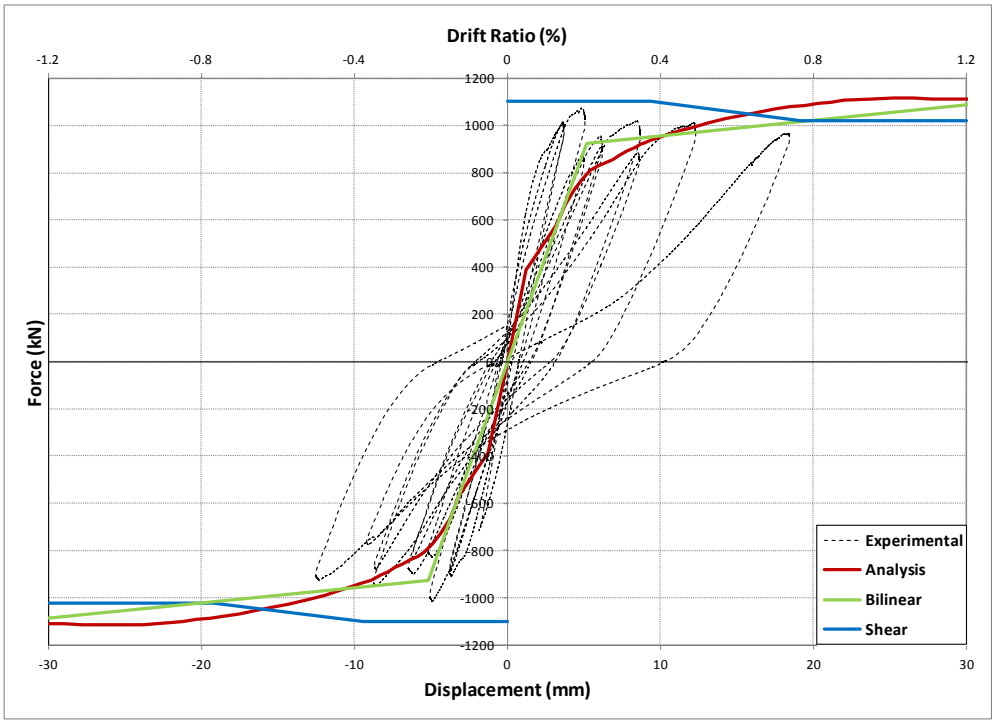

Figure 3-23: Comparison of Flexural and Shear Capacity of Specimen 2 According to Eurocode 8

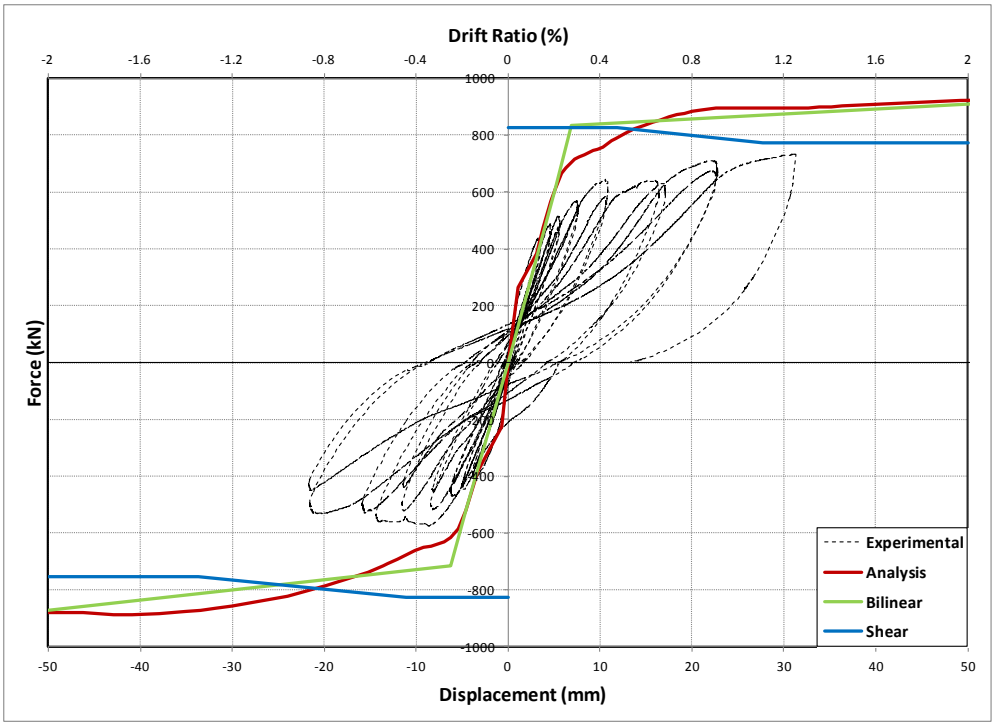

Figure 3-24: Comparison of Flexural and Shear Capacity of Specimen 3 According to Eurocode 8

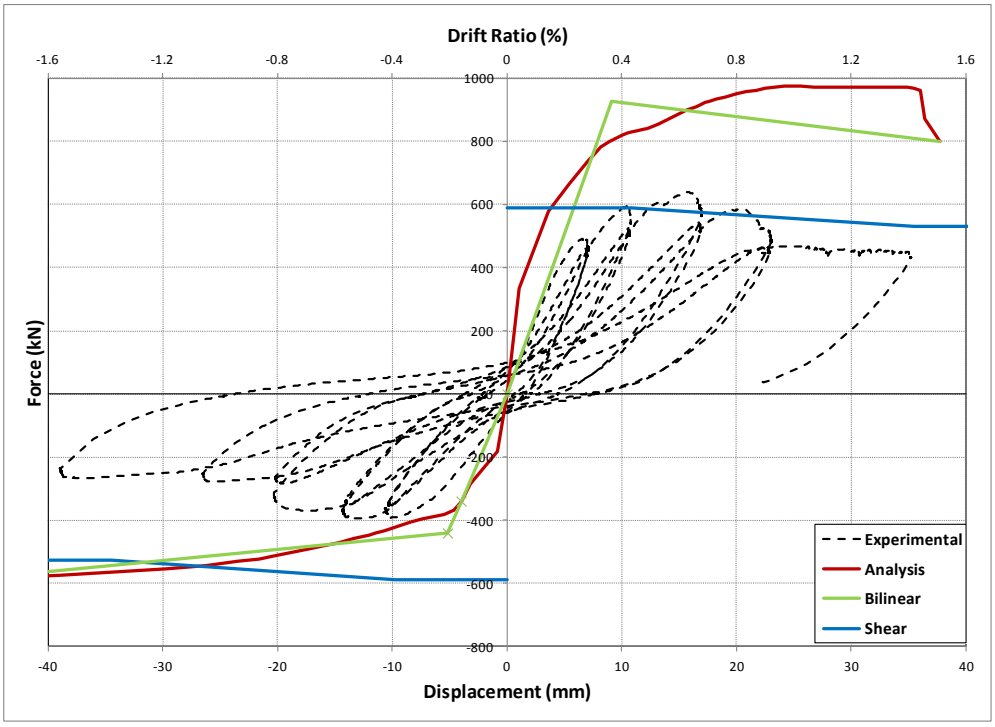

Figure 3-25: Comparison of Flexural and Shear Capacity of Specimen 4 According to Eurocode 8

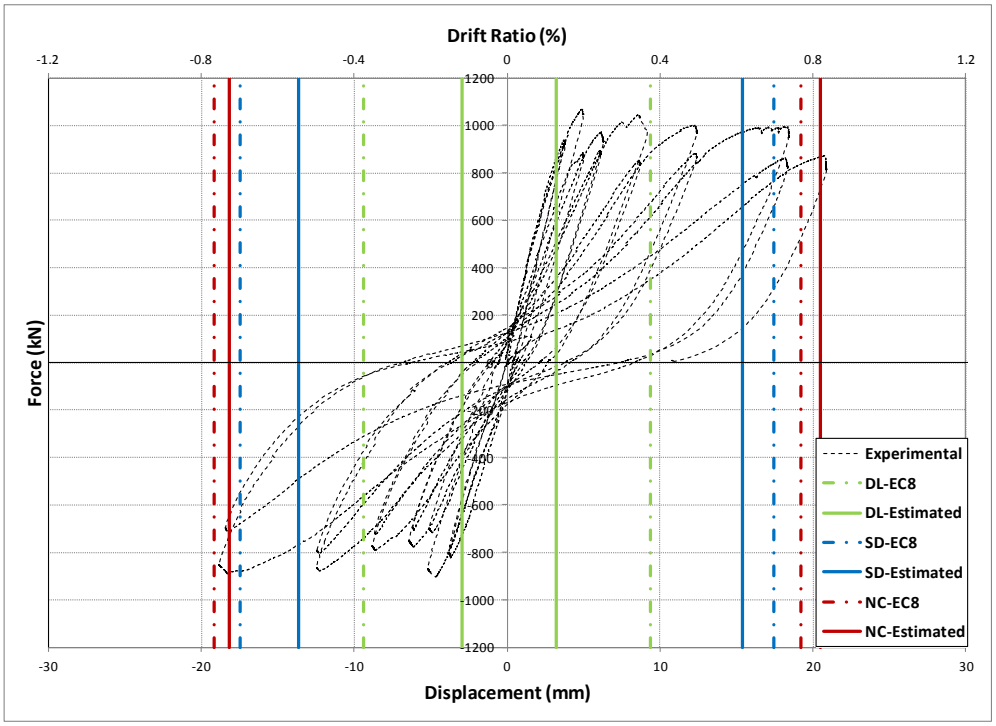

Figure 3-26: Comparison of Experimental Results of Specimen 1 with Damage States According to Eurocode 8

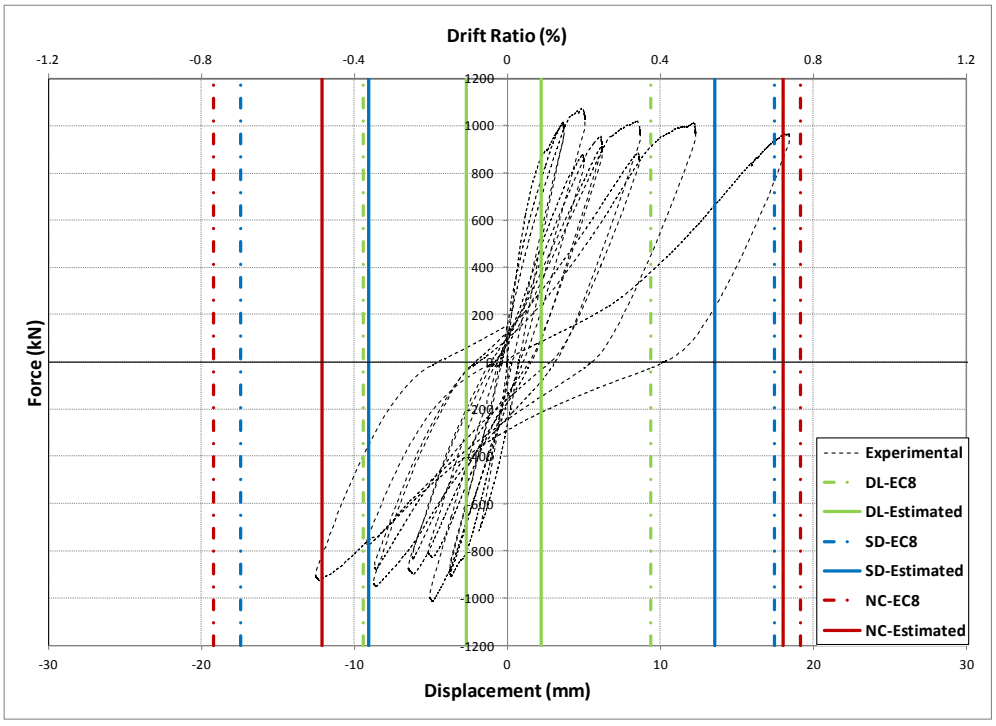

Figure 3-27: Comparison of Experimental Results of Specimen 2 with Damage States According to Eurocode 8

3.5.3 Comparison of the Results According to TEC2007

Deformation limits (material strains) for each performance level are determined for each specimen. Afterwards, the calculated deformations are converted to displacements in order to compare the results using section analysis provided in Sec.2.2.

Shear and flexure capacity of the walls are compared in Figure 3-28 to Figure 3-31. It can be noticed that the results obtained are rather different from the other two codes. According to Turkish Code, the specimen 3 is expected to behave ductile, while according to ASCE41 and EC8 is shear-controlled. Comparing the response of specimen 3 with the damage state criteria defined for ductile elements, it can be seen that there is an overestimation of performance limits.

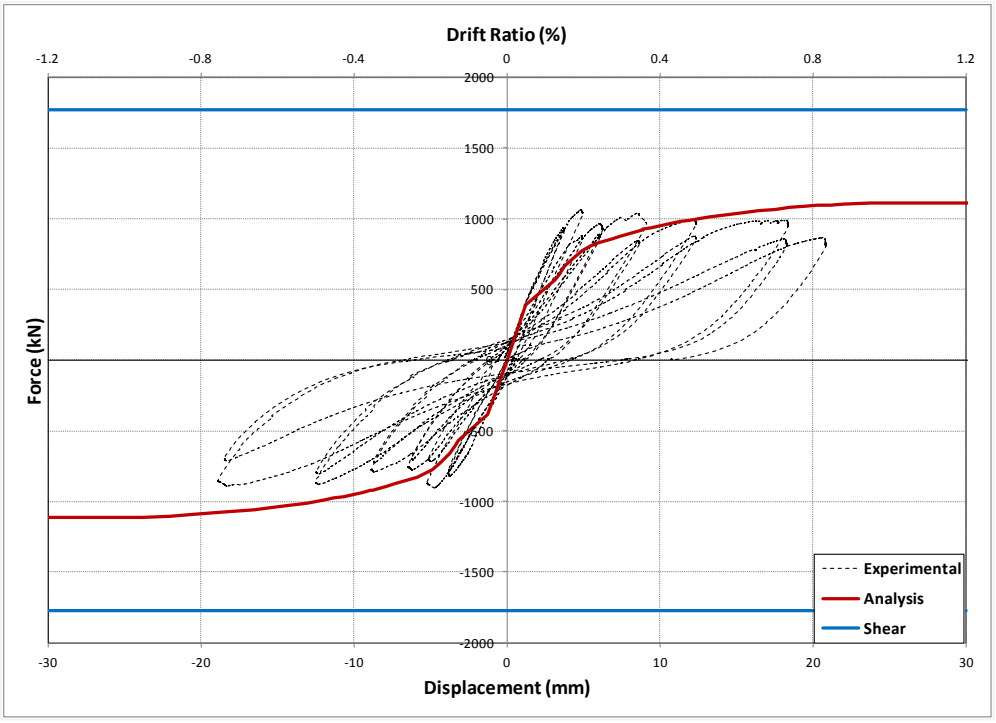

Figure 3-28: Comparison of Flexural and Shear Capacity of Specimen 1 According to TEC2007

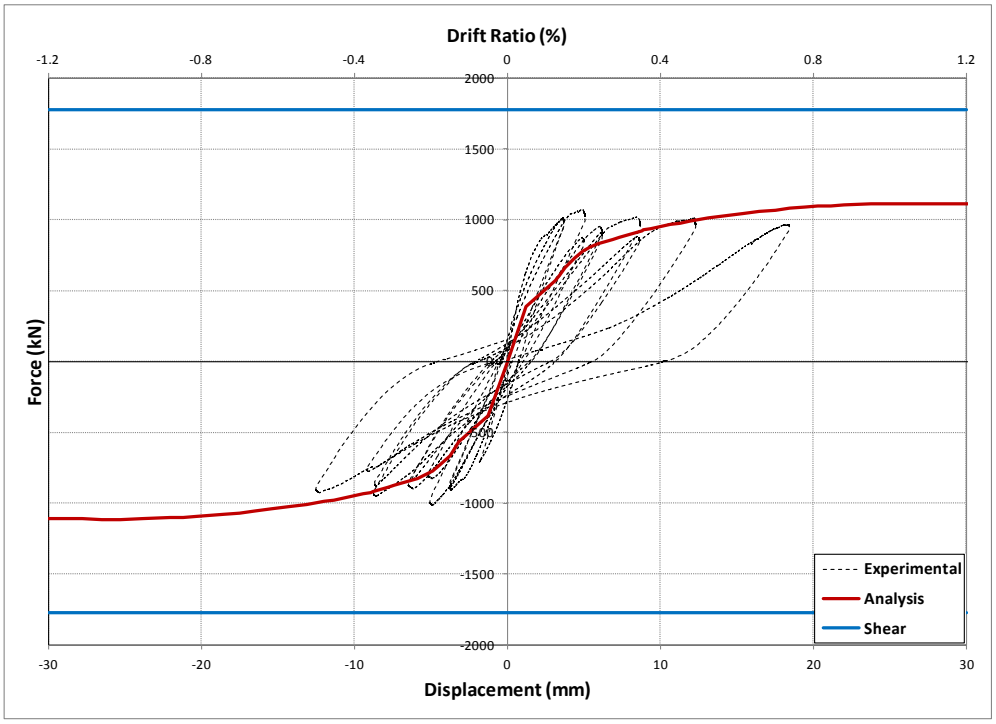

Figure 3-29: Comparison of Flexural and Shear Capacity of Specimen 2 According to TEC2007

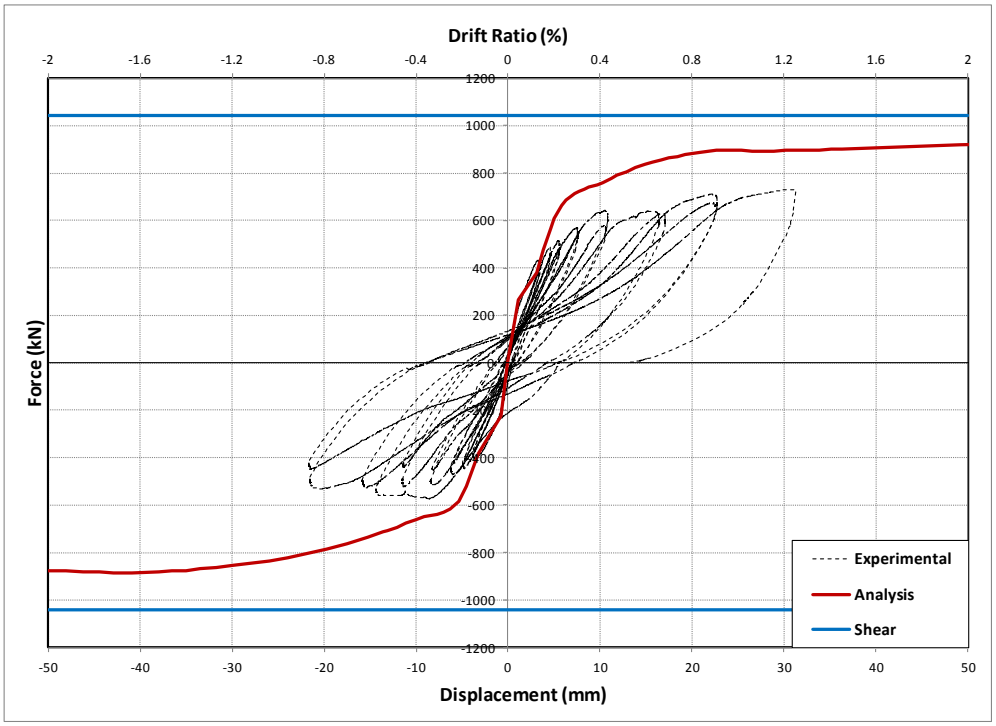

Figure 3-30: Comparison of Flexural and Shear Capacity of Specimen 3 According to TEC2007

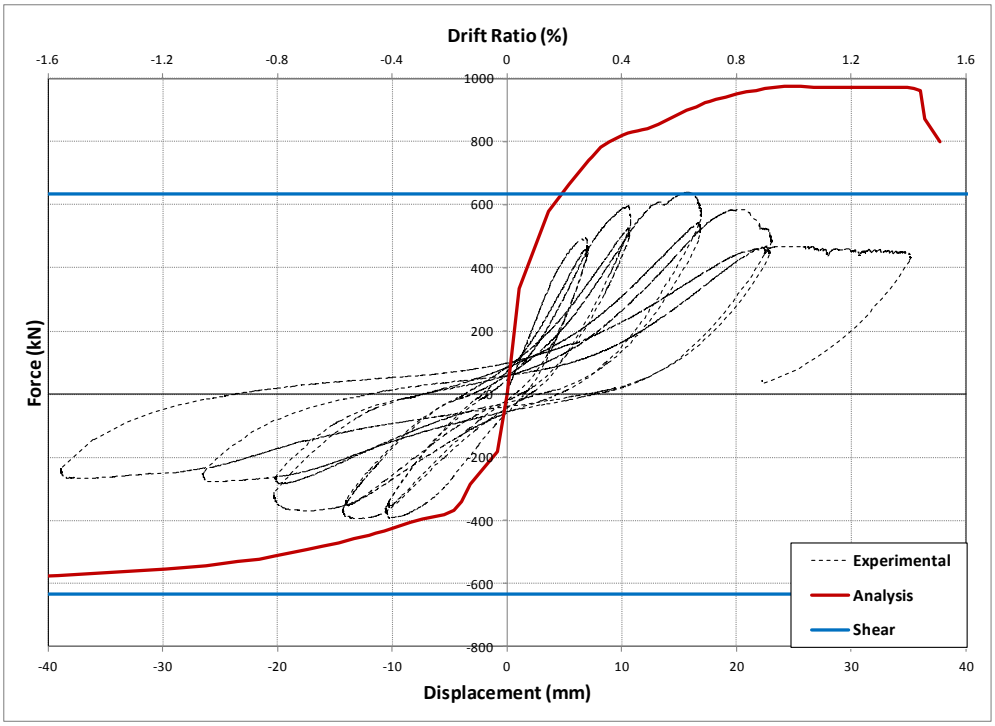

Figure 3-31: Comparison of Flexural and Shear Capacity of Specimen 4 According to TEC2007

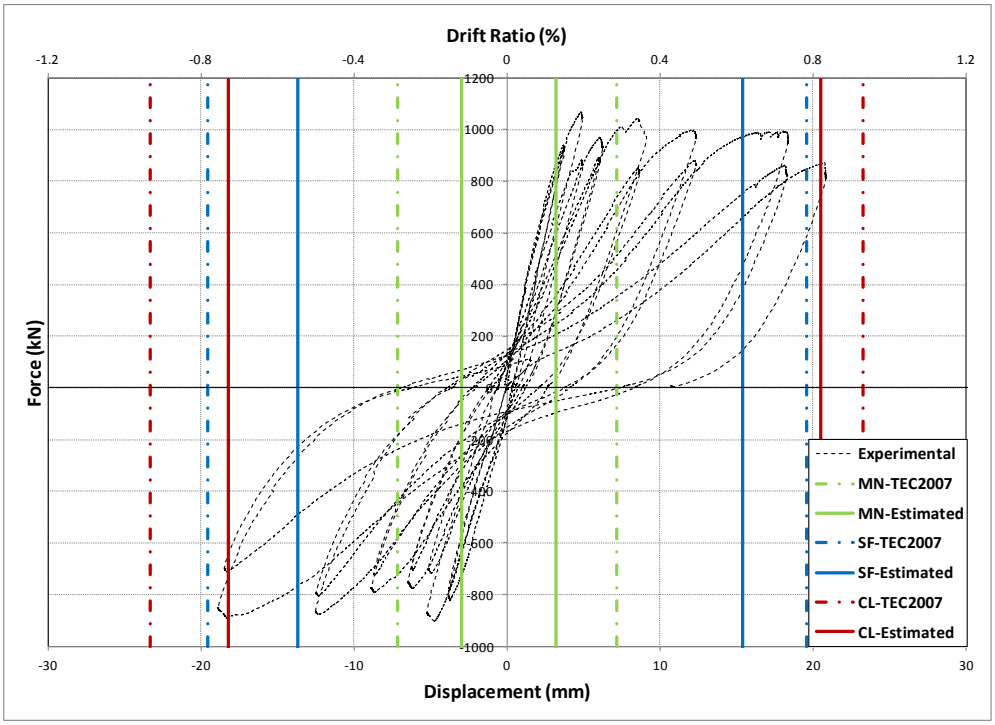

Figure 3-32: Comparison of Experimental Results of Specimen 1 with Damage States According to TEC2007

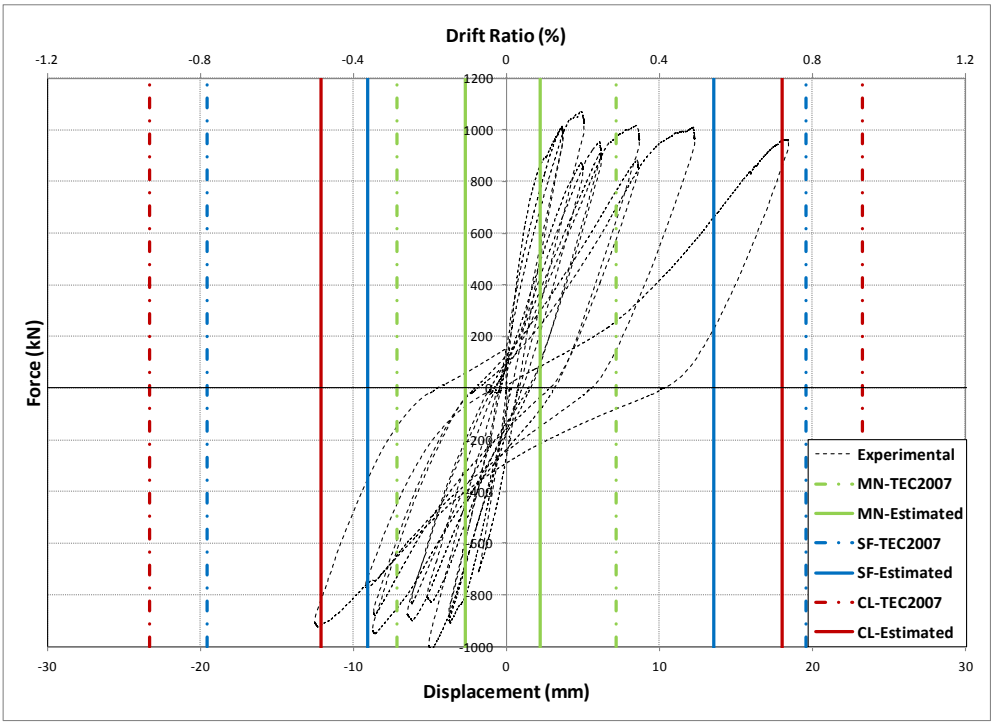

Figure 3-33: Comparison of Experimental Results of Specimen 2 with Damage States According to TEC 2007

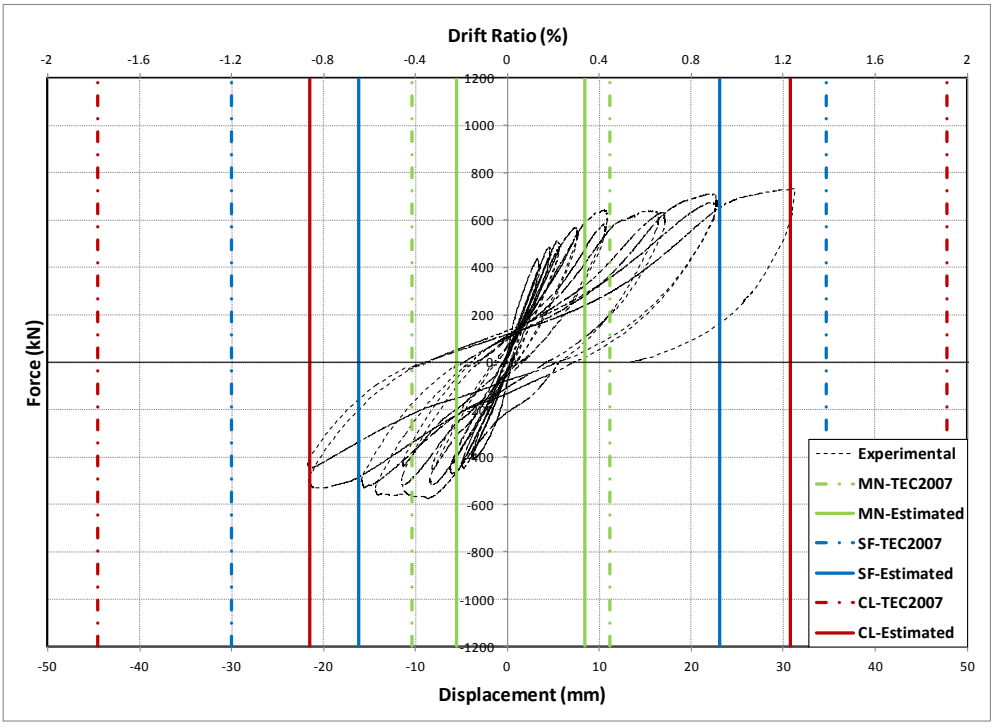

Figure 3-34: Comparison of Experimental Results of Specimen 3 with Damage States According to TEC 2007

3.6 Discussion of the Results

In order to summarize the performance evaluation performed in previous sections, a thorough comparison of the results obtained from different seismic guidelines are presented in Table 3-6 and Table 3-7. Regarding performance limits, Immediate Occupancy were overestimated by all codes, however in shear-controlled walls, this state have a better estimation by ASCE. In flexure-controlled members, Collapse Prevention is best predicted by EC8, while in shear-controlled members ASCE-06 provides a good estimation for this state. Among codes, the updated version of ASCE (ASCE/SEI-41-13) overestimates the performance limits, which results in unsafe predictions.

Comparing the shear capacities of the brittle specimens specified by the codes, ACI318 provides the closest value with respect to test result for specimen 3, while in case of specimen 4, the best estimate is provided by TEC2007. However, TEC2007 provides a completely different result for specimen 3 by determining a high shear capacity in comparison with other codes. Accordingly, the failure mode obtained for this specimen is specified as ductile failure, which is not in accordance with other codes and experimental observations. Capacity estimations provided for first 2 specimens are well-estimated by all codes, while in specimens 3 and 4 the best estimation is obtained according to ASCE. Eurocode provides a good prediction regarding the failure mechanisms of specimens, whereas in TEC2007 it cannot be properly estimated.

Table 3-6: Comparison of the Criteria Proposed by Seismic Guidelines with Experimental Response of Specimens 1 and 2

		ASCE/SEI41-06		ASCE/SEI41-13		Eurocode 8		TEC2007		Experimental	
		(-)	(+)	(-)	(+)	(-)	(+)	(-)	(+)	(-)	(+)
Specimen 1	V_{flex} (kN)	-1017	1077	-1017	1077	-925	925	-925	925	-903	1069
	V_{sh} (kN)	-1645	1645	-1645	1645	-1101	1101	-1772	1772		
	IO (mm)	-8.16	8.16	-8.16	8.16	-9.4	9.4	-7.15	7.15	-2.95	3.2
	LS (mm)	-13.06	13.06	-22.86	22.86	-17.44	17.44	-19.6	19.6	-13.65	15.375
	CP (mm)	-22.86	22.86	-40.01	40.01	-19.18	19.18	-23.31	23.31	-18.2	20.5
	Failure Mode	Flexure		Flexure		Flexure		Flexure		Flexure-Shear	
Specimen 2	V_{flex} (kN)	-1017	1077	-1017	1077	-925	925	-925	925	-1017	1072
	V_{sh} (kN)	-1645	1645	-1645	1645	-1101	1101	-1772	1772		
	IO (mm)	-8.16	8.16	-8.16	8.16	-9.4	9.4	-7.15	7.15	-2.7	2.2
	LS (mm)	-13.06	13.06	-22.86	22.86	-17.44	17.44	-19.6	19.6	-9.08	13.54
	CP (mm)	-22.86	22.86	-40.01	40.01	-19.18	19.18	-23.31	23.31	-12.1	18.05
	Failure Mode	Flexure		Flexure		Flexure		Flexure		Flexure-Shear	

Table 3-7: Comparison of the Criteria Proposed by Seismic Guidlines with Experimental Response of Specimens 3 and 4

		ASCE/SEI41-06		ASCE/SEI41-13		Eurocode 8		TEC2007		Experimental	
		(-)	(+)	(-)	(+)	(-)	(+)	(-)	(+)	(-)	(+)
Specimen 3	**V_{flex} (kN)**	-873	863	-873	863	-715	836	-715	836	-572	732
	V_{sh} (kN)	-687	687	-687	687	-827	827	-1043	1043		
	IO (mm)	-9.8	9.8	-9.8	9.8	-	-	-10.3	11.2	-5.5	8.4
	LS (mm)	-18.4	18.4	-36.8	-36.8	-	-	-30	34.5	-16.1	23.1
	CP (mm)	-24.5	24.5	-49	49	-	-	-44.5	47.9	-21.5	30.8
	Failure Mode	Shear		Shear		Flexure-Shear		Flexure		Flexure-Shear	
Specimen 4	**V_{flex} (kN)**	-597	918	-597	918	-440	928	-440	928	-393	639
	V_{sh} (kN)	-459	459	-459	459	-590	590	-635	635		
	IO (mm)	-9.8	9.8	-9.8	9.8	-	-	-	-	-6.4	6.5
	LS (mm)	-18.4	18.4	-36.8	-36.8	-	-	-	-	-15.2	17.2
	CP (mm)	-24.5	24.5	-49	49	-	-	-	-	-20.3	23
	Failure Mode	Shear		Shear		Shear		Shear		Flexure-Shear	

CHAPTER 4

BUILDING DESIGN

4.1 General

This section is assigned to analysis and design and afterwards, performance assessment of a building incorporating the double wall system. An 8-story building located in high seismic zone is proposed. The load carrying system is composed of double wall system and the slab system is considered as a filigree slab for all floors. A typical plan showing the location of double walls is presented in Figure 4-1. The typical story height is considered as 3m in this project.

Code requirements of Turkish Earthquake Code-2007 (TEC 2007) were used for the structural design. The function of the building is for the purpose of accommodation, thus according to Table 2-3 in TDY 2007, corresponds to an importance factor of 1.0. The seismic design criteria for the shear wall structure and its site are summarized in Table 4-1. The seismic design response spectrum for the building is presented in Figure 4-2.

The building was designed considering the influences of vertical loads and earthquake induced lateral loads. The considered vertical loads are:

- Gravity Loads:

- Concrete specific weight for member loads: 2.5 t/m^3
- Dead loads considered for slabs: 0.237 t/m^2

- Live Loads:

  Typical floor levels: 0.2 t/m^2

Table 4-1: Seismic Design Criteria

Seismic Design Criteria	
Earthquake Zone	1. Zone
Effective Ground Acceleration Coeficient (A_0)	0.4
Behavior Factor (R)	5
Importance Factor (I)	1
Site Class	Z2

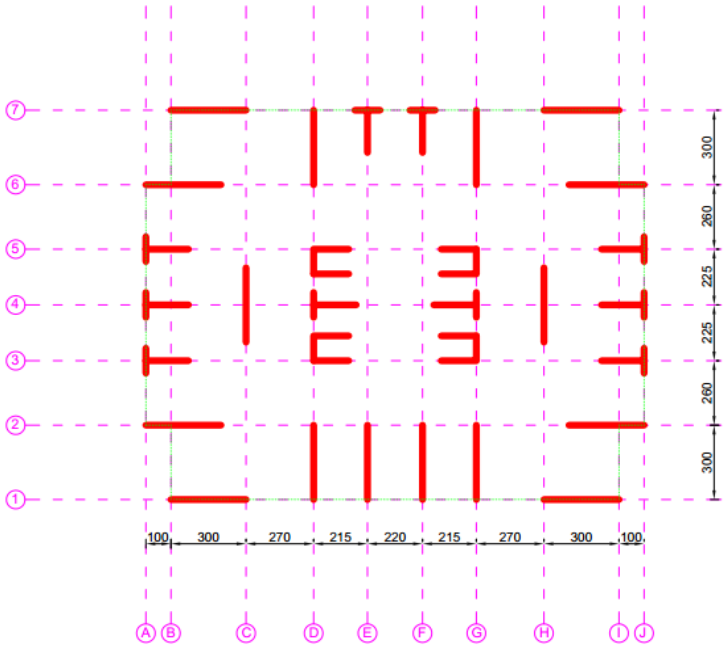

Figure 4-1 Proposed Building Plan

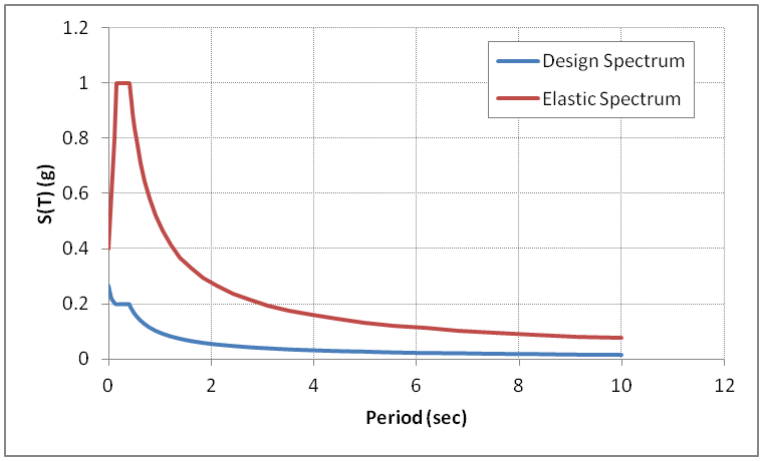

Figure 4-2: Design Spectrum According to TDY 2007

Structural modeling and analysis of the building was conducted using PROBINA ORION program. Modal combination approach using Complete Quadratic Combination (CQC) was employed for the earthquake analysis. Number of modes considered for the analysis was selected such that at least 90% of mass participation was accounted. The design spectrum shown in Figure 4-2 was used to define the effect of earthquake forces. In addition to the gravity load combinations defined as 1.4D+1.6L (D: Dead, L: Live), $1.0D\pm1.0L\pm E_x$, $1.0D\pm1.0L\pm E_y$, $1.0D\pm1.0L\pm E_x\pm 0.3E_y$, $1.0D\pm1.0L\pm E_y\pm 0.3E_x$ combinations were used to determine the critical actions under combined effects of gravity and earthquake loads. Complete load combinations used for this project is presented in Table 4-2. For these load combinations live loads were reduced by a factor of 0.3 to consider the reduced likelihood of full live load acting with earthquake loads.

The building system was selected as an special ductile building system. The mathematical model of the building was prepared by using finite elements (shell elements) for the slabs and middle column model for walls. The building model is shown in Figure 4-3. Building base was fixed against rotations and translations. Structural members for earthquake analysis was considered uncracked and rigid diaphragms were assigned at each level.

Table 4-2: Load Combinations

No	Combination	G	Q	QS1	QS2	SX+	SX-	SY+	SY-
1	G+Q *F	1.4	1.6	0	0	0	0	0	0
2	G+QS1 *F	1.4	0	1.6	0	0	0	0	0
3	G+QS2 *F	1.4	0	0	1.6	0	0	0	0
4	G+Q+Sx+	1	1	0	0	1	0	0	0.3
5	G+Q-Sx+	1	1	0	0	-1	0	0	-0.3
6	G+Q+Sx-	1	1	0	0	0	1	0.3	0
7	G+Q-Sx-	1	1	0	0	0	-1	-0.3	0
8	G+Q+Sy+	1	1	0	0	0	0.3	1	0
9	G+Q-Sy+	1	1	0	0	0	-0.3	-1	0
10	G+Q+Sy-	1	1	0	0	0.3	0	0	1
11	G+Q-Sy-	1	1	0	0	-0.3	0	0	-1
12	G+Sx+	0.9	0	0	0	1	0	0	0.3
13	G-Sx+	0.9	0	0	0	-1	0	0	-0.3
14	G+Sx-	0.9	0	0	0	0	1	0.3	0
15	G-Sx-	0.9	0	0	0	0	-1	-0.3	0
16	G+Sy+	0.9	0	0	0	0	0.3	1	0
17	G-Sy+	0.9	0	0	0	0	-0.3	-1	0
18	G+Sy-	0.9	0	0	0	0.3	0	0	1
19	G-Sy-	0.9	0	0	0	-0.3	0	0	-1

Following material properties were assumed during the course of modeling:

Table 4-3: Material Properties

Members	**Concrete**		**Reinforcement Steel**	
	f_{ck} (MPa)	E_c (MPa)	f_{yk} (MPa)	E_s (MPa)
Walls	35	33200	420	200000
Slabs	25	30250	420	200000

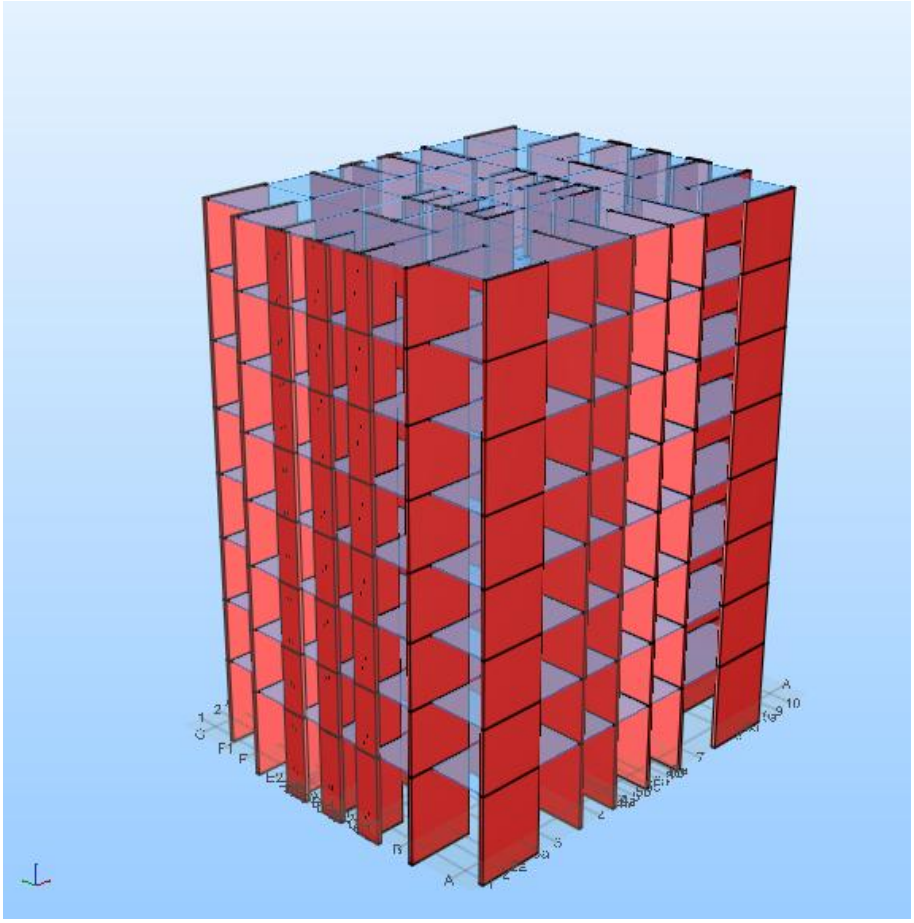

Figure 4-3: PROBINA Model

Total building weight was found as 2621.355 tons for the combined action of dead and reduced live loads used for the seismic analysis.

4.2 Analysis Results

The building vibration periods and the cumulative mass participation factors for three directions are presented in Table 4-4. First five mode shapes are shown in Figure 4-4. It can be observed that considering about 12 modes resulted in about 95% of all the mass participation which is regarded to be sufficiently accurate for response spectrum analysis. One irregularity regarding the elevation, soft story irregularity, were encountered. According to TDY 2007, all internal force and displacement quantities determined by *Mode Superposition Method* shall be amplified in

accordance with equation below with considering β=0.9 (Due to the *soft story* irregularity).

$$B_D = \frac{\beta V_t}{V_{tB}} B_B \qquad (4\text{-}1)$$

Base shear forces calculated using modal combination method are determined as 2313.77 kN in the x direction and 2178.42 kN in the y direction. The expected building story drift ratio (difference between lateral deformations of two consecutive floors divided by the story height) is presented in Table 4-5 to Table 4-8. It can be observed that building has sufficient rigidity in the lateral direction as the computed drift ratios for both directions are below the allowed 2% limit.

Table 4-4: Building Vibration Periods and Cumulative Mass Participations

MODE	PERIOD	UX	UY	RZ	SUM UX	SUM UY	SUM RZ
1	0.92616	0.013839	0	65.91148	0.013839	0	65.91148
2	0.888305	0	65.76969	0	0.013839	65.76969	65.91148
3	0.802811	65.66916	0	0.013705	65.68299	65.76969	65.92518
4	0.159425	0.005178	0	20.43547	65.68817	65.76969	86.36066
5	0.149284	0	20.70527	0	65.68817	86.47496	86.36066
6	0.133357	20.66018	0	0.004738	86.34835	86.47496	86.36539
7	0.061309	0.002942	0	7.058669	86.35129	86.47496	93.42406
8	0.057625	0	7.067998	0	86.35129	93.54296	93.42406
9	0.050942	7.125303	0	0.002636	93.4766	93.54296	93.4267
10	0.034444	0.002277	0	3.411384	93.47887	93.54296	96.83808
11	0.032599	0	3.392589	0	93.47887	96.93555	96.83808
12	0.028607	3.446103	0	0.002162	96.92497	96.93555	96.84024

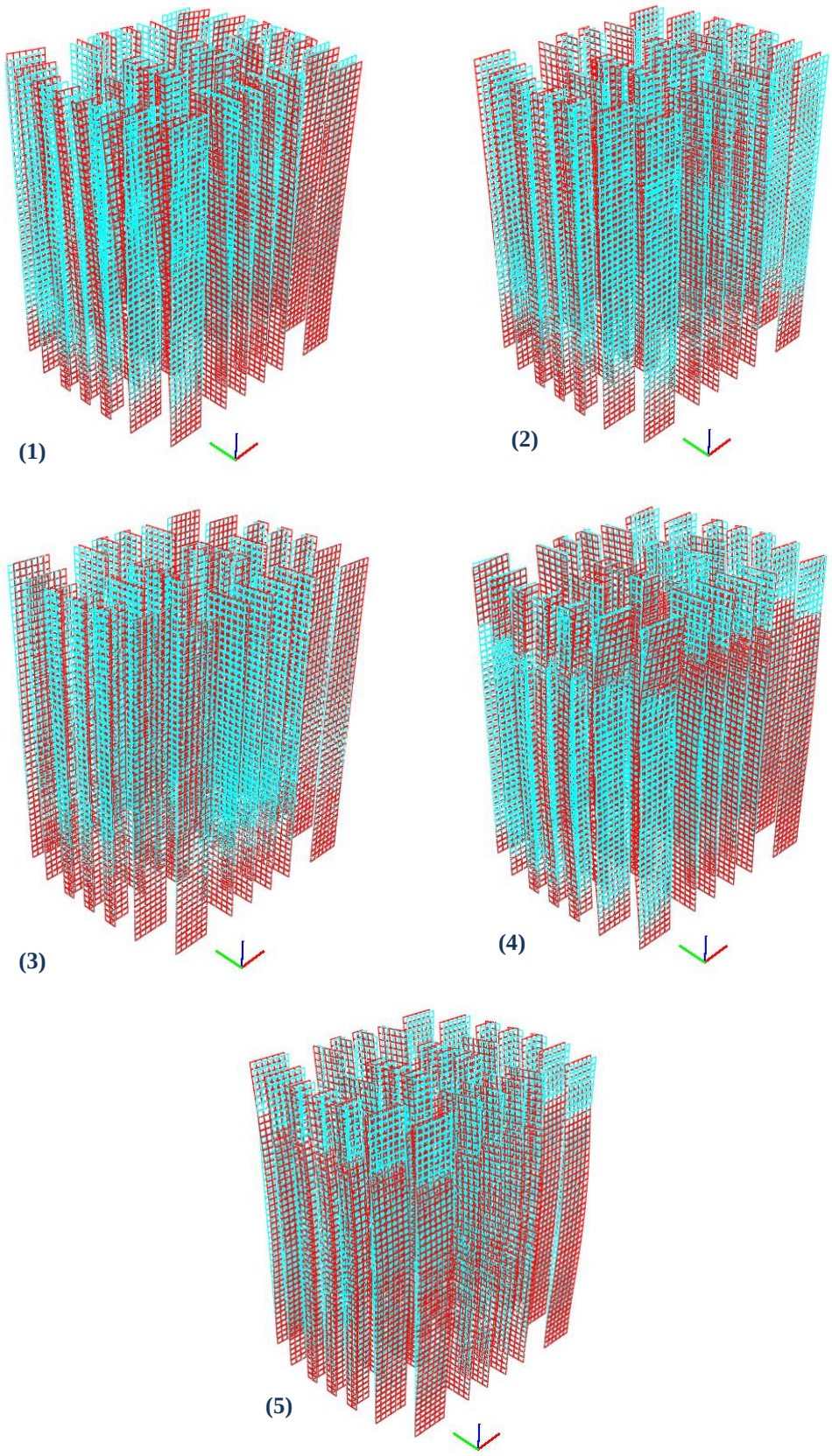

Figure 4-4: First Five Modes Shapes

Table 4-5: Drift Ratio Comparison Under Lateral Load SX+

Floor	Max. Drift(D_i) (m)	Relative Drift (D_i - D_{i-1}) (m)	Effective Drift (D_i - D_{i-1} x R) (m)	Effective Drift Ratio (D_i - D_{i-1} x R)/h	Limit
8	0.035743	0.006205	0.031026	0.010342	0.02
7	0.029537	0.00612	0.030602	0.010201	0.02
6	0.023417	0.005883	0.029414	0.009805	0.02
5	0.017534	0.005442	0.02721	0.00907	0.02
4	0.012092	0.004759	0.023796	0.007932	0.02
3	0.007333	0.003804	0.019019	0.00634	0.02
2	0.003529	0.002551	0.012755	0.004252	0.02
1	0.000978	0.000978	0.004891	0.00163	0.02

Table 4-6: Drift Ratio Comparison Under Lateral Load SX-

Floor	Max. Drift(D_i) (m)	Relative Drift (D_i - D_{i-1}) (m)	Effective Drift (D_i - D_{i-1} x R) (m)	Effective Drift Ratio (D_i - D_{i-1} x R)/h	Limit
8	0.035252	0.006119	0.030593	0.010198	0.02
7	0.029133	0.006035	0.030177	0.010059	0.02
6	0.023098	0.005801	0.029007	0.009669	0.02
5	0.017296	0.005367	0.026834	0.008945	0.02
4	0.011929	0.004694	0.023469	0.007823	0.02
3	0.007236	0.003752	0.018759	0.006253	0.02
2	0.003484	0.002517	0.012583	0.004194	0.02
1	0.000967	0.000967	0.004837	0.001612	0.02

Table 4-7: Drift Ratio Comparison Under Lateral Load SY+

Floor	Max. Drift(D_i) (m)	Relative Drift (D_i - D_{i-1}) (m)	Effective Drift (D_i - D_{i-1} x R) (m)	Effective Drift Ratio (D_i - D_{i-1} x R)/h	Limit
8	0.040785	0.007062	0.035309	0.01177	0.02
7	0.033723	0.006968	0.034842	0.011614	0.02
6	0.026755	0.006702	0.03351	0.01117	0.02
5	0.020053	0.006205	0.031025	0.010342	0.02
4	0.013848	0.005434	0.027168	0.009056	0.02
3	0.008414	0.004352	0.02176	0.007253	0.02
2	0.004062	0.00293	0.014649	0.004883	0.02
1	0.001132	0.001132	0.005662	0.001887	0.02

Table 4-8: Drift Ratio Comparison Under Lateral Load SY-

Floor	Max. Drift(D_i) (m)	Relative Drift (D_i - D_{i-1}) (m)	Effective Drift (D_i - D_{i-1} x R) (m)	Effective Drift Ratio (D_i - D_{i-1} x R)/h	Limit
8	0.040785	0.007062	0.035309	0.01177	0.02
7	0.033723	0.006968	0.034842	0.011614	0.02
6	0.026755	0.006702	0.03351	0.01117	0.02
5	0.020053	0.006205	0.031025	0.010342	0.02
4	0.013848	0.005434	0.027168	0.009056	0.02
3	0.008414	0.004352	0.02176	0.007253	0.02
2	0.004062	0.00293	0.014649	0.004883	0.02
1	0.001132	0.001132	0.005662	0.001887	0.02

4.3 Wall Design

For the design of walls following steps were conducted:

- Internal forces (axial forces, shear forces, bending moments) from all load combinations were obtained.
- Reinforcement amounts of longitudinal and transverse steel were estimated.
- Bending capacity was controlled by ensuring that all the demand points are within the interaction diagrams
- Shear strength was checked according to TDY (2007) (Turkish Earthquake Code) and ACI 318-11 standards
- Reinforcement details were provided following TDY (2007) for the transverse reinforcement, internal ties and boundary regions.

Typical wall design calculations are summarized in Figure 4-6 to Figure 4-8 for selected U-shaped, T-shaped , and rectangular shaped walls, on 1st floor, respectively. The location of selected walls is specified in the plan by blue lines (Figure 4-5). Wire mesh reinforcement along with deformed bars was used in the design of structural elements. Afterwards, the design of the system with the cast in place reinforced concrete system was converted into a double wall system.

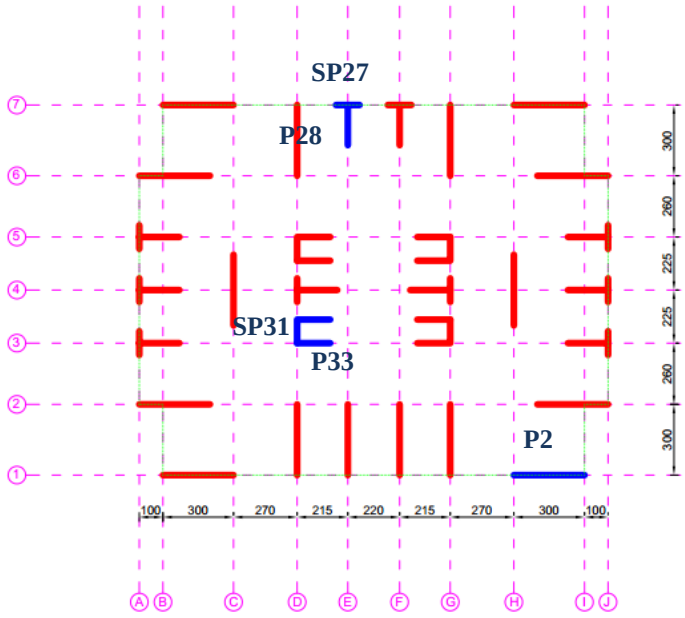

Figure 4-5: Location of Selected Walls

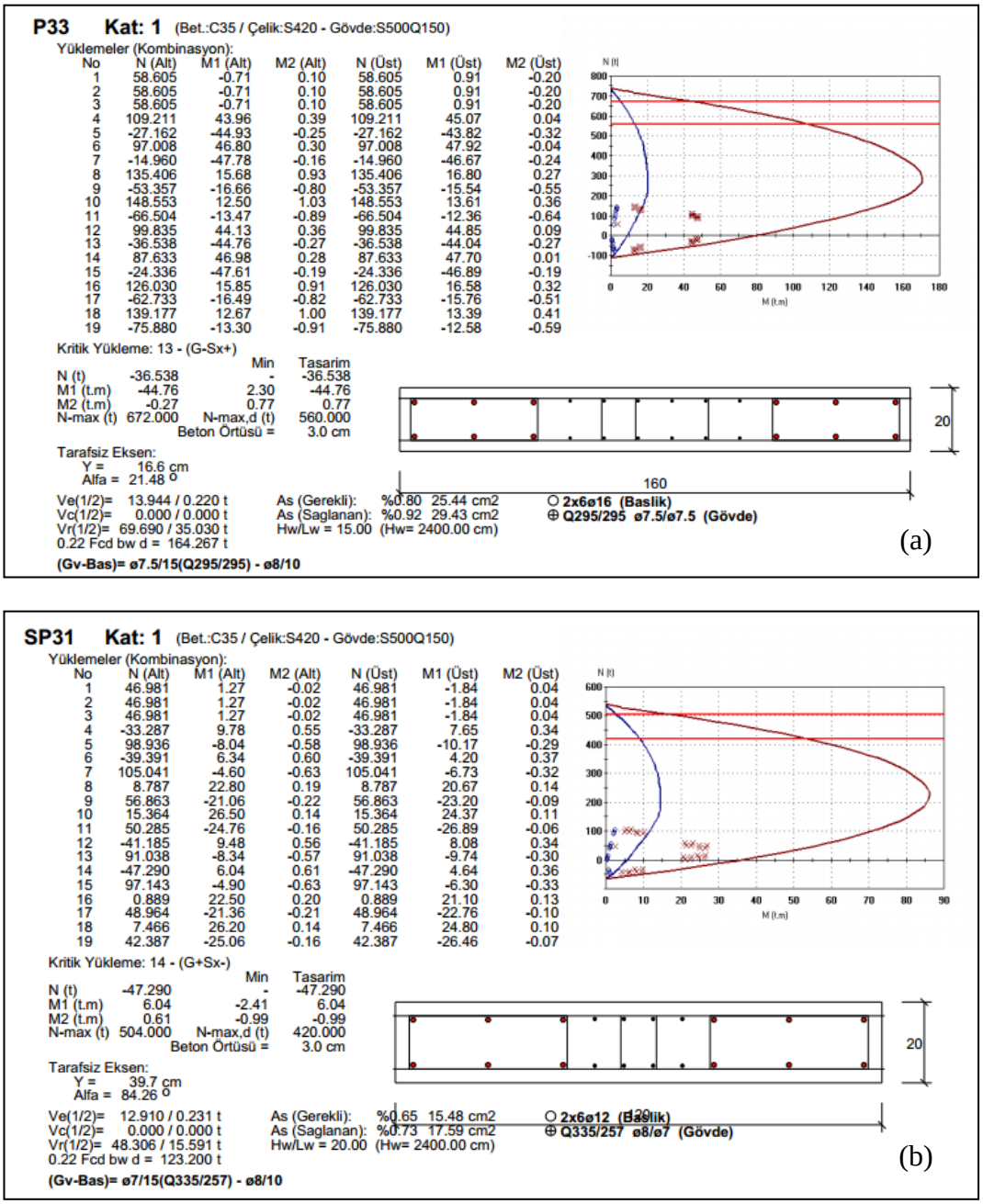

Figure 4-6: Reinforcement Calculation Summary for a Typical U-Shaped Wall; (a) Web, (b) Flange

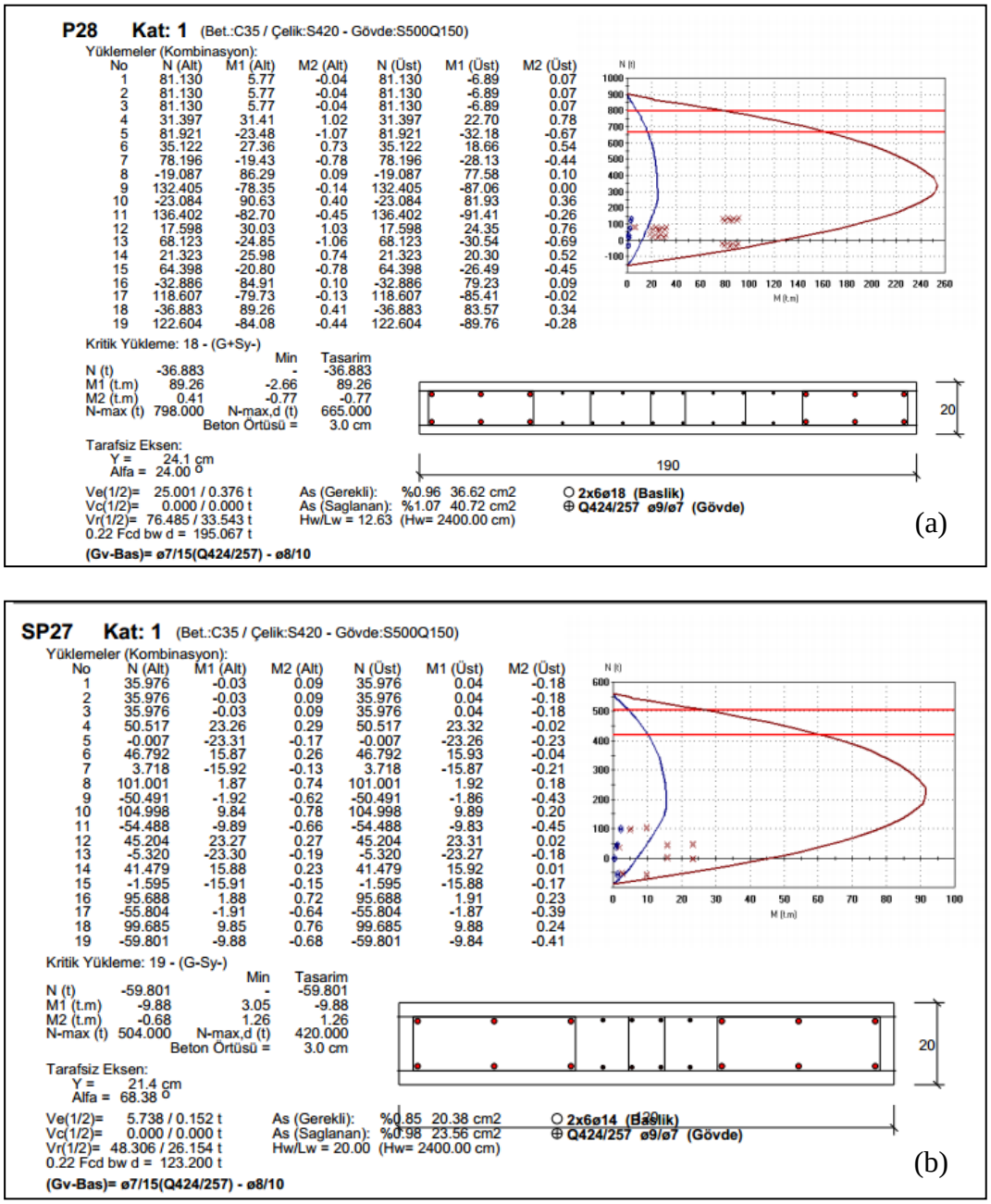

Figure 4-7: Reinforcement Calculation Summary for a Typical T-Shaped Wall; (a)Web, (b) Flange

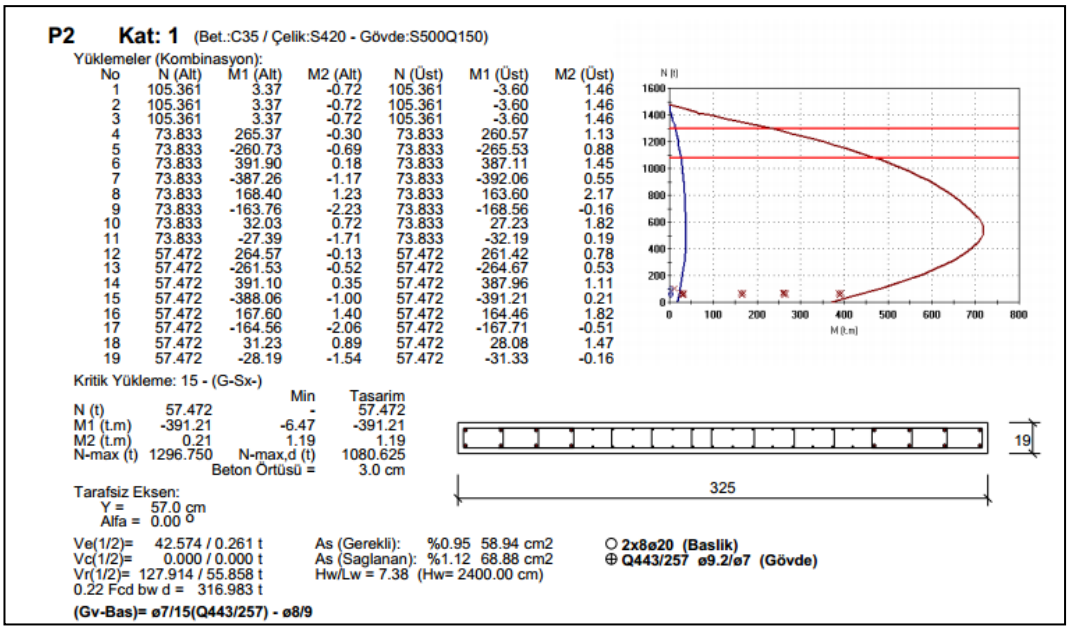

Figure 4-8: Reinforcement Calculation Summary for a Typical Rectangular Wall

Considering the examples above, It can be observed that the applied loads can be carried safely for the reinforcement pattern. These calculated reinforcement amount satisfies the minimum reinforcement calculated according to TDY 2007/TS500 min reinforcement requirements.

4.4 Equivalent Double Walls

After obtaining the wall reinforcement, the design of monolithic walls was converted into a double wall system. The mesh reinforcement was used as the main reinforcement of the shells whereas additional longitudinal reinforcement was assumes in order to satisfy the requirements of boundary zone reinforcement. The connection between adjacent double walls was established by placing horizontal connection cages. With the purpose of modeling cross ties in double wall conversion process, the waves were used owing to the experimental evidence described in Chapter 2. As indicated by TDY 2007, it is required to use 4- 8 mm diameter cross ties with a yield strength of 420 MPa at every wall square meter for ordinary shear

walls. Taking into account that the yield strength of waves is 550 MPa, the necessary amount of waves with 4 mm diameter per leg is 2.5 per meter square. This amount of waves is already available to bear against pressures during concrete casting. The aforementioned procedure outlined for one wall is repeated for all walls in order to convert a regular reinforced concrete design into a double wall configuration. This conversion process is explained for three typical rectangular, U-shaped, and T-shaped walls, which reinforcement calculations were summarized in previous section.

4.4.1 Rectangular Wall

Reinforcement details designed for wall "P2" at 1st story is presented in Figure 4-9. As mentioned before, mesh reinforcement is considered as the main reinforcement of shells. In order to provide additional bars for end zone, length of end zones shall be calculated according to TDY 2007.

Code. $\quad Along\ the\ critical\ height \quad \rightarrow \quad l_u \geq max\ (0.2l_w, 2b_w)$

$$l_u \geq \max(0.2 \times 3, 2 \times 0.2) = \max(0.6, 0.4) = 0.6\ \text{m}$$

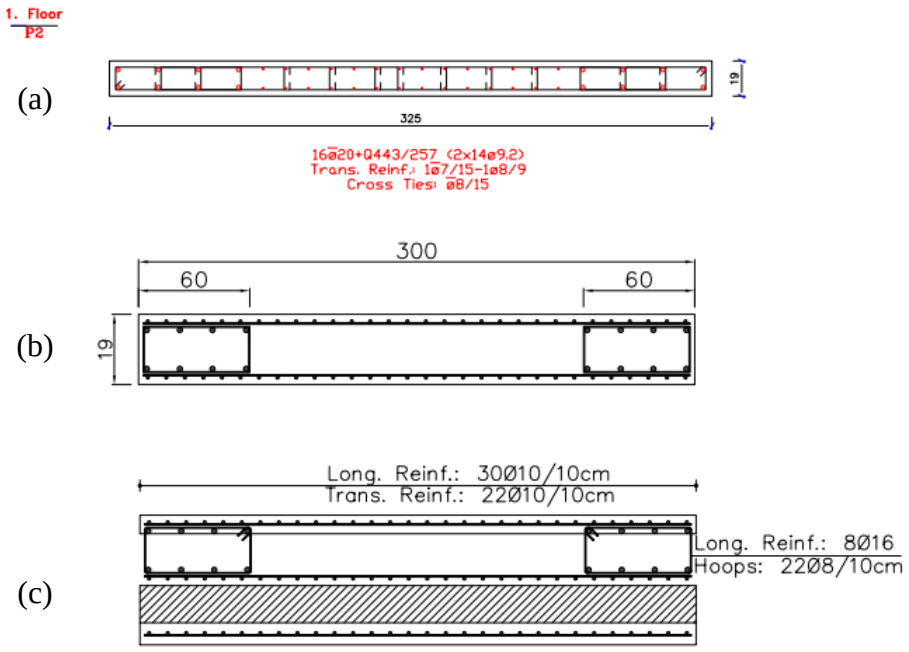

Figure 4-9: "P2" Double Wall Conversion; (a) Monolithic Wall, (b) Structural Part of Equivalent Double Wall, (c) Equivalent Double Wall

Along 60cm from each end points, additional bars are considered so that the equivalent bar area is obtained and TDY 2007 regulations are respected.

In cast-in-place wall, area of 8 ϕ20: 2513.27 mm^2

In double wall, area of 2x6 ϕ10 + 2x4 ϕ16 : 2550 mm^2

4.4.2 U-Shaped Wall

Reinforcement details designed for wall "P33" and "SP31" at 1st story is presented inFigure 4-10. As mentioned before, mesh reinforcement is considered as the main reinforcement of shells. In order to provide additional bars for end zone, length of end zones shall be calculated according to TDY 2007.

For Web Part:

<u>Code.</u> $Along\ the\ critical\ height \rightarrow l_u \geq max\ (0.2l_w, 2b_w)$

$$l_u \geq \max(0.2 \times 1.4, 2 \times 0.2) = \max(0.28, 0.4) = 0.4\ \text{m}$$

Along 40cm from each end points, additional bars are considered so that the equivalent bar area is obtained and TDY 2007 regulations are respected.

In cast-in-place wall, area of 6 ϕ16: 1206.37 mm^2

In double wall, area of 2x4 ϕ8 + 2x4 ϕ12 : 1306.9 mm^2

For Flange Part:

<u>Code.</u> $Along\ the\ critical\ height \rightarrow l_u \geq max\ (0.2l_w, 2b_w)$

$$l_u \geq \max(0.2 \times 1, 2 \times 0.2) = \max(0.2, 0.4) = 0.4\ \text{m}$$

Along 40cm from each end points, additional bars are considered so that the equivalent bar area is obtained and TDY 2007 regulations are respected.

In cast-in-place wall, area of 6 ϕ12: 678.58 mm^2

In double wall, area of 2x4 ϕ8 + 2x4 ϕ8 : 804.25 mm^2

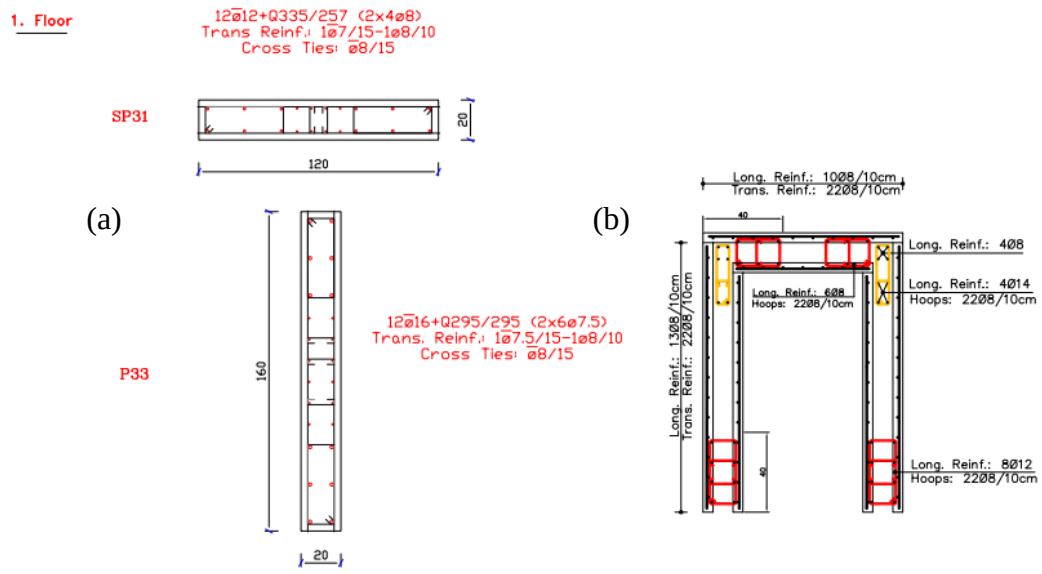

Figure 4-10: "P33" and "SP31" Double Wall Conversion; (a) Monolithic Wall, (b) Equivalent Double Wall

4.4.3 T-Shaped Wall

Reinforcement details designed for wall "P28" and "SP27" at 1st story is presented in Figure 4-11. As mentioned before, mesh reinforcement is considered as the main reinforcement of shells. In order to provide additional bars for end zone, length of end zones shall be calculated according to TDY 2007.

For Web Part:

Code. $\quad Along\ the\ critical\ height \quad \rightarrow \quad l_u \geq max\ (0.2l_w, 2b_w)$

$$l_u \geq \max(0.2 \times 1.7, 2 \times 0.2) = \max(0.34, 0.4) = 0.4\ \text{m}$$

Along 40cm from each end points, additional bars are considered so that the equivalent bar area is obtained and TDY 2007 regulations are respected.

In cast-in-place wall, area of 6 ϕ18: 1526.81 mm^2

In double wall, area of 2x4 ϕ10 + 2x4 ϕ12 : 1533.1 mm^2

For Flange Part:

Code. $Along\ the\ critical\ height \rightarrow l_u \geq max\ (0.2l_w, 2b_w)$

$$l_u \geq \max(0.2 \times 1, 2 \times 0.2) = \max(0.2, 0.4) = 0.4\ \text{m}$$

Along 40cm from each end points, additional bars are considered so that the equivalent bar area is obtained and TDY 2007 regulations are respected.

In cast-in-place wall, area of 6 ϕ14: 923.63 mm^2

In double wall, area of 2x4 ϕ10 + 2x4 ϕ8 : 1030.44 mm^2

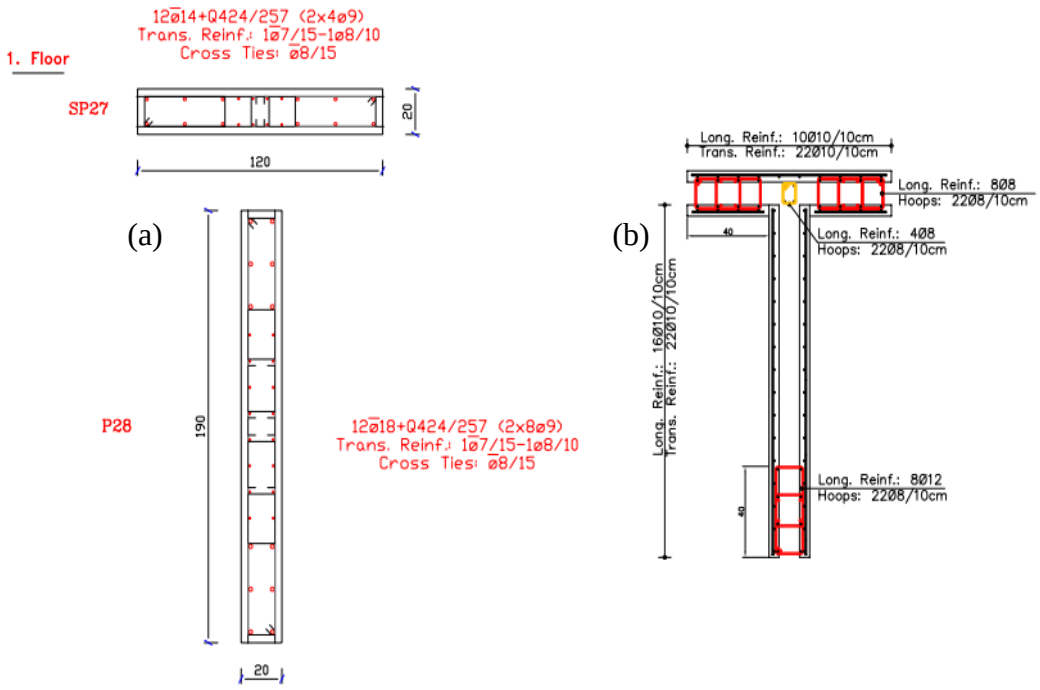

Figure 4-11: "P28" and "SP27" Double Wall Conversion; (a) Monolithic Wall, (b) Equivalent Double Wall

4.5 Assessment According to TEC2007

As explained in previous section, ultimate strain limits regarding each state, for both concrete and steel, must be determined in detailed assessment procedure of TEC2007. Afterwards, the overall structural performance can be obtained by specifying the distribution of member damages over the building. The related rules according to TEC2007 are as follows:

- **Immediate Occupancy:** Up to 10 percent of the beams in the direction of the earthquake loads at any story, are in the significant damage state, beyond the MN limit. All other structural members shall be in the minimum damage state.
- **Life Safety:** Up to 30 percent of the beams and a proportion of the columns are in the extreme damage state, beyond the SF limit. All other structural members should be in the minimum or significant damage states. Total shear, however, carried by the columns that are in the extreme damage state shall not exceed 20 percent of the story shear at each story.
- **Collapse Prevention:** At any story, in the direction of the applied earthquake loads, up to 20 percent of beams are in the collapse state, beyond the CL limit. All other structural members are in the minimum, significant or extreme damage states. However, total shear carried by the columns, whose both the top and bottom sections are beyond the MN limit, shall not exceed 30 percent of the story shear at each story. In other words, such columns should not lead to a stability loss.
- **Collapse:** If the building fails to satisfy the CP performance level above, it is decided to be in the collapse state.

According to TEC2007, the limit state for residential buildings shall be Life Safety, under an expected earthquake with a probability of exceedance of 10 percent in 50 years.

In order to evaluate the performance of the building designed in previous section, a nonlinear static analysis (pushover analysis) was performed. The slab of each floor was idealized as rigid diaphragm and was modeled as shell elements. Degrees of freedom in two perpendicular horizontal directions and rotation around the axis passing through the center of mass of the building were considered. Regarding reinforced concrete element under flexure, effective stiffness values for cracked section given in TEC2007 were used. For all walls, axial load values were determined considering all vertical loadings (G+0.3Q). After performing the analysis and determining the required performance state, plastic hinge locations, plastic hinge rotation and hence, plastic curvature may be calculated. By adding the yielding curvature (the point where the plastic behavior begins) to plastic curvature, the total demand curvature of each section is attained. Considering the critical section of each wall, the concrete and reinforcement strain related to the demand curvature were determined using the moment-curvature analysis developed in Chapter 2. After evaluating the performance state related to demand curvatures for each element, total performance state of the building can be specified. In this study, this procedure was performed for the elements of the critical story, the ground story.

Before this process, the shear capacity investigation and comparison regarding the failure modes (i.e. brittle failure and ductile failure) are done; capacity values of the walls were compared with the shear demand values obtained from the nonlinear analysis. The results for walls in x-direction and y-direction are presented in Table 4-9 and Table 4-10, respectively. It can be seen that no brittle failure mode is expected and the shear demand value are below the corresponding capacity.

In Figure 4-13, lateral displacement demands calculated from plastic hinge rotation demands using procedures described in Chapter 2, are compared with performance limits specified by TEC2007. It can be concluded that since the building under investigation comprises of significant amount of double walls capable of sufficient seismic performance, all the walls' displacement demands remain in Minimum and

Significant Damage states (before Safety Limit), and hence, this building meets the performance required by TEC2007.

Table 4-9: Comparison of Shear Capacities with Demands for Elements in x-Direction

X-Direction	V_r	V_e	V_d	V_d/V_r
P1 (R)	1772.4	869.2	800	0.451365
P2 (R)	2417.1	1295	800	0.330975
P3 (R)	2417.1	1105.7	750	0.310289
P4 (R)	2417.1	1105.7	750	0.310289
P5 (R)	2417.1	1105.7	750	0.310289
P6 (R)	2417.1	1105.7	750	0.310289
P7 (R)	2417.1	1295	800	0.330975
P8 (R)	2417.1	1295	800	0.330975
P17 (U)	1685.1	519.9	370	0.219572
P18 (U)	1685.1	519.9	370	0.219572
P19 (U)	1685.1	519.9	370	0.219572
P20 (U)	1685.1	519.9	370	0.219572
P21 (T)	1388.4	469.2	320	0.230481
P22 (T)	1388.4	469.2	320	0.230481
P25 (T)	1388.4	469.2	340	0.244886
P26 (T)	1388.4	469.2	320	0.230481
P27 (T)	1388.4	469.1	350	0.252089
P28 (T)	1388.4	469.2	340	0.244886
P29 (T)	1388.4	469.2	320	0.230481
P30 (T)	1388.4	469.2	350	0.252089

The values are in kN.

Table 4-10: Comparison of Shear Capacities with Demands for Elements in y-Direction

Y-Direction	V_r	V_e	V_d	V_d/V_r
P9 (R)	2417.1	1105.7	900	0.372347
P10 (R)	2417.1	1105.7	850	0.351661
P11 (R)	2417.1	1105.7	850	0.351661
P12 (R)	2417.1	1105.7	900	0.372347
P13 (R)	2417.1	1105.7	950	0.393033
P14 (R)	2417.1	1105.7	950	0.393033
P15 (R)	2417.1	1105.7	910	0.376484
P16 (R)	2417.1	11.5.7	910	0.376484
P23 (T)	1388.4	469.2	420	0.302506
P24 (T)	1388.4	469.2	420	0.302506

The values are in kN.

Shear walls are labeled according to Figure 4-12. Response of all walls in ground story, calculated using moment-curvature analysis are provided in Appendix A.

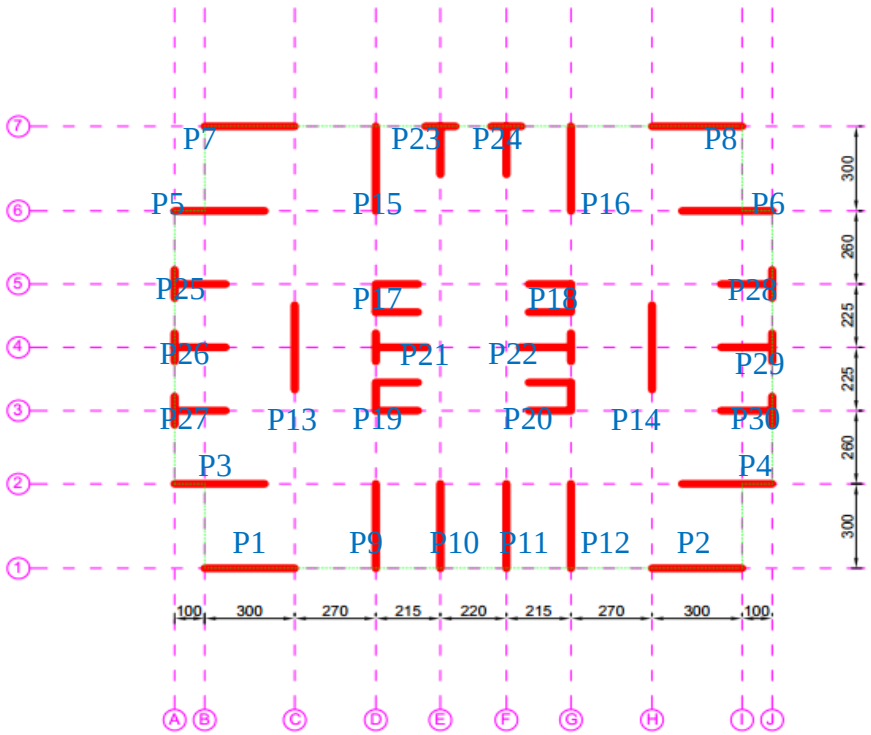

Figure 4-12: Labels of Shear Walls in Ground Story

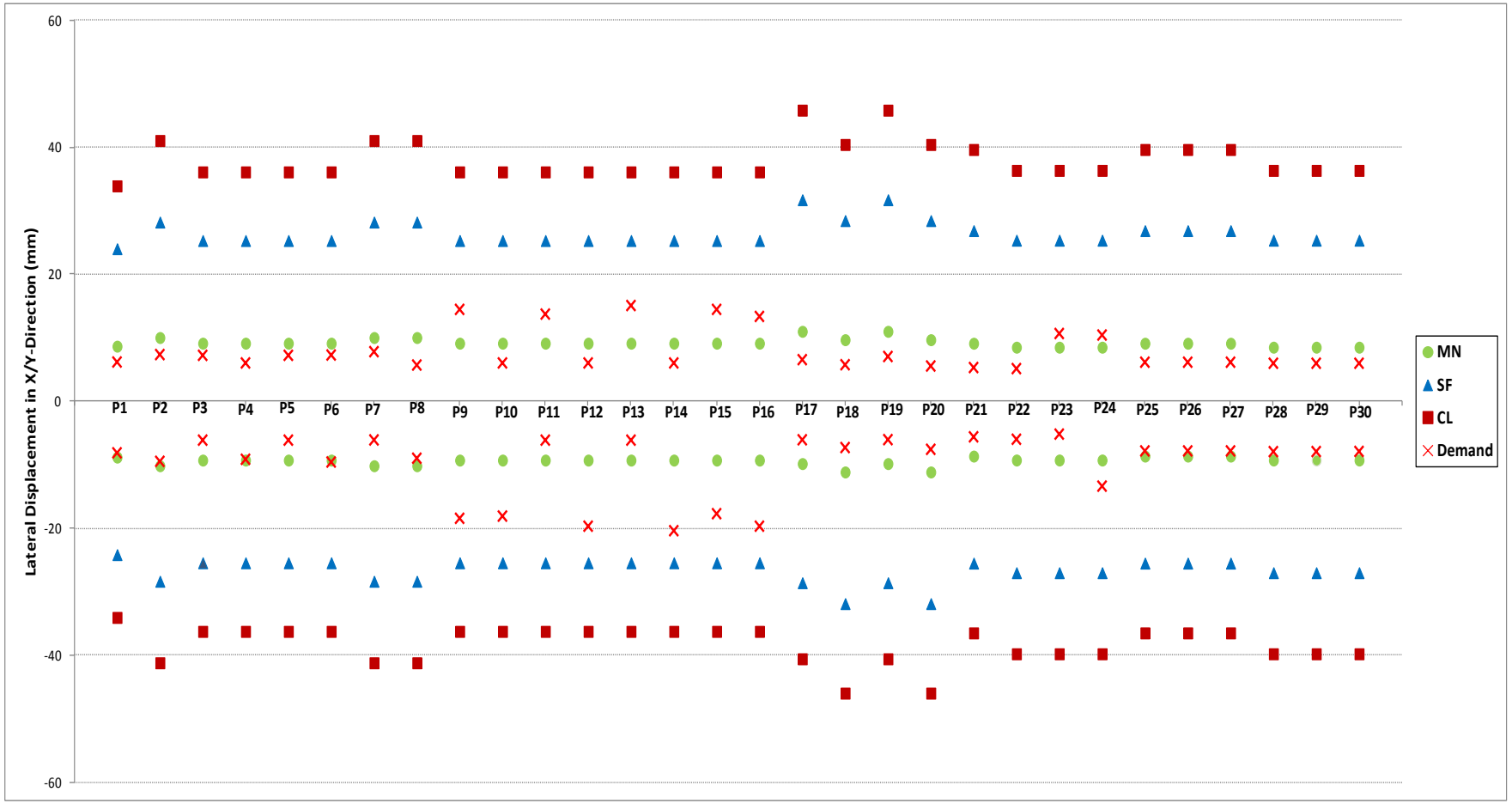

Figure 4-13: Comparison of Lateral Displacement Demands of Ground Story Walls with Performance States According to TEC2007

CHAPTER 5

CONCLUSION

5.1 Summary

The use of precast concrete in construction has gained a significant popularity since 1960's. Although the use of precast components is now well-established in non-seismic countries and they have been utilized as gravity loading members for decades, in high seismic zones, the widespread use of precast concrete construction was hindered due to poor design and construction mistakes done by engineers and contractors. This resulted in an adverse impression and non-monolithic construction has been regarded with suspicious. However, considering the needs of the society, moving forward towards high quality production and fast construction, implementing precast construction for buildings is inevitable. Accordingly, correct techniques has to be utilized for earthquake resistant design of precast concrete structures. Significant research efforts were spent on investigation of earthquake resistant precast details and diaphragms in both North America and Europe with projects such as SAFECAST or NEES based projects, and PRESSS coordinated research program between the United States and Japan on the seismic design and performance of precast concrete structural systems. However, a limited studies have been done regarding the seismic performance of double walls and thus, this study was formed to evaluate the seismic performance of double walls, in order to provide applicable

designing document and to confirm its application as a seismic resisting system in future.

5.2 Conclusions

This study focused on the confirmation of the applicability of the double walls in seismic zones. Through the experimental study of different types of single shear walls, providing the appropriate analytical model, performance assessment of each single wall, and a double wall-incorporated building, seismic behavior of double walls were evaluated. Based on the above study, several useful observations and conclusions are summarized to contribute to better understanding of the double wall's seismic mechanism.

- Comparing the moment curvature results with the experimental results shows that the strength and section response of the double walls can be predicted with standard section analysis procedures of cast-in-place reinforced concrete. This fact enables the use of existing analysis tools for structural design of double wall systems.
- Although specimens 3 and 4 exhibited significant shear strains during the tests and a brittle mode of failure were diagnosed through moment-curvature analysis and performance assessment of the walls, they were able to sustain lateral load considerably and a rather ductile behavior was detected until the ultimate capacity. It can be seen that full ductile behavior may be attained by increasing the shear reinforcement and hence, the shear capacity of the members.
- The range of the displacement ductility levels of the specimens were between about 4 and 7.5. It is obvious that tested walls were squatter with respect to the walls incorporated in buildings. Therefore, it can be easily realized that the seismic behavior of building walls will even be more ductile.

- This study is valid only when double walls are connected with waves and with cages having sufficiently long development length. Any deviations from these may dismiss the results here.
- The detailed evaluation procedures of ASCE/SEI-41, TEC2007 and EC8-3 were performed. In the elements controlled by flexure, it seems that ASCE/SEI-41-06 provide a better agreement with the experimental results, while the updated version of this document, overestimates the damage limits indicating that after complete analysis, collapse state should be determined.
- In brittle elements, comparing the related shear capacities specified by the codes, ASCE/SEI-41 (ACI318) provides the closest value to test result. It may be concluded that the shear strength expressions of ACI318 are found to be safe to compute the capacity of double walls. Among these codes, TEC2007 provides the most improper values.
- Eurocode 8 provides the best prediction of the failure mechanisms of specimens.
- Analysis results of the building under investigation comprising of significant amount of double walls capable of sufficient seismic performance, demonstrate that such semi-precast multi-story buildings with about 2% wall area are expected to sustain limited displacement demands resulting in damages states mostly below MN and few below LS.

REFERENCES

"PCI Design Handbook: Precast and Prestressed Concrete, 7th Edition," Precast/Prestressed Concrete Institute, 2008.

"Seismic Design of Precast Concrete Building Structures: State of the art Report," FIB Bulletins, 2003.

A. Al-Einea, D. Salmon, M. Tadros and T. Culp, "A New Structurally and Thermally Efficient Precast Sandwich Panel System," *PCI Journal,* vol. 39, no. 4, pp. 90-101, 1994.

A. Benayoune, A. Abdul Samad, D. Trikha, A. Abang Ali and S. Ellinna, "Flexural Behaviour of Precast Concrete Sandwich Composite Panel, Experimental and Theoretical Investigations," *Construction and Building Materials,* vol. 22, no. 4, pp. 580-592, 2008.

ACI Committee 318, Building Code Requirements, Structural Concrete and Commentary, American Concrete Institute, 2011.

ACI Committee 533, "Guide for Precast Concrete Wall Panels," American Concrete Institute, 1993.

A. Haas, Precast Concrete, Design and Applications, Applied Science Publishers, 1983.

A. Hamid and M. Fudzee, "Seismic Performance of Insulated Sandwich Wall Panel Under In-Plane Lateral Cyclic Loading," *International Journal of Emerging Technology and Advanced Engineering,* vol. 3, no. 3, pp. 1-7, 2013.

A. Yakut and T. Solmaz, "Performance based Displacement Limits for Reinforced

Concrete Columns under Flexure," in *15 WCEE*, Lisboa, 2012.

B. Binici and E. Canbay, "Component Testing of the Double Wall System for Seismic Qualification," Department of Civil Engineering, Middle East Technical University, Ankara, 2014.

C. H. Goodchild and J. Glass, "Best Practice Guidance for Hybrid Concrete Construction," The Concrete Center, September, 2004.

D. King, M. Priestley and R. Park, "Computer Programs for Concrete Column Design," Research Report 86/12, Department of Civil Engineering, University of Canterbury , New Zealand, May 1986.

E. Karaesmen, Prefabrication in Turkey: Facts and Figures, Ankara, Turkey: Department of Civil Engineering, Middle East Technical University, 2001.

E. P. Koehler, D. W. Fowler, E. H. Foley, G. J. Rogers, S. Watanachet and M. J. Jung, "Self-Consolidating Concrete for Precast Structural Applications," The University of Texas at Austin, August, 2007.

EERI, "Armenia Earthquake Reconnaissance Report," Earthquake Spectra, Earthquake Engineering Research Institute, Special Supplement, August 1989, 175 p.

EERI, "Kocaeli, Turkey, Earthquake of August 17, 1999 Reconnaissance Report," Earthquake Spectra, Earthquake Engineering Research Institute, Supplement to Volume 16, 1999, 461 p..

EERI, "Learning from Earthquakes: The M 6.3 Christchurch, New Zealand, Earthquake of February 22, 2011," EERI Special Earthquake Report, Oakland, CA, 2011.

G. De Matteis and R. Landolfo, "Structural Behaviour of Sandwich Panel Shear Walls: An Experimental Analysis," *Materials and Structures*, vol. 32, pp. 331-341, 1999.

J. J. Waddell, Precast Concrete: Handling and Eretion, The Iowa State University

Press; American Concrete Institute, 1974.

J. Mander, M. Priestley and R. Park, "Theoretical Stress-Strain Model for Confined Concrete," *ASCE Journal of Structural Engineering,* vol. 114, no. 8, August 1988.

K. J. Elwood, "Performance of Concrete Buildings in the 22 February 2011 Christchurch Earthquake and Implications for Canadian Codes," *Canadian Journal of Civil Engineering,* vol. 40, pp. 759-779, 2013.

L. Xu, X. Shen and J. Shen, "Seismic Study of Hybrid Shear Wall," in *10th National Conference in Earthquake Engineering, Earthquake Engineering Research Institute,* 2014.

M. Fintel, "Performance of Buildings with Shear Walls in Earthquakes of the Last Thirty Years," *PCI Journal,* vol. 40, no. 3, pp. 62-80, May/June 1995.

M. Mahendran and S. Subaahara, "Shear Strength of Sandwich Panel Systems," *Australian Journal of Structural Engineering,* vol. 3, no. 3, pp. 115-126, 2002.

M. Priestley, G. Calvi and M. Kowalsky, Displacement-Based Seismic Design of Structures, IUSS Press, 2007.

M. Saatcioglu, D. Mitchell, R. Tinawi, N. Gardner, A. Gillies, A. Ghoborah, D. Anderson and D. Lau, "The August 17,1999 Kocaeli (Turkey) Earthquake Damage to Structures," *Canadian Journal of Civil Engineering,* vol. 28, no. 4, pp. 715-737, August 2001.

PCI Committee, "State of the Art Precast/Prestressed Concrete Sandwich Wall Panels," Second Edition.

R. B. Fleischman, J. I. Restrepo, S. Pampanin, J. R. Maffei, K. Seeber and F. A. Zahn, "Damage Evaluations of Precast Concrete Structures in the 2010–2011 Canterbury Earthquake Sequence," *Earthquake Spectra, Earthquake Engineering Research Institute,* vol. 30, no. 1, pp. 277-306, February2014.

R. E. Englekrik, "Design-Construction of The Paramount - A 39-Story Precast Prestressed Concrete Apartment Building," vol. 47, no. 4, 2002.

R. Park, "Seismic Design and Construction of Precast Concrete Buildings in New Zealand," *PCI Journal,* vol. 47, no. 5, pp. 60-75, September/October 2002.

S. K. Ghosh, "Earthquake Resistant Precast Buildings," *MC magazine,* Winter 2001.

S. L. Wood, J. K. Wight and J. P. Moehle, "THE 1985 CHILE EARTHQUAKE, Observations on Earthquake-Resistant Construction in Vina del Mar," Civil Engineering Studies, Structural Research Series No. 532, University of Illinois, Urbana, Ill, 1987.

S. Pessiki and A. Mlynarczyk, "Experimental Evaluation of the Composite Behavior of Precast Concrete Sandwich Wall Panels," *PCI Journal,* vol. 48, no. 2, pp. 54-71, 2003.

Seismic Evaluation and Retrofit of Existing Buildings, Reston, Virginia, USA: American Society of Civil Engineers, 2014.

Seismic Rehabilitaion of Existing Buildings, Report No: ASCE/SEI 41 - Supplement 1, Reston, Virginia, USA: American Society of Civil Engineers (ASCE), 2007.

Turkish Earthquake Code 2007, Specification for Buildings to be Built in Seismic Zones, Ministry of Public Works and Settlement, 2007.

T. Holden, J. Restrepo and J. B. Mander, "Seismic Performance of Precast Reinforced and Prestressed Concrete Walls," *Structural Engineering,* vol. 129, no. 3, pp. 286-296, March, 2003.

U. Ersoy and G. Özcebe, "Moment-Curvature Relationship of Confined Concrete," *First Japan-Turkey Workshop On Earthquake Engineering,* vol. 1, pp. 10-21, 1997.

U. Ersoy, T. Tankut and G. Özcebe, Damages Observed in the Precast Framed Structures in the 1998 Ceyhan Earthquake and their Rehabilitation, Ankara, Turkey: Department of Civil Engineering, Middle East Technical University, 1999.

V. Mpampatsikos, "A Critical Rreview of the R.C. Frame Existing Building

Assessment Procedure According to Eurocode 8 and Italian Seismic Code," M.Sc. Thesis, Rose School, 2008.

APPENDIX A

RESPONSE OF SHEAR WALLS

Using moment-curvature procedure described in Chapter 2, response of walls under study in Chapter 4 are determined as follows.

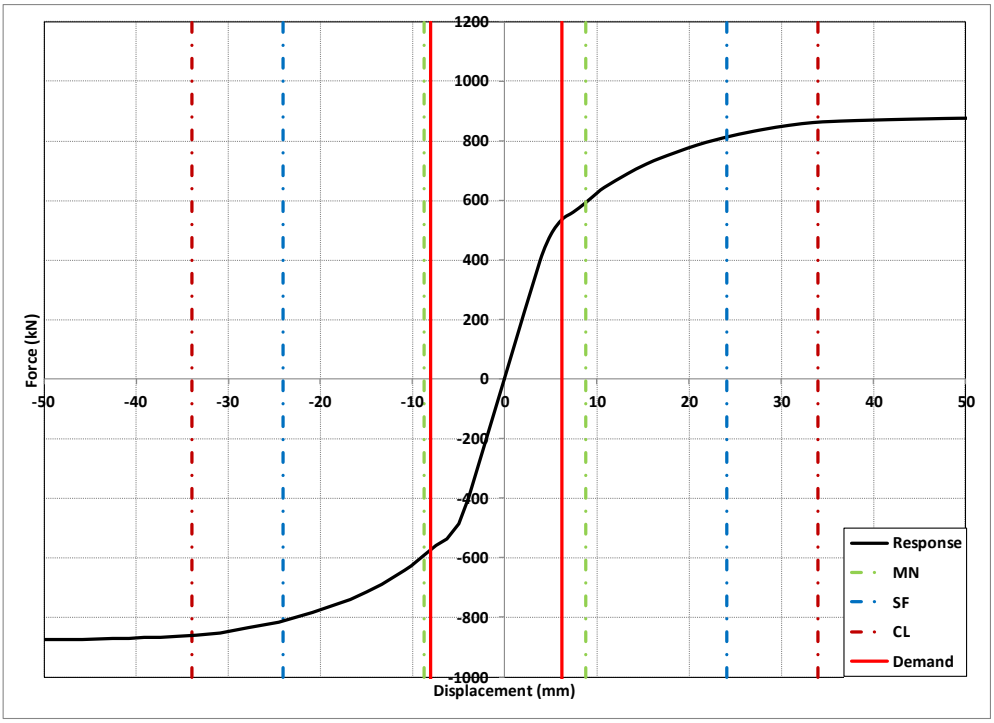

Figure A-1: Response of Wall P1

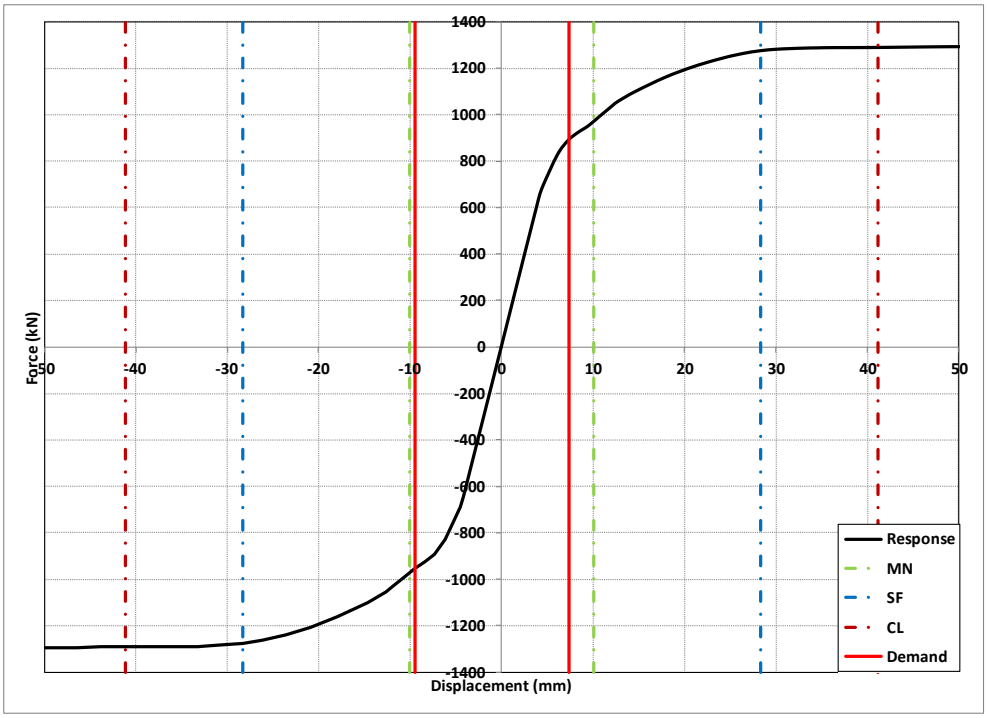

Figure A-2: Response of Wall P2

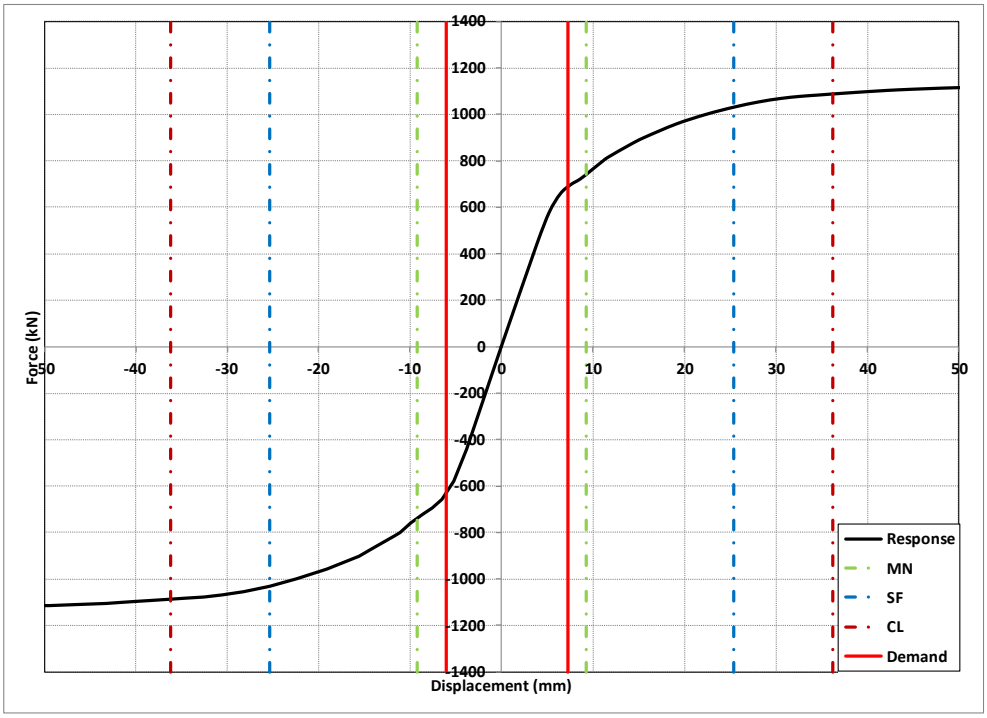

Figure A-3: Response of Wall P3

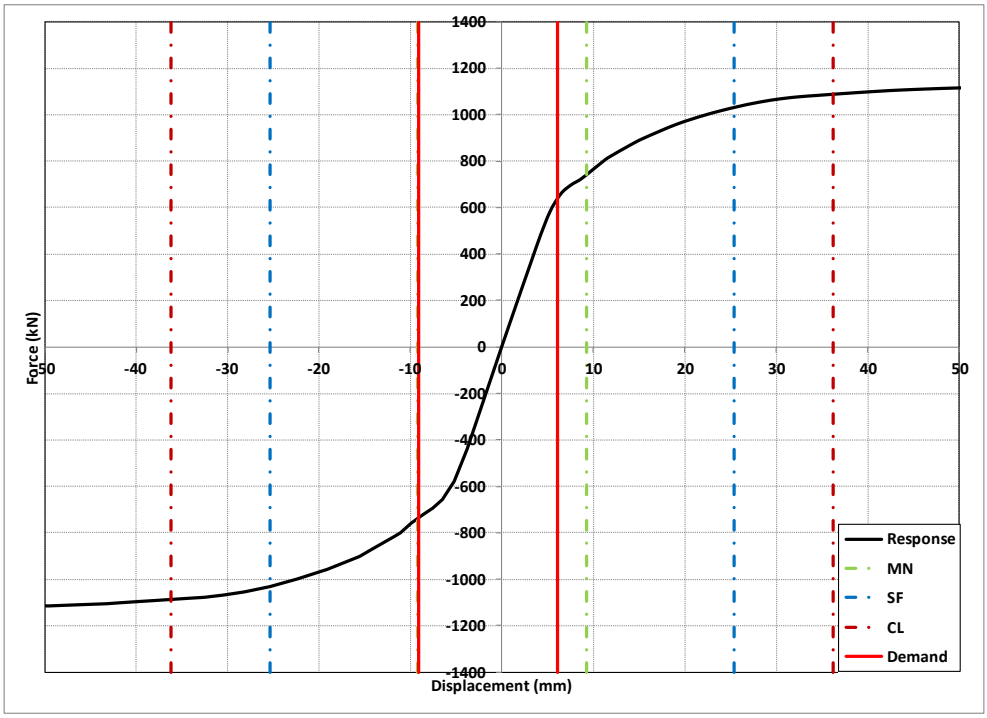

Figure A-4: Response of Wall P4

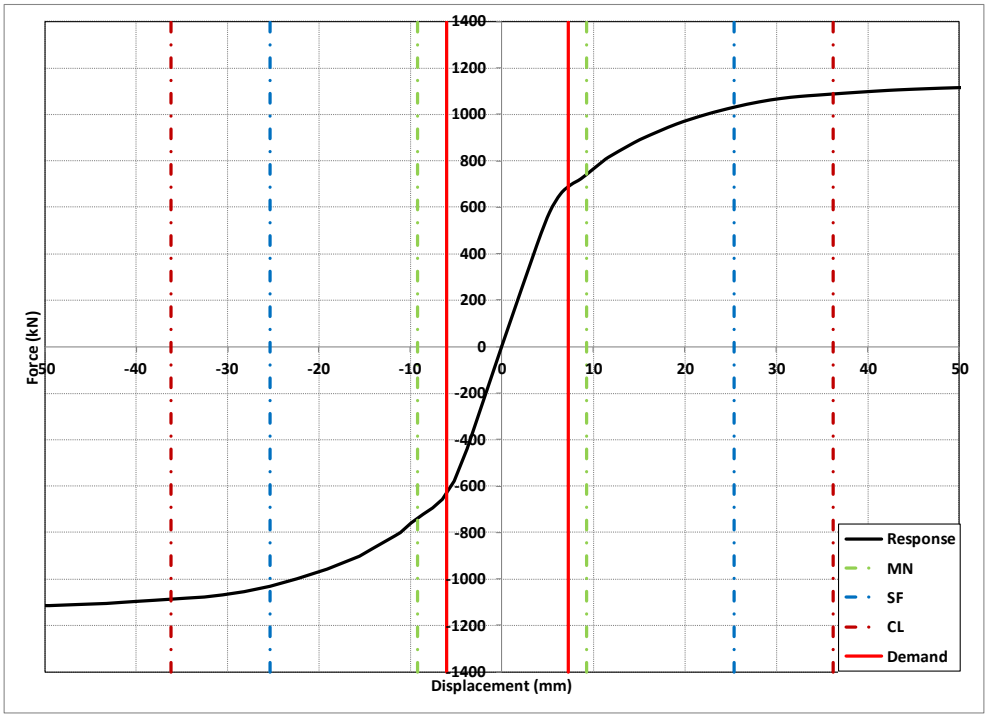

Figure A-5: Response of Wall P5

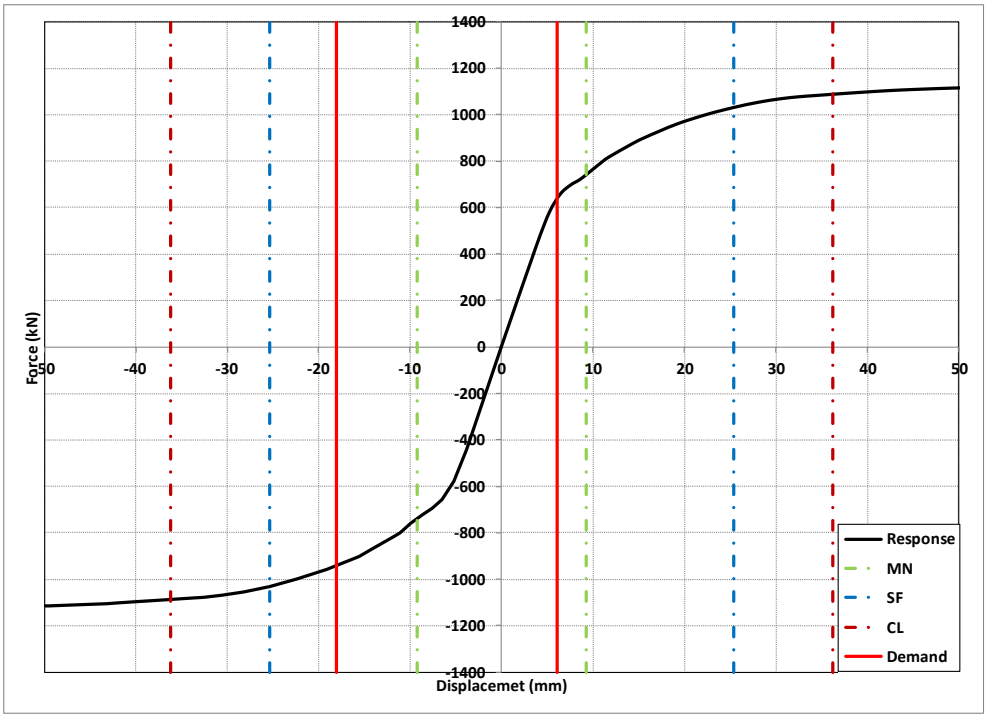

Figure A-6: Response of Wall P6

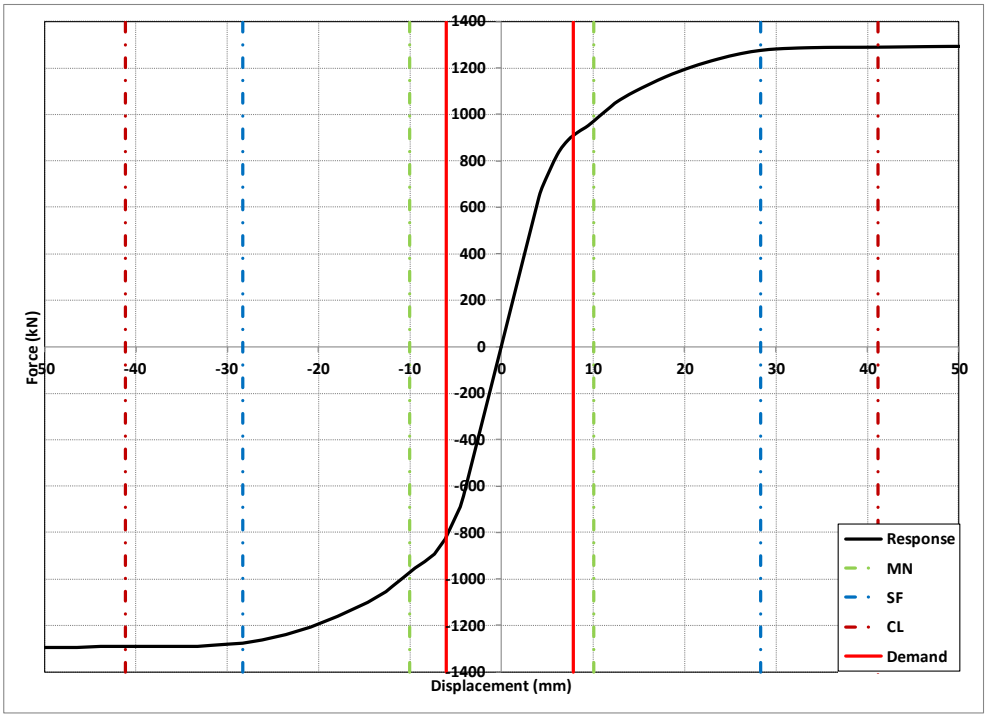

Figure A-7: Response of Wall P7

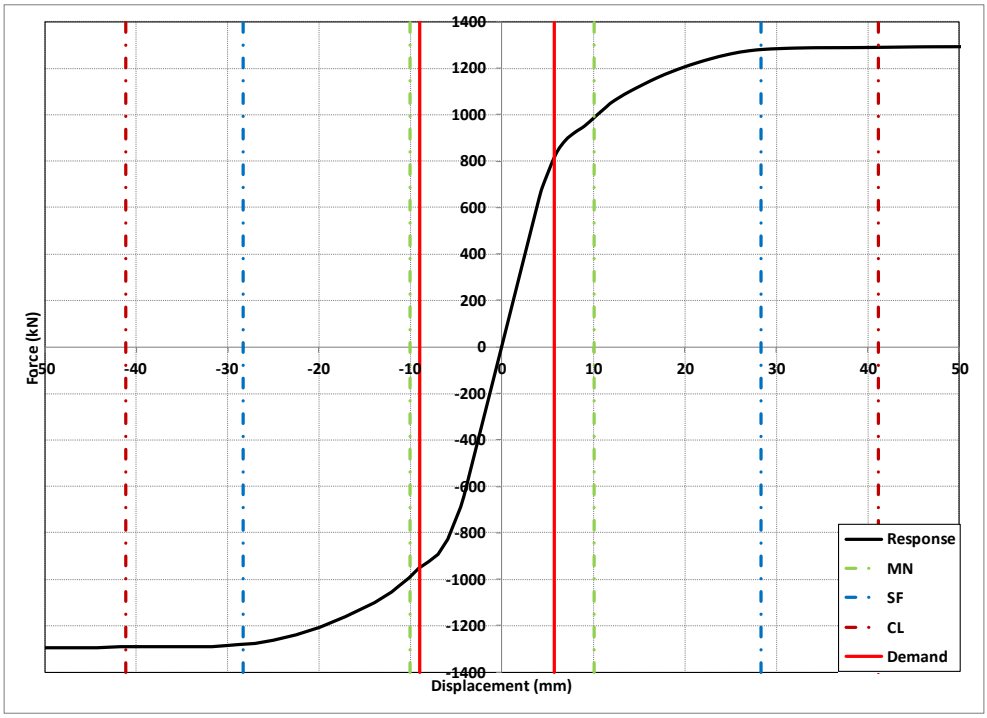

Figure A-8: Response of Wall P8

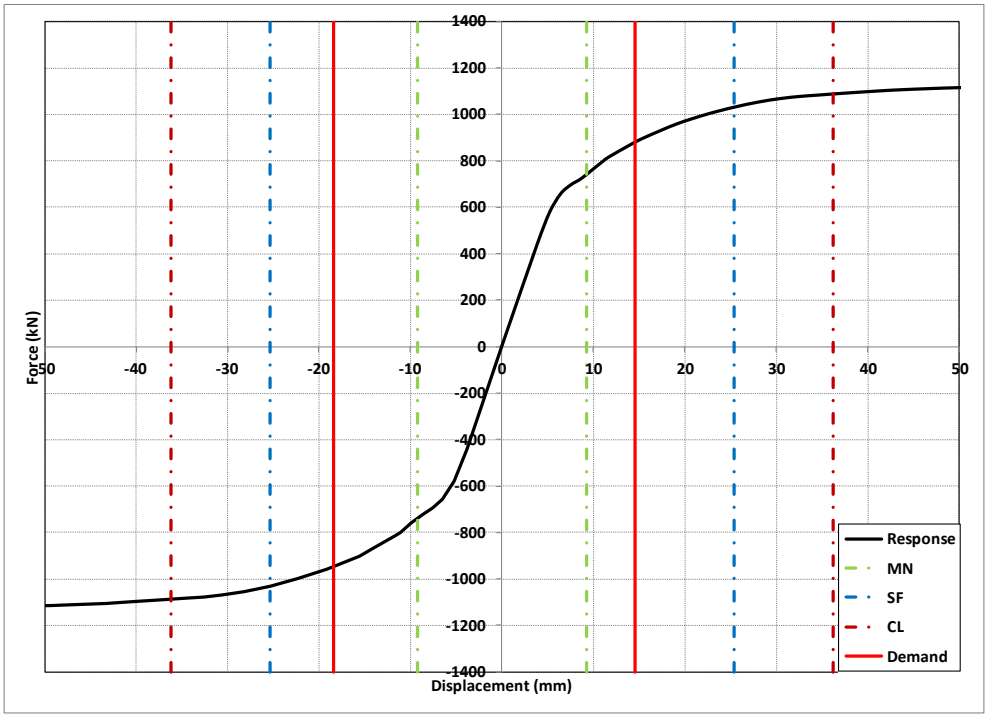

Figure A-9: Response of Wall P9

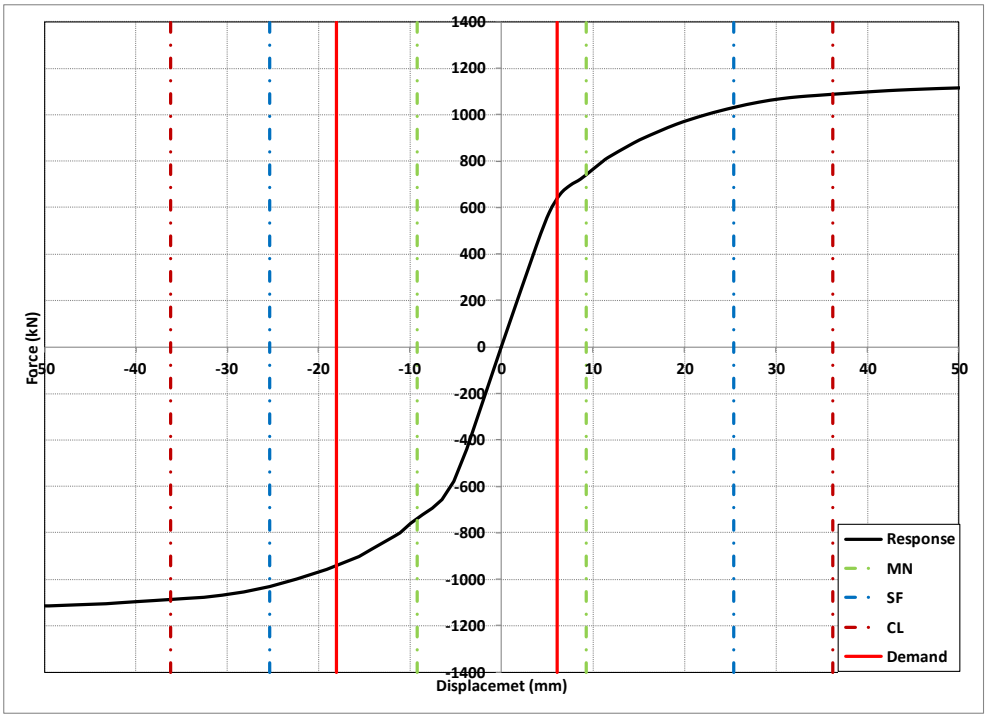

Figure A-10: Response of Wall P10

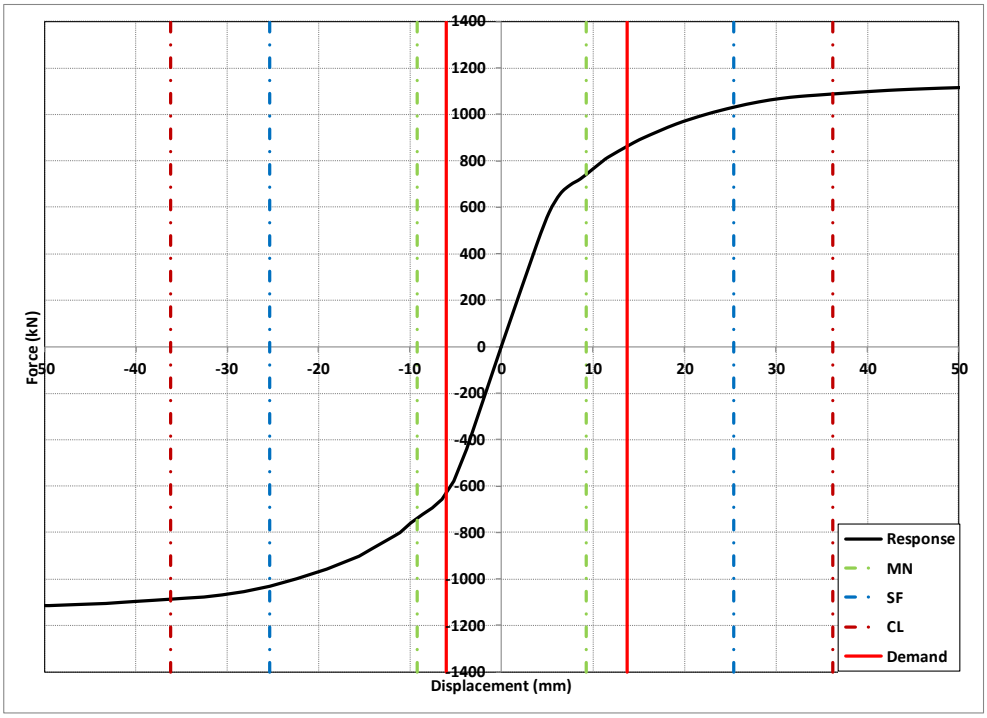

Figure A-11: Response of Wall P11

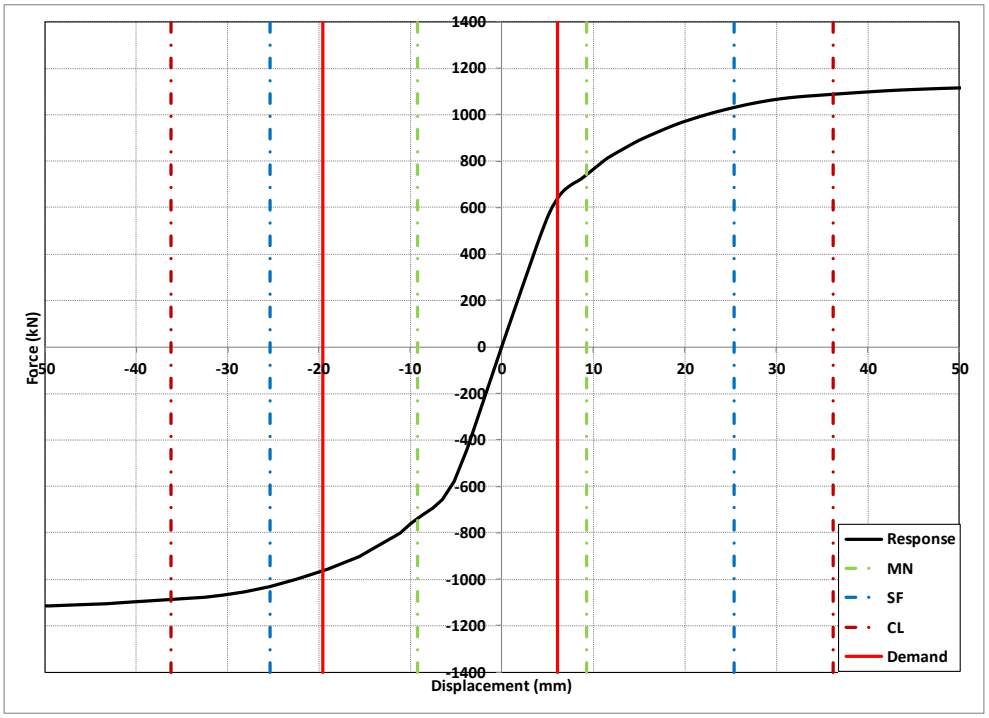

Figure A-12: Response of Wall P12

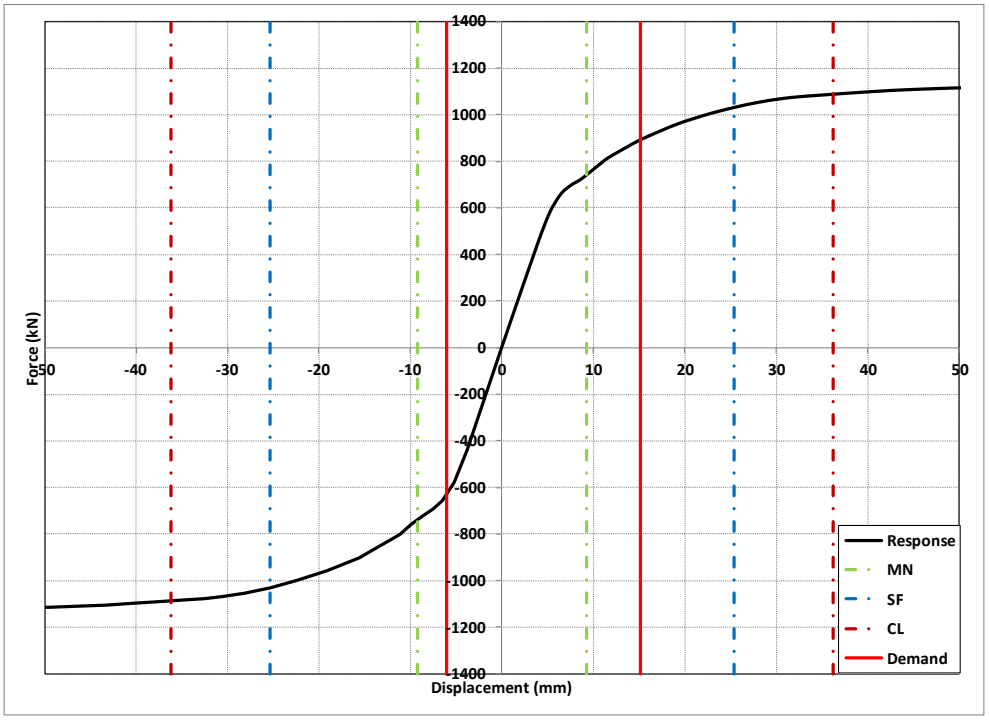

Figure A-13: Response of Wall P13

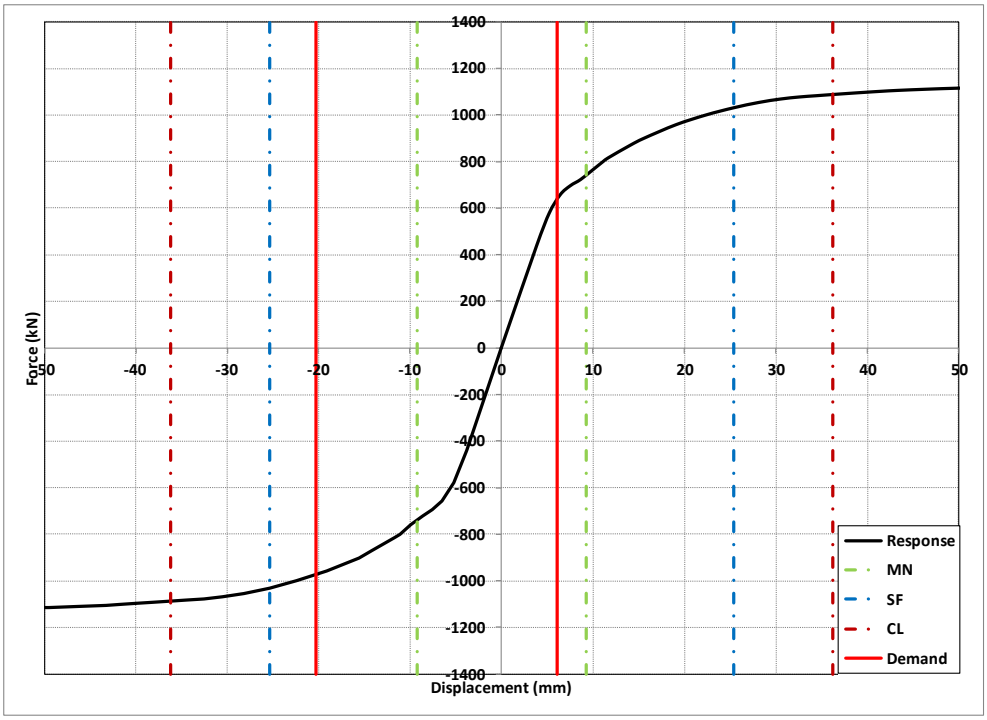

Figure A-14: Response of Wall P14

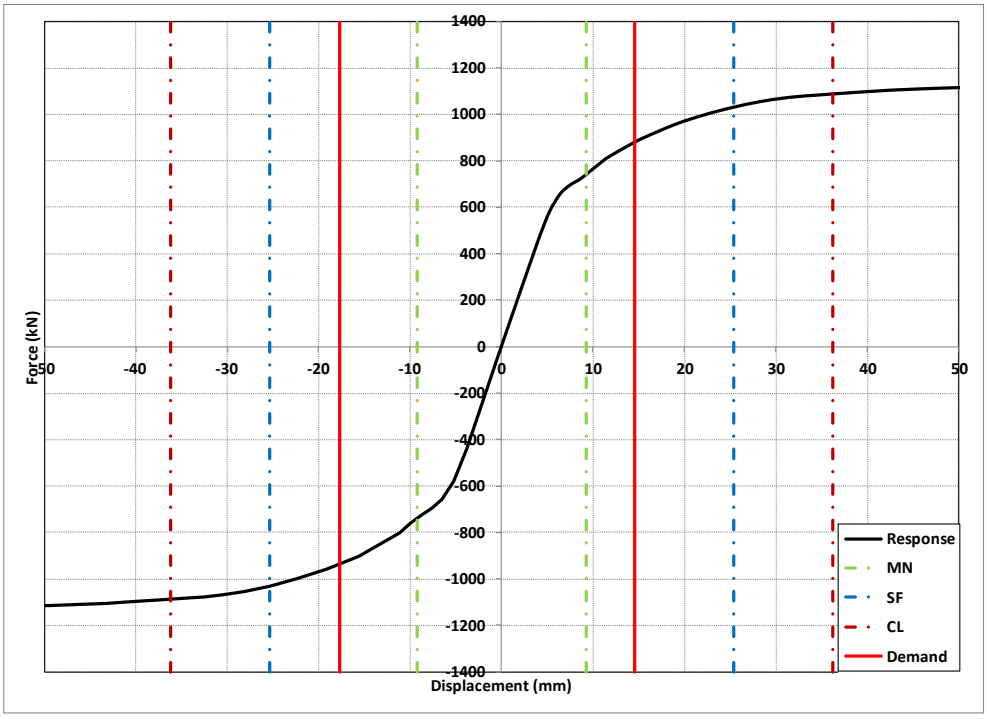

Figure A-15: Response of Wall P15

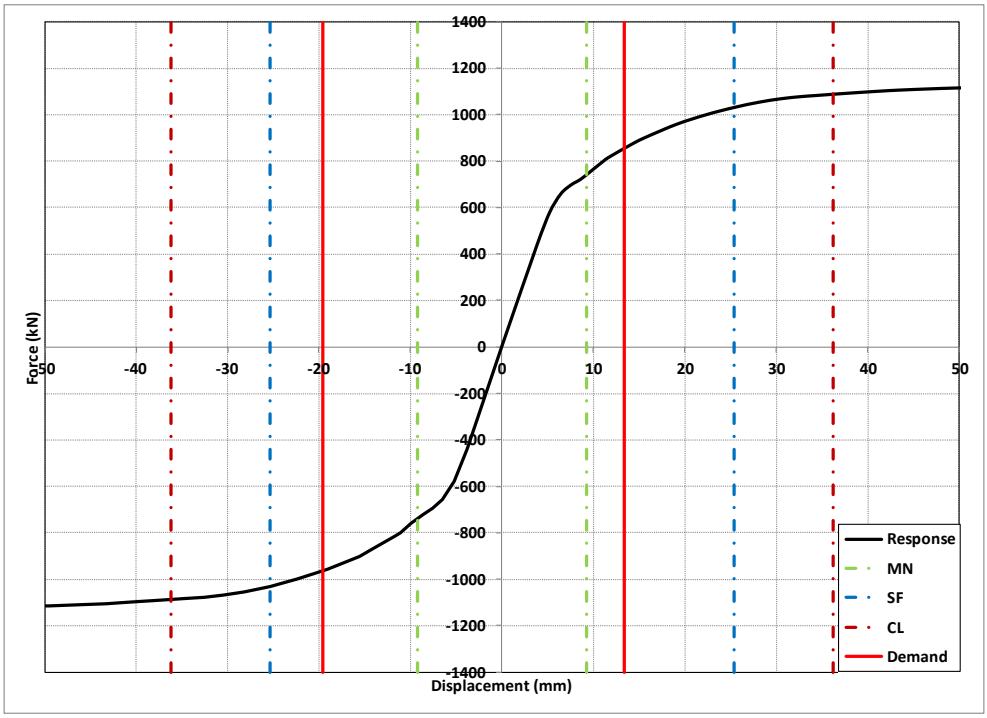

Figure A-16: Response of Wall P16

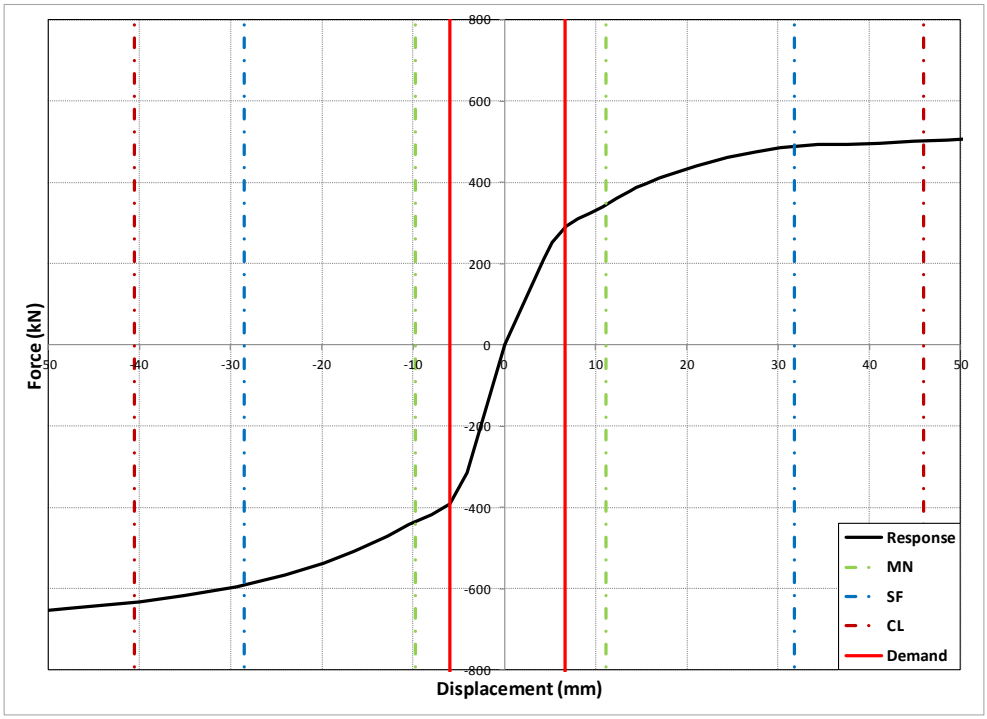

Figure A-17: Response of Wall P17

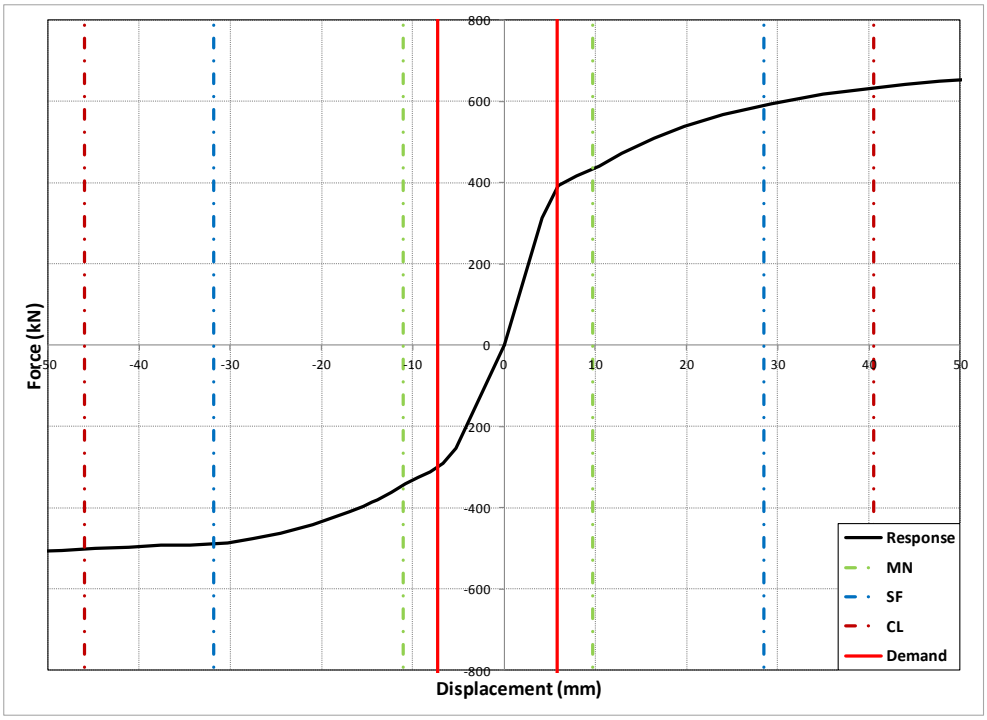

Figure A-18: Response of Wall P18

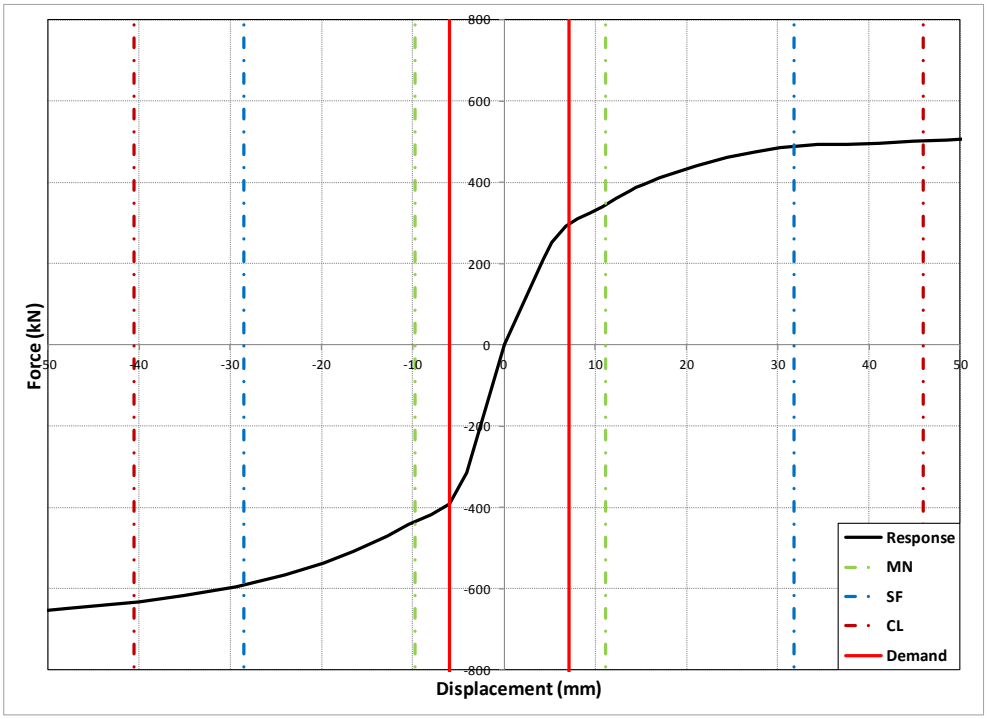

Figure A-19: Response of Wall P19

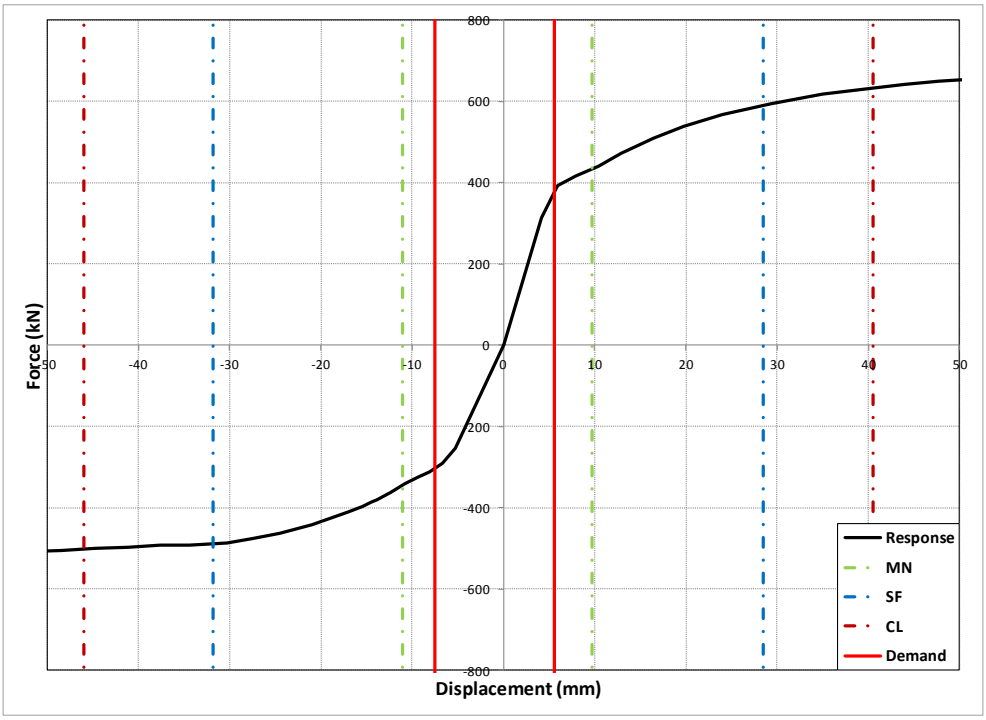

Figure A-20: Response of Wall P20

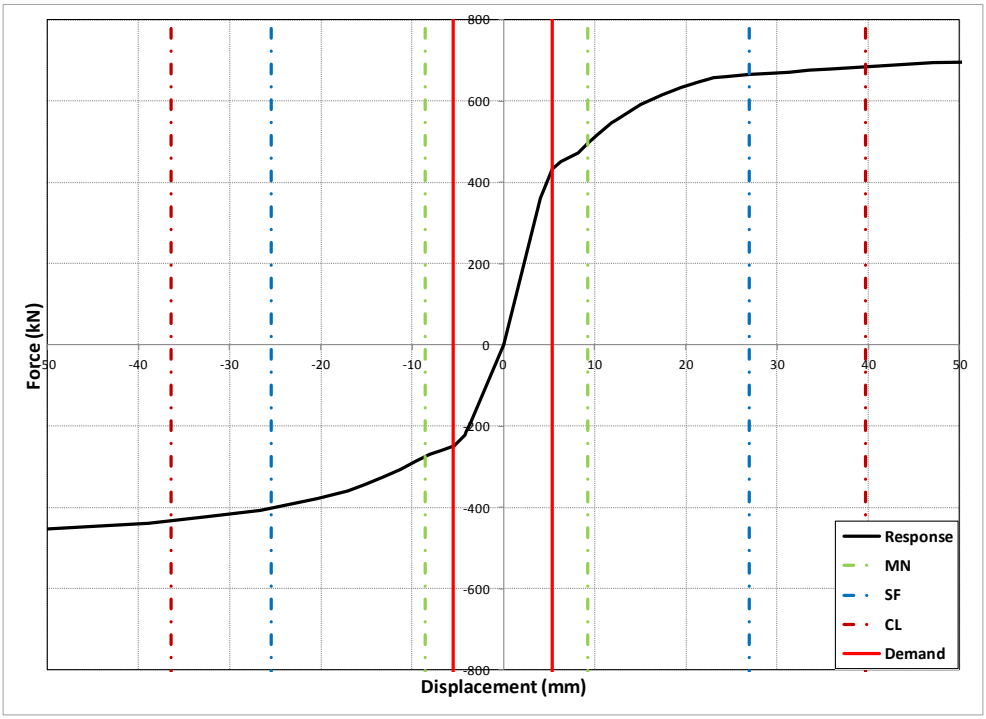

Figure A-21: Response of Wall P21

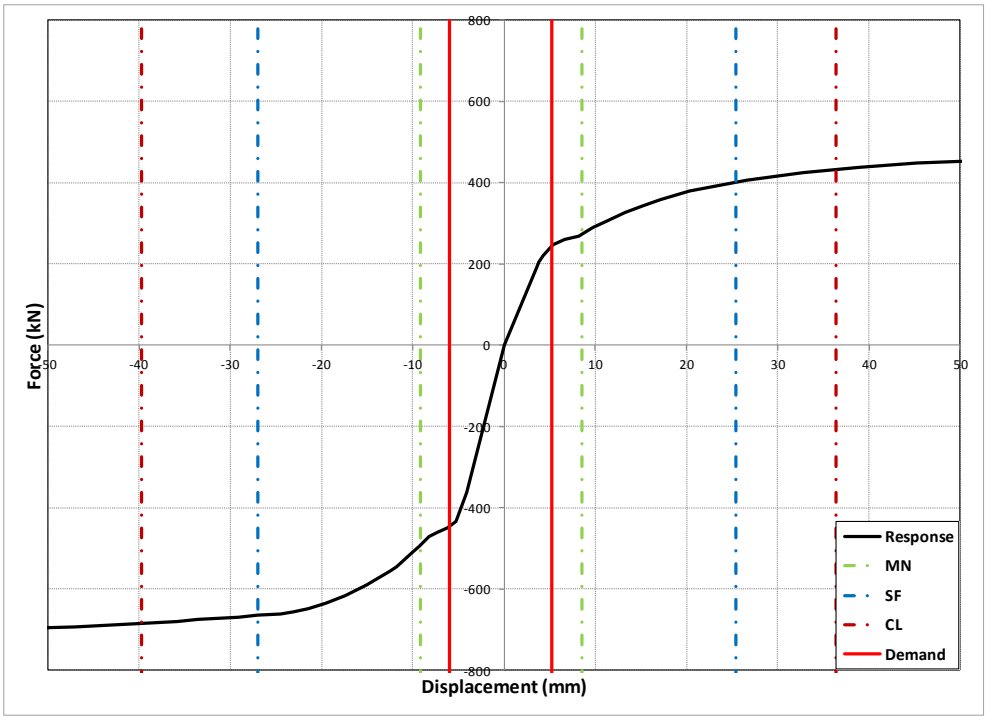

Figure A-22: Response of Wall P22

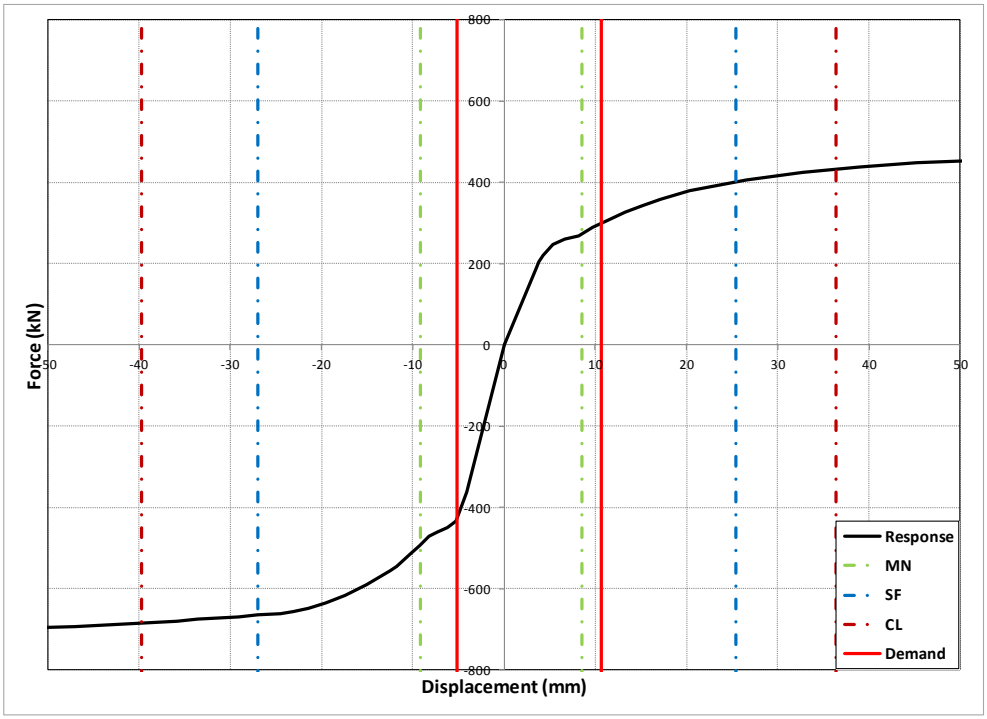

Figure A-23: Response of Wall P23

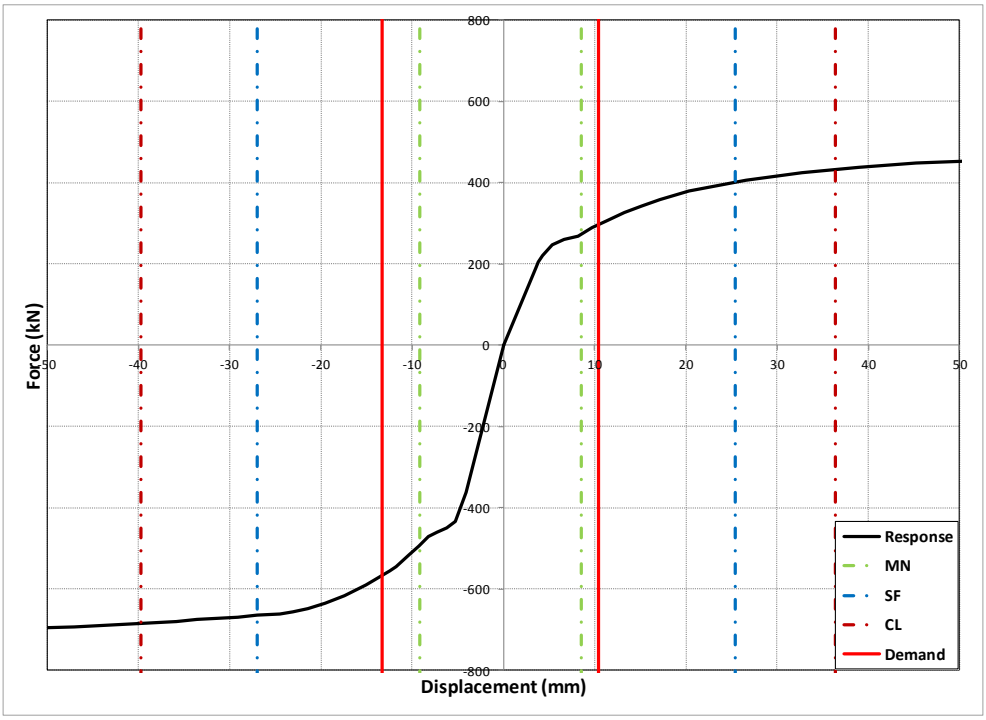

Figure A-24: Response of Wall P24

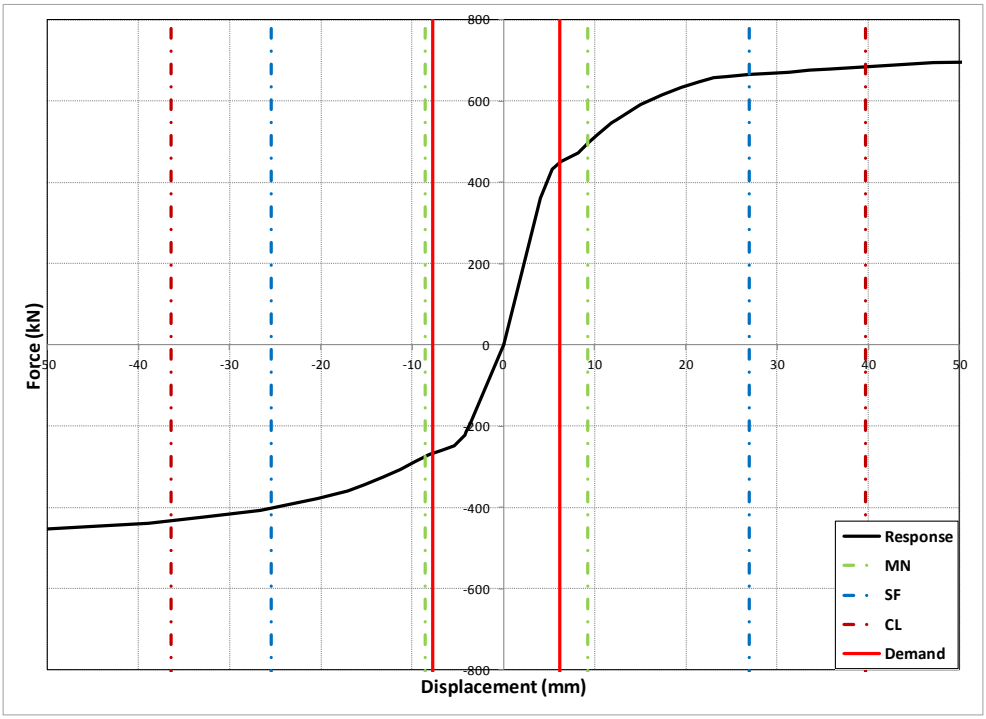

Figure A-25: Response of Wall P25

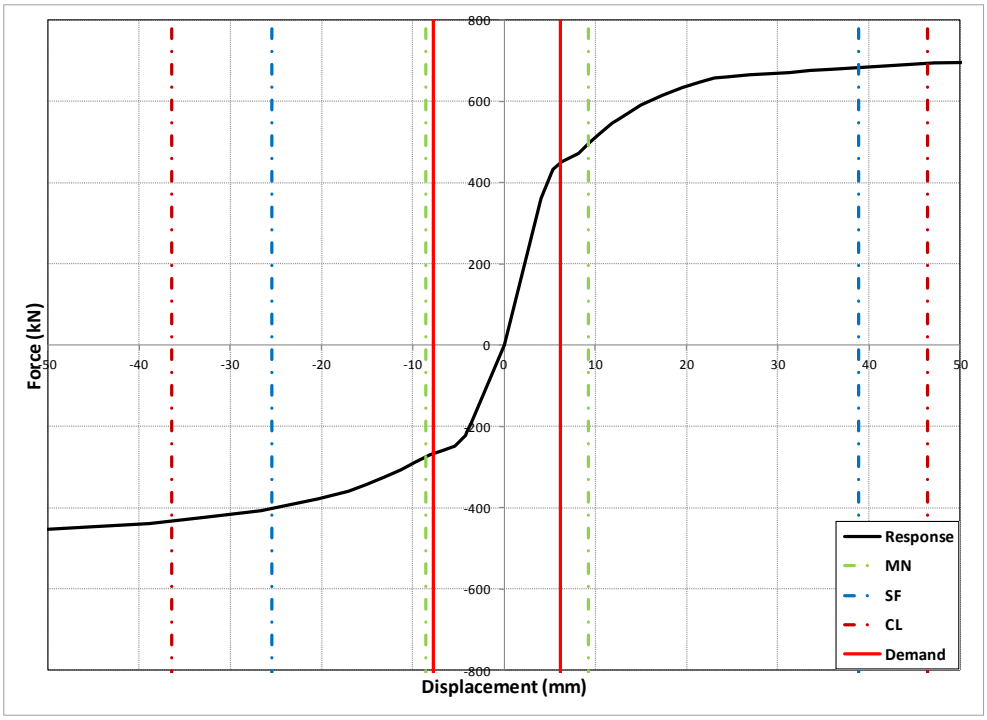

Figure A-26: Response of Wall P26

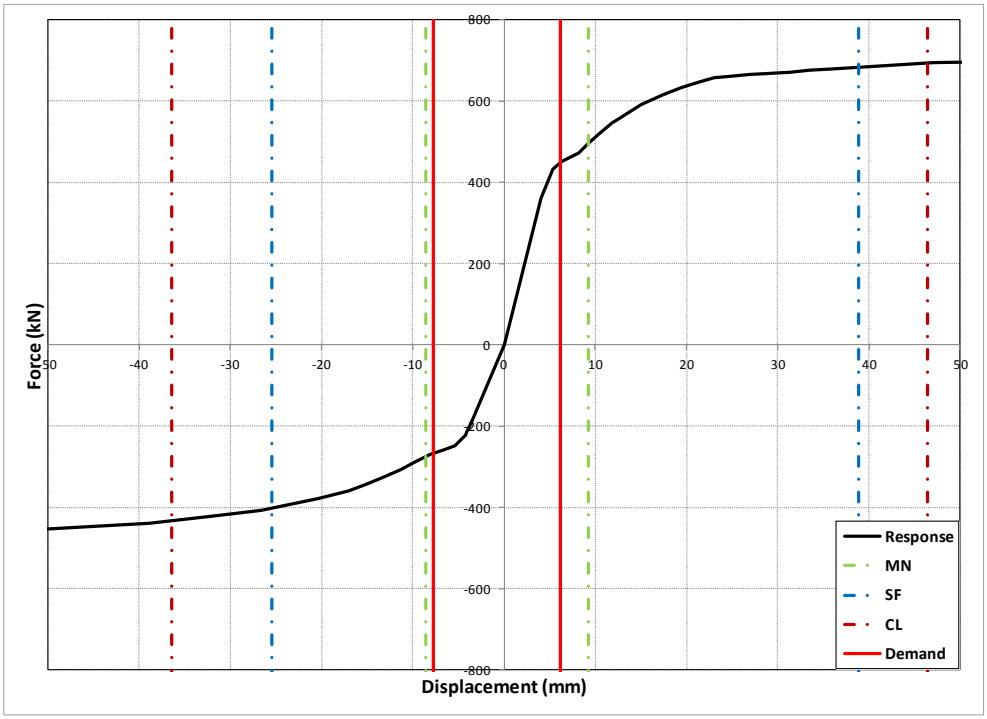

Figure A-27: Response of Wall P27

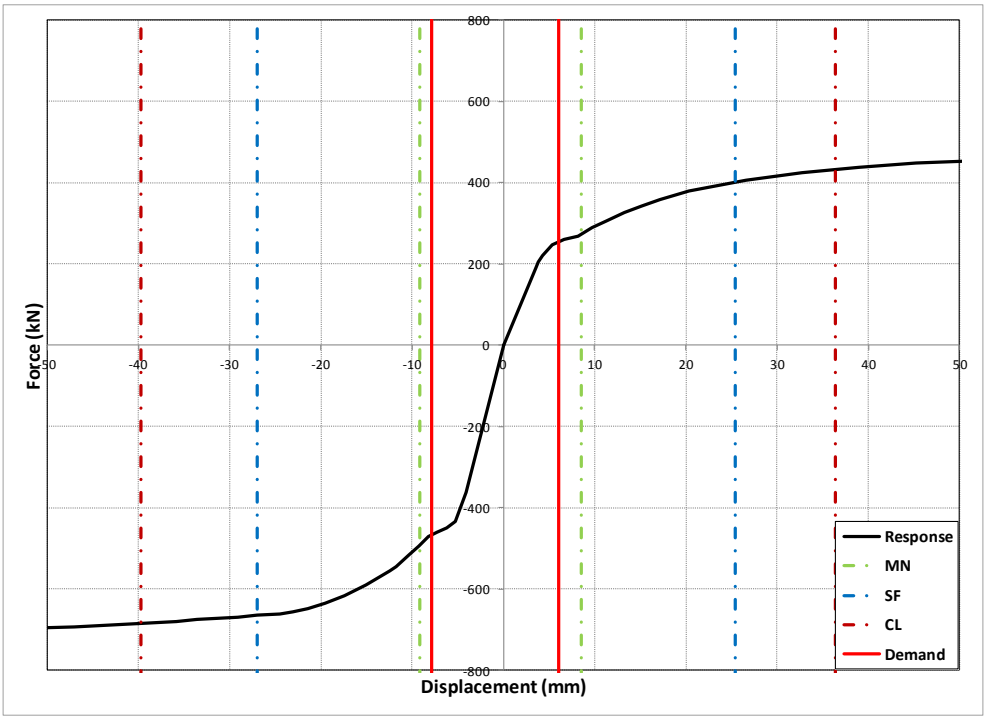

Figure A-28: Response of Wall P28

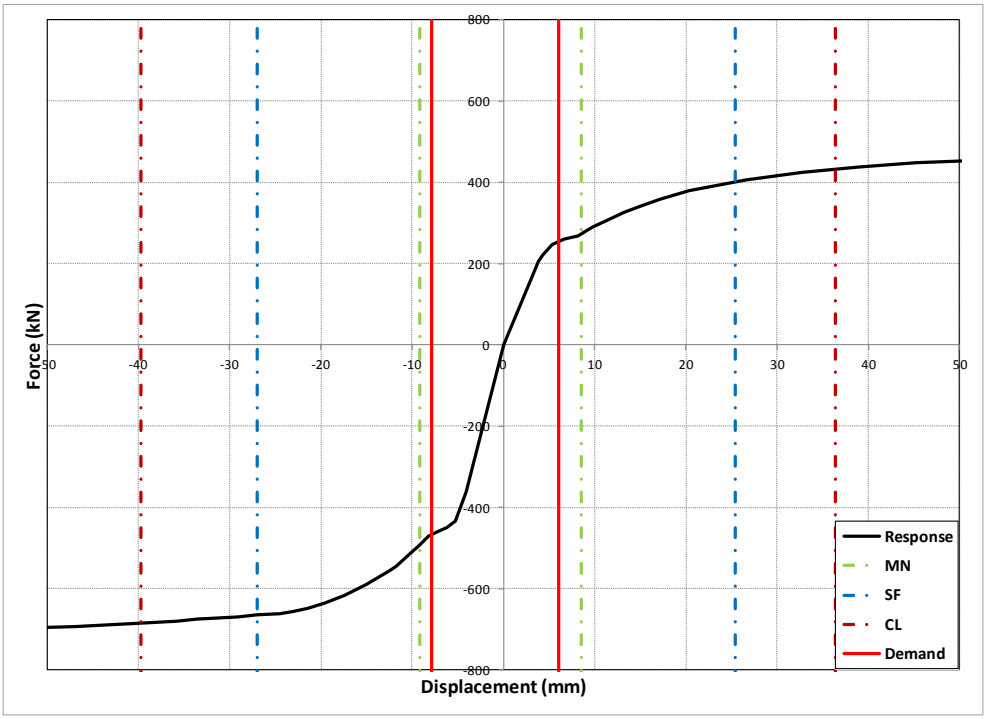

Figure A-29: Response of Wall P29

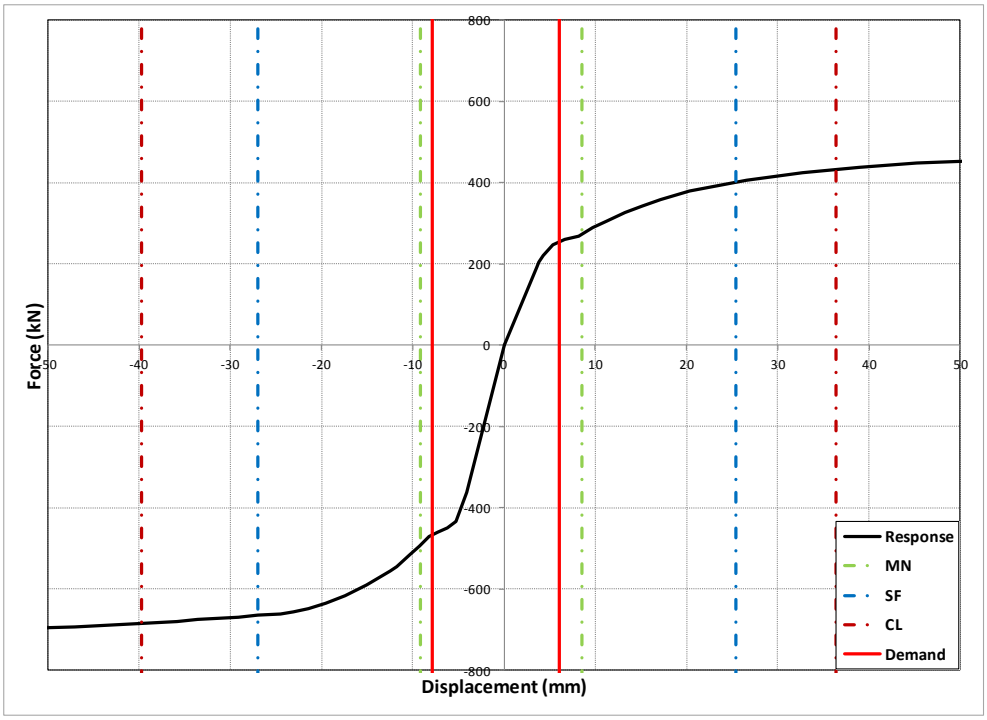

Figure A-30: Response of Wall P30